Professor Dr. rer. nat. S. Schmauder am

**Institute for Materials testing,
Materials Science and Strength of Materials
University of Stuttgart**

Professor Dr.-Ing. habil. Eberhard Roos

Master Thesis No. 752 438

Title:	Fatigue strength analysis and end-of-life crack propagation in thin stainless steel structures by means of comparing FE-analyses and experimental results
Candidate:	Muhmmad Ajmal Choudhary
Address:	Pfaffenwaldring 42a / 303 70569 Stuttgart, Germany
Starting date:	November 02, 2008
Completing date:	April 30, 2009
Supervisor:	Dr.-Ing. Ulrich Weber

Professor Dr. rer. nat. S. Schmauder am
Institute for Materials testing,
Materials Science and Strength of Materials
University of Stuttgart
Professor Dr.-Ing. habil. Eberhard Roos

MASTER THESIS

Fatigue Strength Analysis of Welded Thin Steel Sheets Structures in Exhaust Systems by Means of Comparing FE- and Experimental Results

To check the fatigue strength of components of exhaust systems, hydro-pulse-tests are used, in which the component is tested under the operating temperature and real loading conditions. The pipe inlet or outlet is under cyclical bending moments in two directions for different loading levels. The results of the hydro-pulse-tests are s-n-curves, which give the high cycle fatigue strength and durability of the components.

FE-analyses are to be done under the same thermal-mechanical conditions for the parts like welded thin steel sheets under cyclical tension load, pipe inlets of mufflers and catalyst converters under cyclical bending moments in two directions. There exist already experimental hydro-pulse-test results for these parts under different temperatures. Direct frequency analysis can be used to follow the hydro-pulse-test with the FE-method. In the FE-analysis, different temperatures and different geometries of weld seams are to be considered. To estimate the high cycle fatigue strength of the components from the FE-modelling the stress analysis will be performed by using different FE-models such as shell elements and solid elements for the weld seams and by comparing FE- and experimental results.

To obtain a better understanding and a general approach for the prediction of s-n-curves or fatigue strength of components of exhaust systems, a combination of stress-analysis and fatigue theory considering the influences of temperature, weld seam geometry and notch-effects will be taken into account in this work.

Accepted by: *Professor Schmauder*

Professor Roos

This project is dedicated to my beloved parents, teachers and friends

whose prayers, inspiration and love led to this accomplishment

Preface

The research presented in this Master thesis was initiated by the Institute for Materials Testing, Materials Science and Strength of Materials (IMWF) at the Universität Stuttgart. It was carried out under the supervision of Dr.-Ing. Ulrich Weber from November 2008 to April 2009.

I give my sincere appreciation and gratitude to Mr. Thomas Stark of Whirlpool for introducing me to this project. The experimental study was carried out at Whirlpool with his support. His invaluable advice, guidance and support were of great help to me throughout this thesis.

I would especially like to thank and express my deepest thankfulness and admiration to Dr.-Ing. Ulrich Weber for his support and guidance throughout this project. His encouragement and enthusiasm has been a great inspiration for me.

A special thanks goes to Professor Dr. rer. nat. Siegfried Schmauder for spreading his knowledge and founding my interest in fracture mechanics through his discussion and courses at Universität Stuttgart.

In the end I would like to thank the members of my family for their emotional and moral support throughout my academic career. No personal development could ever take place without proper guidance of parents. I also acknowledge with gratitude, the inspiration and encouragement of my grand parents, brothers and sisters.

Stuttgart, May 2009

Muhammad Ajmal Choudhary

Table of Contents

List of Figures

List of Tables

Nomenclature

Abbreviations

ALT	- Accelerated life test
CAL	- Constant amplitude loading
CL	- Cyclic loading
CPP	- Crack propagation path
DKC	- Discrete Kirchhoff constraint
DOF	- Degrees of freedom
FCG	- Fatigue crack growth
FCP	- Fatigue crack propagation
FE	- Finite Element
FEA	- Finite Element analysis
FEM	- Finite Element Method
LEFM	- Linear elastic fracture mechanics
RMC	- Rest moisture content
RT	- Room temperature
SIF	- Stress intensity factor
WM	- Washing machines
2D	- Two dimensional
3D	- Three dimensional

Symbols

Greek Symbols

σ_{ij} - Second order stress tensor

σ - Remote stress applied to the component

σ_n - Normal stress

τ_{ij} - Shear stress tensor

ε_{ij} - Second order strain tensor

ν - Poisson's ratio

Π - Potential energy

ΔK - Stress intensity factor range

Lower Case Latin Symbols

a - Crack length

$\{d\}$ - Global nodal point displacement vector

n - Unit vector

r - Distance from the crack tip

u - Displacement vector

w - Crack width

Upper Case Latin Symbols

C, m	- Material constants used in Paris law
E	- Young's modulus
$\{F\}$	- Global load vector
G	- Energy release rate
G_C	- Critical energy release rate
K	- Stress intensity factor
K_I	- Mode I stress intensity factor
K_{II}	- Mode II stress intensity factor
K_{Ic}	- Fracture toughness
$\{K\}$	- Global stiffness matrix
N	- Number of load cycles
P	- Applied load
U	- Elastic strain energy stored in the body
W	- Work done by external forces.
Y	- Dimensionless geometric parameter

Abstract

The study of fatigue crack growth (FCG) is an important consideration in design of engineering components and during their service life. The aim of this Master thesis is to use a combination of experimental investigation and finite element analysis (FEA) for fatigue strength analysis and to predict crack locations and crack propagation in thin stainless steel structures. Washing machines (WM) have perforated highly stressed thin-walled rotating stainless steel structures with the trend to continuously increase the internal capacity as well as spinning speeds. Initially, the background to the project and the description of the investigation are presented. An introduction of the theories that has been applied is given and a description of the modeling procedures in ANSYS, ABAQUS and Franc2D is presented.

The experimental investigations provided the shape deformation of the drum under the applied load conditions and it also provided the crack locations and the corresponding fatigue data. These experimental results are verified by means of FEA.

The FEA has been done initially using ANSYS and results are compared with the experimental results. Later on, ABAQUS is used to ensure the ANSYS results. The numerical investigations are divided into two categories: deformation and stress analysis as well as crack propagation with fatigue strength analysis. The deformation and stress analysis shows that lifter holes are the most critical location for the cracks to appear because the maximum stresses are at these locations. Based on these results crack propagation and fatigue strength analysis is performed in Franc2D using a simplified FE model. The results from this FE model agree with the experimental findings. Finally, the effects of loading and inner lifter hole radius on the crack propagation and fatigue life is considered in order to optimize the design with better resistance to crack growth.

Keywords: finite element analysis, fatigue strength, crack propagation, optimized design.

1. Introduction

Most engineering components and structures subjected to repeated fluctuating load cycles, contain some form of stress raisers that results from geometrical or metallurgical discontinuities. In most of the cases such components fail due to the phenomenon known as fatigue [1].

1.1 Background

During the past few years, extensive efforts have been devoted to develop methodologies that permit the prediction of fatigue failure. As the knowledge related to fatigue expanded, it becomes clear that in certain cases fatigue could be treated from the crack propagation point of view. The understanding of the crack initiation and crack propagation behavior has led to an increase in the life of structures subjected to cyclic loading (CL). To efficiently utilize mechanical components and structures one would like to avoid fatigue crack propagation (FCP) which results in fatigue failure. However, because of operating conditions and performance requirements it is not always possible. Thus, prediction of expected crack location and crack propagation behavior are the main objectives for the researchers in this field.

The concept of fracture mechanics developed during the early research which is applicable to linear elastic materials is known as linear elastic fracture mechanics (LEFM). LEFM has been used to estimate fatigue life of engineering components and structures. In this approach, the growth of a fatigue crack under CL is principally controlled by the stress intensity factor (SIF) K, which defines the elastic stress field around the crack tip. The SIF plays a major role in LEFM problems and several methods were proposed to derive it using analytical, experimental and numerical techniques. For general cases SIF can be obtained from handbooks. The handbook solutions of elementary cases are derived from FE-analysis and are often expressed in analytical formulas. The application of the elementary solutions in the design and sizing process involves and requires engineering judgments in a conservative manner.

However, the crack extension per cycle versus the SIF range is a typical presentation of FCP data. The results of FCG rate is usually correlated using Paris law [3].

$$\frac{dA}{dN} = C(\Delta k)^m \tag{1.1}$$

In most fracture mechanics problems possibility of fatigue failure is expected. Because the crack propagation concept is highly dependent on the state of stress in the vicinity of the crack tip, SIF is considered as the most important parameter that can be used to predict the crack propagation path (CPP). However, for many fracture mechanics problems involving complex geometry and load configuration, an approximate analytical solution for the determination of the SIF is not feasible. In addition, due to the latest research and advancements in computational methods, numerical techniques are also employed in this regard. Finite Element Method (FEM) is most commonly used to estimate the SIF numerically and thus, the CPP can be predicted. In FEM the elements are related mathematically with nodal points and the forces are transmitted through these nodal points. Using singular elements around the crack tip, singularity behavior can be achieved and the SIF can be calculated numerically which is used later on for the prediction of the CPP and fatigue life prediction. Thus, the research conducted in this Master thesis, is an attempt to investigate the problem of fatigue failure.

1.2 Statement of the problem

Currently, most of the engineering components and structures are designed with the trend to continuously increase the overall performance of the components and structures. As a result of this rapid and continuous advancement the designers and researchers have to face a lot of new challenges in terms of reliability and better fatigue life of these engineering components and structures. Thus, need for specialized fatigue strength analysis for such engineering components and structures has gone from a non-issue to a serious concern over the recent few years.

WM have perforated highly stressed thin-walled rotating stainless steel structures, called drums. For the analysis purpose one spinning cycle can basically be considered as one load cycle, however, with reduced forces since water is getting extracted from the laundry during the cycle. Based on the loading conditions, low cycle fatigue is expected for the rotating structure. Since spinning occurs at room temperature (RT) after rinsing with cold water, the temperature effects can be neglected during the structural analysis.

With the passage of time there is a trend to continuously increase the internal capacity as well as spinning speeds of the WM drum. In order to meet the customer requirements, a process change for the longitudinal seam connection from crimping to laser welding has been performed. Therefore, the wrapper connection is now very robust and it exceeds multiple lifetimes as compared to the crimped structure. Thus, by using this technique the wrapper connection has been secured against cracks but on the other hand the possibility that the cracks appear on other areas of the drum is still there. Hence, after the intended lifetime it is expected that the cracks appear at the so called lifer holes because of overload conditions. Accelerated life tests (ALT) on component level are performed on an available drum-test-bench in parallel to show the correlation of the damage around the lifter holes with the numerical findings.

From experimental investigations it has been found that cracks appear near the lifter holes. To obtain a well defined CPP and the fatigue strength of the structure, FEA is applied. FEA techniques provide good understanding of crack propagation and fatigue strength of the structures. With the help of these results the overall design of the structure is improved with a controlled failure in order to avoid risks, which usually lead to a total and dramatic damage of the washing equipment.

1.3 Scope of the present work

The main purpose of this research is to verify the results obtained from the experimental analysis by means of FEA techniques and then apply the experimental investigation along with FEA techniques in order to predict the expected crack locations and crack propagation. Finally, with this combined approach the fatigue strength is investigated. The experimental investigations are performed to evaluate the drum performance under the fatigue loading conditions. The experimental investigation results are obtained in the form of shape deformations and crack propagation behaviour. Different numerical FE models are used for a better understanding of the whole damage process and to get a better control over the damage parameters. Initial FEA is performed by using ANSYS [36] as FEM tool. Later on, the results from ANSYS simulations are further verified through simulation results from ABAQUS [38]. The FE model is created by using PATRAN [37] as a meshing tool. The structural deformations and stress distribution results from numerical analysis provide good agreement with the experimental findings. In order to get symmetric results a cylindrical coordinate system is used during numerical analysis in ABAQUS. Consequently by using symmetry

conditions, the FE model is modified which results in a simplified FE model for the analysis. The results obtained from ABAQUS simulations in terms of stresses and deformations are used as input for the analysis of crack propagation. The crack propagation analysis is performed by using Franc2D code [28] which provides a variety of options in order to get better understanding of crack propagation behaviour and fatigue strength. Finally, the influence of loading and inner radius of the lifter holes on the crack propagation and fatigue life of the component is studied by using different FE models in Franc2D.

1.4 Thesis layout

This introductory chapter is intended to summarize the problem statement and the scope of the present work. This chapter provides the basic motivation for the study of crack propagation and to perform the fatigue strength analysis of the stainless steel structures.

In chapter 2, the theoretical aspects are presented, that constitute the basis of the techniques used in this thesis. This chapter briefly describes the physical phenomenon of fatigue and fracture mechanics. Other theoretical aspects that are discussed are the plane stress concept, residual strength and thermodynamics of crack growth.

In chapter 3, a detail description of analytical models is presented which are used for crack propagation and fatigue strength calculations.

In chapter 4, the experimental procedures and the corresponding results are described in detail. These experiments are carried out to evaluate the performance of drum under the fatigue loading conditions.

In chapter 5, the procedure of creating a FE model is presented. This chapter briefly explains the geometric model, assumptions, boundary conditions and the loading conditions that are used in this thesis.

In chapter 6, the results of the FE modeling in ANSYS are presented. These results include the deformation behavior and the stress distribution plots. The results of the FE modeling in ABAQUS and the formulation of modified FE models based on the ANSYS simulation results are also presented. This chapter also briefly describes the modifications in the FE model and the corresponding results. The modifications include formulating FE model in cylindrical coordinate system and model simplification due to symmetry conditions.

In chapter 7, the FE model formulation and the results for the crack propagation and the fatigue strength analysis are presented. The FE model formulation includes the details of creating a geometric outline of the model, loading conditions, meshing and material properties. The influence of loading and notch radius on the crack propagation and fatigue life is also described in this chapter.

In chapter 8, a summary of the main conclusions drawn from this research is discussed. Some recommendations for the possibility of further research in this field are also given in this chapter.

2. Literature review

In recent years, considerable efforts have been made for the development of analytical as well as numerical models for the better estimation of crack propagation and fatigue life. The ultimate goal for the researchers who are working in the mechanical design field is to develop structures with high reliability and crack growth resistant. In most of the design cases, the knowledge of FCG behaviour helps the designer to predict the number of load cycles before the structure fails [2].

Although, in most of the practical cases the service loading can not be characterized as a constant amplitude loading (CAL). However, it is believed that assuming CAL can reveal valuable characteristic information about the behavior of the structure which is under investigation. Local strain and fracture mechanics approaches have been involved extensively in fatigue life analysis.

In general, the crack propagation behavior is used particularly to prove the damage tolerance of the structure. In many cases with the help of this information researchers are able to develop procedures for damage control and to increase the reliability of the structure which increases the lifetime of structures. The literature survey, carried out for this study, is being presented under different categories and the details are given below.

2.1 Fatigue

In most of engineering failures are caused by fatigue. Fatigue failure is defined as the tendency of a material to fracture by mean of progressive cracking under repeated alternating or cyclic stresses of intensity considerably below the strength [4]. Although, the fracture is of a brittle type, it may take some time to propagate, depending on both the intensity and frequency of the stress cycles. Nevertheless, there is very little, if any, warning before failure if the crack is not noticed. ASTM E-206 definition of the fatigue [5] is as follows;

"The process of progressive, localized, permanent structural change occurring in a material, subjected to conditions which produce flucturing stresses and strains at some point(s) and which may culminate in cracks of complete fracture after a certain number of flucturings"

Fatigue is a damage process and mostly failure occurs due to its cumulative nature [6]. It keeps on increasing till the material can not withstand load (stress, strains) anymore and,

hence, as a result the structure fails. The maximum stress values are less than the ultimate tensile stress limit and may be below the yield stress limit of the material. Thus, the fatigue damage of a structure that is subjected to normally elastic stress fluctuations occurs at regions of stress raisers where the localized stress exceeds the yield strength of the material. Macroscopically, the surface is usually perpendicular to the direction of principal tensile stress. These stress raisers are usually unavoidable as they exist in the surroundings of voids, sharp edges or notches and material discontinuities like inclusions etc.

2.1.1 Demonstration of crack propagation

In many engineering structures and components cracks are initiated by different ways. It is important to understand the basic phenomenon associated with the crack initiation process, since these cracks will ultimately lead to failure of the material if they are not detected and recognized. There are various ways of crack initiation but three of them are most important and usually in most engineering applications cracks are initiated due to these three processes as illustrated in figure 2.1.

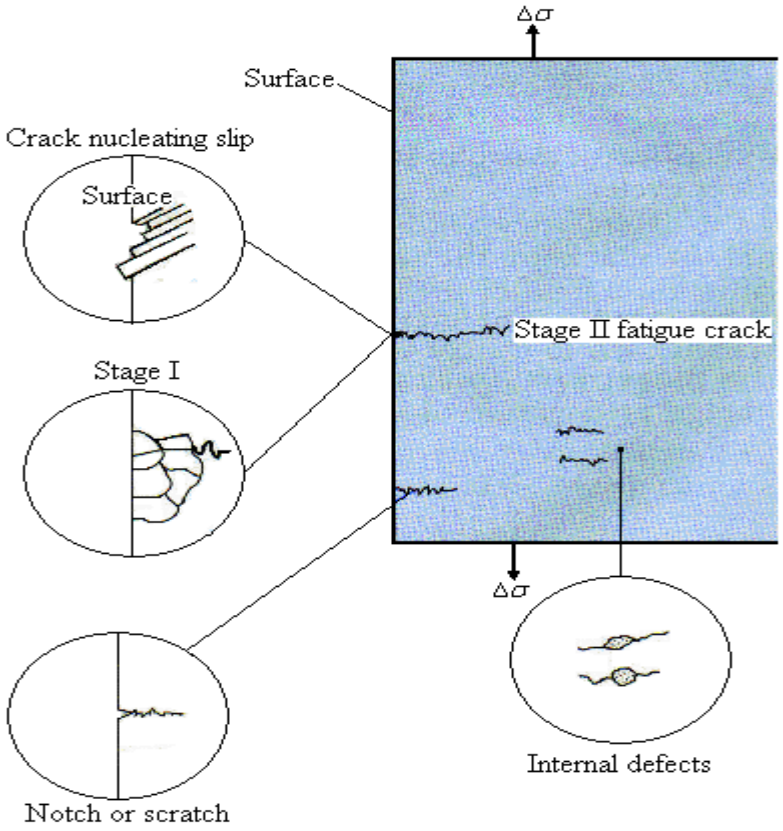

Figure 2.1: Various ways of crack initiation.

The details of most common causes of crack initiation are as follow:

1. Nucleating slip planes: Slip occurs when a material is stressed to the point of plastic deformation. When this happens the planes of crystals actually slip from their original positions leaving slip bands which resemble steps. When the material slips it forms a crack at the point of the intersection of the deformed material and the non-deformed material. If the stress is still applied after the crack is formed it continues to propagate and at some point the material fails.

2. Notches: There seems to be confusion among many engineers between notches and cracks. This is not surprising as the boundary between notch and crack is sometimes blurred, especially under fatigue conditions. However, a notch can be defined as geometric discontinuity which has a definite depth and root radius as demonstrated in figure 2.1. Notches always results in areas of stress concentration in a structure. Since the surface area of the notch is smaller than the surface area of the rest of the solid, hence, in most cases it is observed that notches are the first part to fail in any structure because of stress concentration effects.

3. Internal defects: Internal defects are a lot like notches in the respect that they cause a stress concentration in the material in which they are inhabited. There are several reasons for internal defects like grain boundaries, concentrations of point defects in the area and defects that occurred during processing. The internal defects are illustrated in figure 2.1. In most cases it has been seen that a material usually fails from a crack generated externally long before it fails from a crack generated internally.

2.1.2 Fatigue life

It is well established that fatigue is essentially a two stage process; crack initiation and crack propagation. In the same way fatigue life can be defined as the sum of crack initiation life [7] and crack propagation life. ASTM defines fatigue life as [8];

"The number of stress cycles of a specified character that a specimen sustains before failure of a specified nature occurs."

The crack initiation stage is governed by number of load cycles required for a fatigue crack to initiate and to become a potential stress raiser. However, crack propagation stage comprise of

the loading cycles required to grow the initiated crack until the final failure of the structure is reached.

2.1.3 Factors that affect fatigue

There are many factors that affect fatigue life of engineering structures and components. The details of most important factors which affect the fatigue life of structure are as follows:

1. Stress state: Depending on the complexity of the geometry and the loading, one or more properties of the stress state need to be considered, such as stress amplitude, mean stress, biaxiality, in-phase or out-of-phase shear stress and load sequence.

2. Geometry: Any discontinuity in the geometry of the structure has a great influence on the fatigue strength. Generally, the geometric discontinuities in the form of notches and variation in cross section throughout a part lead to stress concentrations. In most of the crack models the stress concentration is considered to be a major factor which makes a crack to appear and it is the stress concentration location where fatigue cracks initiate.

3. Surface quality: Surface roughness cause microscopic stress concentrations that lower the fatigue strength. The compressive residual stresses can be introduced in the surface by e.g. shot peening to increase fatigue life. Laser peening and ultrasonic impact treatment also give rise to surface compressive stresses and it increase the fatigue life of the component. This improvement is normally observed only for high cycle fatigue.

4. Material Type: Fatigue life, as well as the behavior during CL, varies widely for different materials. Different analytical approaches are available in order to deal with different material models. Thus, the changes in the materials used in parts can also improve fatigue life [9].

5. Residual stresses: In many engineering components residual stresses are produced as a result of metal forming processes. Welding, cutting, casting, and other manufacturing processes involving heat or deformation can produce high levels of residual stresses. As a result of high level tensile residual stresses the fatigue life of the component decrease.

6. Size and distribution of internal defects: It is commonly observed that the cracks appear due to the discontinuities in the structures at the micro level. In general, casting defects such as gas porosity, non-metallic inclusions and shrinkage voids can significantly reduce the fatigue strength.

7. Direction of loading: Although in the case of isotropic materials the direction of loading has no significant effect on the fatigue strength but for non-isotropic materials, fatigue strength depends on the direction of the principal stresses.

8. Grain size: In most of engineering components grain size has a direct impact on the fatigue life of the component. For most metals, smaller grains yield longer fatigue lives, however, the presence of surface defects or scratches will have a greater influence than in a coarse grained alloy.

9. Environmental conditions: Environmental conditions have a strong impact on many physical phenomenon which are mostly related to the surface of the structures. Environmental conditions can cause erosion, corrosion, or gas-phase embrittlement, which all affect fatigue life. Temperature also has some influence on the fatigue strength of a component and in general higher temperatures decrease fatigue strength.

2.1.4 Design against fatigue

A designer can minimize the possibility of fatigue failure by a proper design of engineering structures. Many fatigue failures may be attributed to lack of sufficient consideration of design details or a lack of appreciation of engineering principles [10]. There are three principal approaches to life assurance for engineering structures that display increasing degrees of sophistication:

2.1.4.1 Infinite lifetime approach

In this approach structures are designed in order to keep stress level below the threshold of fatigue limit. In reality this approach is not applicable on most of engineering designs because in most of the cases failure occurs because of fatigue.

2.1.4.2. Safe-life design approach

This approach is based on a fixed life criterion and the user is instructed to replace the part with a new one when the life time is expired. This approach is generally used for small mechanical components however, for large mechanical structure certain maintenance procedures are available that can be used in order to avoid failure.

2.1.4.3. Damage tolerance design

This is a famous design criterion which is usually used in most of the industries. In this approach the component is inspected periodically for cracks and the part is replaced once a crack exceeds a critical length. This approach usually uses the technologies of nondestructive testing and requires an accurate prediction of the rate of crack-growth between inspections.

2.2 Fracture mechanics

The establishment of fracture mechanics [11] is closely related to some well known disasters in recent history. Several hundred liberty ships fractures extensively during the World War II. The failure occurred primarily because of the change from a riveted to a welded construction. Of the roughly 2700 liberty ships, approximately 400 sustained serious fracture. The comet accidents in 1954 sparked an extensive investigation of the cause, leading to significant progress in the understanding of fracture and fatigue.

The term “fracture mechanics” refers to a vital specialization within solid mechanics in which the presence of a crack is assumed, and quantitative relations between the crack length, the material’s inherent resistance to crack growth, and the stress at which the crack propagates are defined [12]. It deals with the behavior of cracked bodies subjected to stresses and strains. These can arise from primary applied loads or secondary self-equilibrating stress fields (e.g. residual stresses). The power of fracture mechanics really lies in the fact that local crack tip phenomena can, to a first order, be characterized by relatively easily measured global parameters, e.g. crack length and nominal global stresses (calculated in the absence of the crack), together with geometry correction factors.

The crack propagation behavior is an important parameter which plays a vital role in the fatigue strength analysis of the structures [13]. As long as the load is small enough, the structure will only deform elastically. A crack starts to propagate when the crack driving force is larger than the material resistance. If however, the structure is sensitive to cracking due to e.g. inadequate design, defects from manufacturing, handling or bad quality, materials fracture will occur. There are a number of parameters that affect the crack propagation mechanism i.e. material properties, fatigue, loading rate, environment etc. Figure 2.2 illustrates the important factors that influence the crack propagation process.

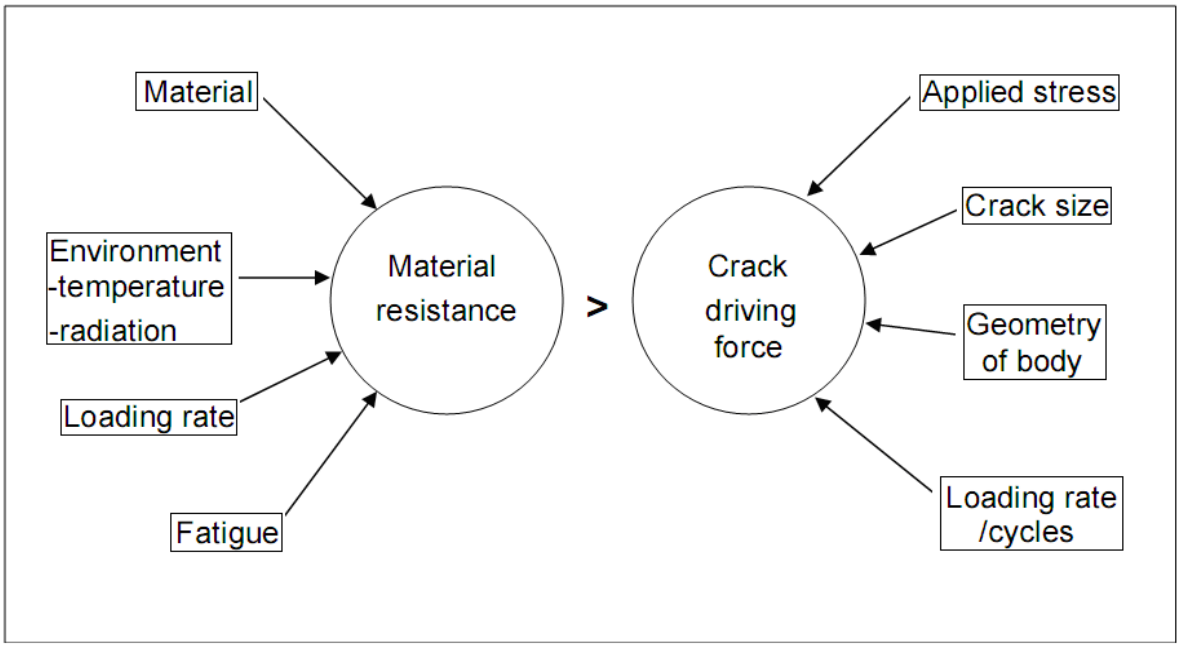

Figure 2.2: Factors influencing the crack propagation.

In general, fracture mechanics is a set of theories describing the behavior of solids or structures with geometrical discontinuity at the scale of the structure [14]. The discontinuity features may be in the form of line discontinuities in two dimensional (2D) media (such as plates, and shells) and surface discontinuities in three dimensional (3D) media. Fracture mechanics has now evolved into a mature discipline of science and engineering. One of the important impacts of fracture mechanics is the establishment of a new design philosophy: damage tolerance design methodology, which has now become a commonly used design criteria in the engineering industries [15].

In short, fracture mechanics is used to answer some main questions such as: will the crack grow, will it grow fast and unstable or slow and stable, if it grows stable at what rate does it grow, to what size can the crack grow and how many cycles or how long time does it take to become an unstable crack. When fracture takes place in any structure it may lose the function it was initially designed for. Thus, the knowledge about what happens with a loaded structure with crack initiations is important in order to avoid failure.

2.3 Linear elastic fracture mechanics (LEFM)

LEFM principles are used to relate the stress magnitude and distribution near the crack tip to the remote stresses applied to the cracked component, crack size, crack shape and the material

properties of the cracked component [16]. The general form of the LEFM equation is given as:

$$\sigma_{ij} = \frac{K_I}{\sqrt{2\pi r}} f_{ij}(\theta) + \ldots \quad (2.1)$$

where:

r = distance from the crack tip

K_I = Mode I SIF

$f_{ij}(\theta)$ = function that represents the stress dependence on θ

2.3.1 LEFM assumptions

LEFM is based on the application of the theory of elasticity to bodies containing cracks or defects. The assumptions used in elasticity are also inherent in the theory of LEFM: small displacements and general linearity between stresses and strains.

The general form of the LEFM equations is given in equation 2.1. As seen, a singularity exists such that as r, the distance from the crack tip, tends toward zero, the stresses go to infinity. As the yield stress is exceeded, material deforms plastically and a plastic zone is formed near the crack tip. The basis of LEFM remains valid if this region of plasticity remains small in relation to the overall dimensions of the crack and cracked body.

2.3.2 Crack propagation modes

There are generally three modes of loading, which involve different crack surface displacements as shown in figure 2.3. The three modes are:

Mode I: Opening or tensile mode (the crack faces are pulled apart)

Mode II: Sliding or in-plane shear (the crack surfaces slide over each other)

Mode III: Tearing or anti-plane shear (the crack surfaces move parallel to the leading edge of the crack and relative to each other)

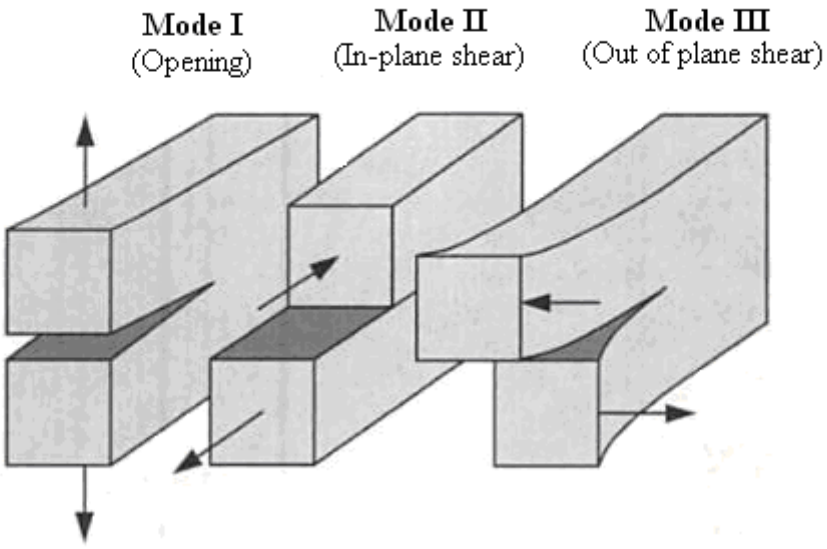

Figure 2.3: The three crack propagation modes.

The following discussion deals with Mode I since this is the predominant loading mode in most engineering applications. Similar treatments can readily be extended to Modes II and III.

2.3.3 Stress intensity factor

The SIF (K) introduced in equation 2.1, defines the magnitude of the local stresses around the crack tip. This factor depends on loading, crack size and geometry. It can be expressed in a general form given by

$$K = \sigma\sqrt{\pi a}\, f\left(\frac{a}{w}\right) \tag{2.2}$$

where:

σ = remote stress applied to the component

a = crack length

$f\left(\frac{a}{w}\right)$ = correction factor that depends on specimen and crack geometry

2.3.4 Energy release rate

Griffith was the first to propose the energy criterion for fracture, but Irwin is primarily responsible for developing the present version of this approach [17]. First, the potential energy Π of an elastic body [18] is defined as :

$$\Pi = U - W \tag{2.3}$$

where U is the elastic strain energy stored in the body and W is the potential energy or the work done by external forces. The energy release rate G is defined as the rate of change in potential energy with respect to the crack area [18].

$$G = \frac{d\Pi}{da} \tag{2.4}$$

The energy release rate G is a measure of the energy available for an increment of a crack extension. To define the fracture criteria in an energy consideration the same discussion used for the stress intensity can be employed. An unstable crack growth occurs when the energy release rate reaches a critical value $G = G_C$, where G_C is a measure of fracture toughness and can be considered as a material property.

2.3.5 Fracture toughness

In materials science, the fracture toughness K_{Ic} is a property which describes the ability of a material containing a crack to resist fracture. The subscript I denotes mode I crack opening under a normal tensile stress perpendicular to the crack.

Fracture toughness is a quantitative way of expressing the resistance of a material to brittle fracture when a crack is present. It is independent of the size and geometry of the cracked body under certain conditions [17]. The materials with higher values of fracture toughness are more likely to undergo a ductile fracture; however, the materials with low value fracture toughness usually undergo a brittle fracture [19]. The largest crack a structure can sustain under specific residual strength requirements can be predicted through this critical value of the SIF where the crack propagation becomes unstable. The fracture criteria can be expressed as:

$$K = K_{Ic} \tag{2.5}$$

2.3.6 Thermodynamics of crack growth

If we consider a crack in a deformable continuum subjected to arbitrary loading, then the first law of thermodynamics gives: the change in energy is proportional to the amount of work performed.

The first law of thermodynamics states that the time-rate of change of the total energy (i.e. sum of the kinetic energy and the internal energy) is equal to the sum of the rate of work done by length $2a$ located in an infinite plate subjected to load P. Griffith assumed that it is possible to produce a macroscopic load displacement $(P-u)$ curve for two different crack lengths a and $a+da$.

Two different boundary conditions will be considered, and in each one the change in potential energy as the crack extends from a to $a+da$ will be determined:

Fixed grip: $(u_1 = u_2)$ loading, an increase in crack length from a to $a+da$ results in a decrease in stored elastic strain energy ΔU,

$$\Delta U = \frac{1}{2}P_2 u_1 - \frac{1}{2}P_1 u_1 \tag{2.6}$$

$$= \frac{1}{2}(P_2 - P_1)u_1 \tag{2.7}$$

$$< 0$$

Furthermore, under fixed grip there is no external work $(u_1 = u_2)$, so the decrease in potential energy is the same as the decrease in stored internal strain energy, hence

$$\Pi_2 - \Pi_1 = \Delta W - \Delta U \tag{2.8}$$

$$= -\frac{1}{2}(P_2 - P_1)u_1 = \frac{1}{2}(P_1 - P_2)u_1 \tag{2.9}$$

Figure 2.4 demonstrates the energy transfer in a cracked plate by using fixed grip technique.

Fixed load: $(P_2 = P_1)$ the situation is slightly more complicated since in this case the external work not zero and the loads acting in this case are fixed. The external work can be expressed as follows:

$$\Delta W = \frac{1}{2} P_1 (u_2 - u_1) \tag{2.10}$$

Furthermore, due to the non-zero external work the change in potential energy is no more equal to the change in internal energy. Thus, the net effect is a change in potential energy and it can be determined by using equation 2.8.

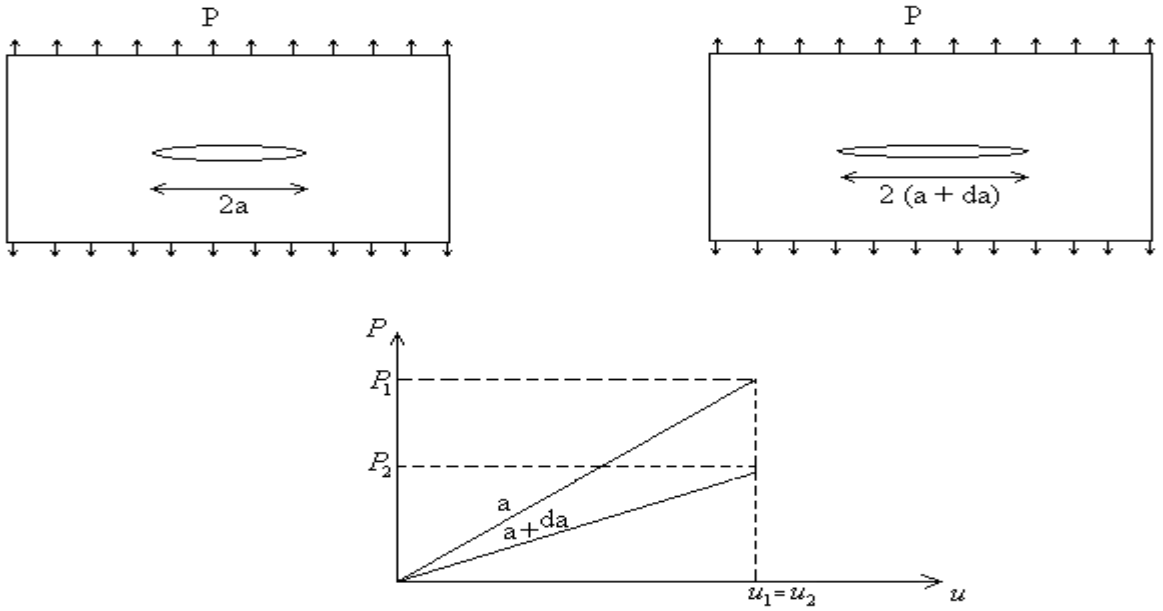

Figure 2.5: Energy transfer in a cracked plate (Fixed grip).

2.4 Plane stress condition

A state of plane stress exists when one of the three principal $(\sigma_1, \sigma_2, \sigma_3)$ stresses is zero. This usually occurs in structures where one dimension is very small compared to the other two, i.e. the structure is flat or thin. In this case, the stresses are negligible with respect to the smaller dimension as they are not able to develop within the material and are small compared to the in-plane stresses. Figure 2.5 demonstrates the plane stress state in a continuum. Therefore, the face of the element is not acted by loads and the structural element can be analyzed as two-dimensional, e.g. thin-walled structures such as plates subject to in-plane loading. The stress tensor can then be approximated by:

$$\sigma_{ij} = \begin{bmatrix} \sigma_x & \tau_{xy} & 0 \\ \tau_{yx} & \sigma_y & 0 \\ 0 & 0 & 0 \end{bmatrix} \tag{2.12}$$

The corresponding strain tensor is:

$$\varepsilon_{ij} = \begin{bmatrix} \varepsilon_{11} & \gamma_{12} & 0 \\ \gamma_{21} & \varepsilon_{22} & 0 \\ 0 & 0 & \varepsilon_{33} \end{bmatrix} \tag{2.13}$$

In above expression the non-zero ε_{33} term arises from the Poisson's effect.

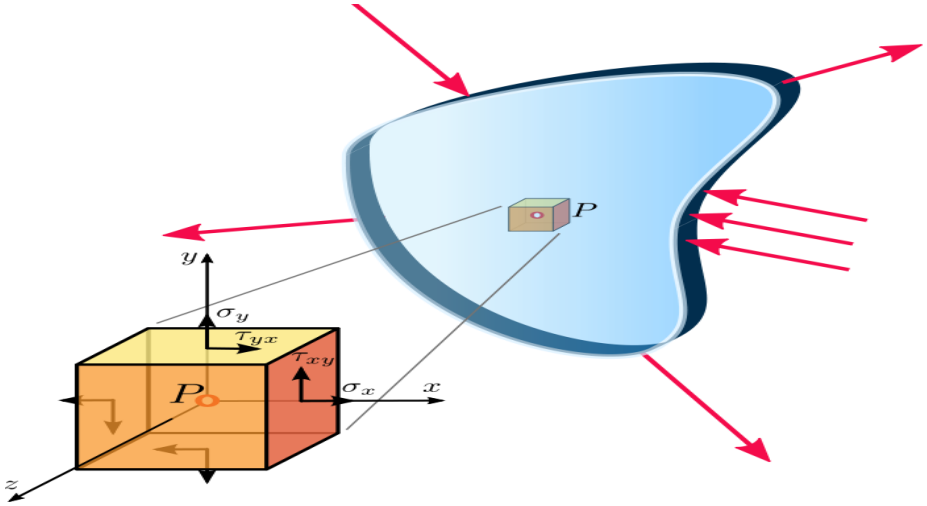

Figure 2.5: Plane stress state in a continuum.

Consider a point P in a continuum under a state of plane stress, or plane strain, with stress components $(\sigma_x, \sigma_y, \tau_{xy})$ and all other stress components equal to zero as shown in figure 2.6. From static equilibrium of an infinitesimal material element at P, the normal stress σ_n and the shear stress τ_n on any plane perpendicular to the $x-y$ plane passing through P with a unit vector n making an angle of θ with the horizontal, i.e. $\cos\theta$ is the direction cosine in the x direction, is given by:

$$\sigma_n = \frac{1}{2}(\sigma_x + \sigma_y) + \frac{1}{2}(\sigma_x - \sigma_y)\cos 2\theta + \tau_{xy}\sin 2\theta$$

$$\tau_n = -\frac{1}{2}(\sigma_x - \sigma_y)\sin 2\theta + \tau_{xy}\cos 2\theta \tag{2.14}$$

Mohr's circle provides a graphical representation of equation 2.14. These equations indicate that in a plane stress or plane strain condition, one can determine the stress components at a point on all directions, i.e. as a function of θ, if one knows the stress components

$(\sigma_x, \sigma_y, \tau_{xy})$on any two perpendicular directions at that point. It is important to remember that we are considering a unit area of the infinitesimal element in the direction parallel to the $y - z$ plane.

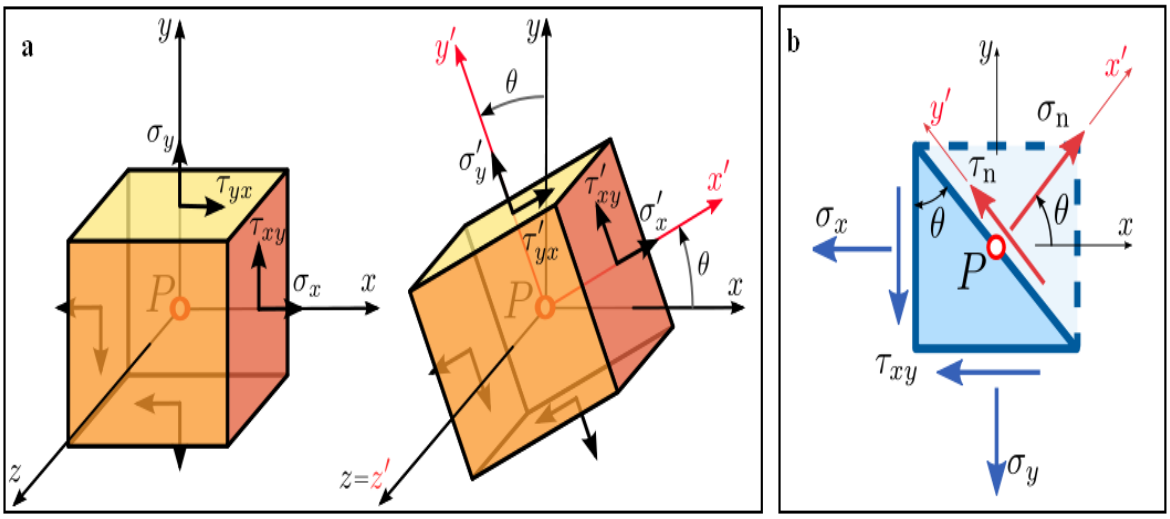

Figure 2.6: (a) Stress transformation at a point in a continuum under plane stress condition. (b) Stress components at a plane passing through a point in a continuum under plane stress condition.

3. Analytical evaluation methods

As discussed earlier, the fatigue life prediction of a component consists of two parts: crack initiation and crack propagation until final failure. Crack initiation life represents the number of cycles spent in forming and growing short cracks at a highly strained region. Whereas the crack propagation life represents the portion of life spent in growing the cracks size to an unstable length. In most cases it is very difficult to determine when this transition occurs.

In general, results from numerical simulations show that fatigue life propagation can constitute over 90 percent of the total fatigue life, and thus the main focus of the present investigation will be placed on the FCP studies. In this chapter different analytical models and techniques are presented which are generally used to determine different parameters related to crack propagation and the fatigue strength of the components.

3.1 Model for stress intensity factor (SIF)

The SIF is extracted from either the stress or displacement field or by any energy based method. There are three basic ways to calculate the SIF, namely the crack opening displacement method, the stiffness derivative technique and the J-integral method, where the latter two are energy based methods. The crack opening displacement method is the simplest but least accurate one and the other two methods have approximately equal accuracy [20]. The stiffness derivative method can be applied to both 2D and 3D bodies. The stiffness derivative technique proceeds as follows for a cracked body subjected to mode I loading. The potential energy in terms of the FEM is given by [20]

$$\Pi = \frac{1}{2}\{d\}^T[K]\{d\} - \{d\}^T\{F\} \tag{3.1}$$

Where $\{d\}$ is the global nodal point displacement vector, $\{K\}$ is the global stiffness matrix and $\{F\}$ is the global load vector. The energy release rate G, defined in equation 2.4 as the rate of change in potential energy with respect to the crack area may now be applied to equation 3.1. The determination of G is evaluated for a 2D body under fixed load conditions and the crack area is therefore replaced with the thickness times the crack length, $A = ta$.

$$G = -\frac{\partial \Pi}{\partial A} = -\frac{\partial\{d\}^T}{t\partial a}\{[K]\{d\} - \{F\}\} - \frac{1}{2}\{d\}^T\frac{\partial[K]}{t\partial a}\{d\} + \{d\}^T\frac{\partial\{F\}}{t\partial a} \tag{3.2}$$

The first term must be zero since the stiffness equation is $[K]\{d\}=\{F\}$, and the third term must also be zero because of a constant load. Finally, the energy release rate can be calculated by the following equation [20];

$$G=\frac{K_I^2}{E}=-\frac{1}{2}\{d\}^T\frac{\partial[K]}{t\partial a}\{d\} \tag{3.3}$$

Where,

$$E'=E \text{ for plane stress}$$

$$E'=\frac{E}{1-\nu^2} \text{ for plane strain}$$

The SIF can now be computed numerically by first solve the stiffness equation $[K]\{d\}=\{F\}$ for $\{d\}$, then increase the crack a small amount, determine a new stiffness matrix and finally approximate the stiffness derivative as $\frac{\partial[K]}{\partial a}=\frac{\Delta K}{\Delta a}$.

3.2 Fatigue crack initiation life

Various models have been suggested to estimate the number of cycles to initiate a detectable crack. In literature there is no standard definition of initial crack and it depends upon the technique used to measure the fatigue parameters. Because the maximum local strain at the notch root is thought to be the controlling parameter during initiation process, consideration of local strains at the highly strained regions are essential for fatigue initiation life assessment.

Sato and Shimada proposed a new procedure to estimate fatigue crack initiation life for notched members of different materials using low-cycle fatigue tests [21]. Under constant amplitude fatigue testing, they observed that the maximum strain value at the notch decreases rapidly reaching a minimum value and then increase gradually as the number of elapsed cycles increase. One of the main results of their experiments was that the maximum local strain value at the first cycle coincided with the local maximum strain value at crack initiation. Crack initiation life was determined experimentally by microscopic observation of small crack propagation having a length of 10-15 μm.

3.3 Fatigue crack propagation

Significant portion of fatigue life may be spent in the propagation of cracks inherently present in the components. These cracks can be the result of manufacturing defects, welds, surface flaws or excessive plastic deformation at notched regions. LEFM presently offers the most powerful applicable analytical technique in predicting the remaining life of such members. In this approach, pre-cracked panels are subjected to constant-amplitude CL. There are many crack propagation models but the most commonly used law which relates the SIF to sub-critical crack growth under a fatigue stress regime is the Paris law [22].

Life prediction for fatigue cracks was made very much easier and far more quantitative, in the 1960's when Paris [23] postulated that the range of SIF might characterise sub-critical crack growth under fatigue loading in the same way that K characterised critical, or fast fracture. He examined a number of alloys and realised that plots of crack growth rate against range of SIF gave straight lines on log-log scales. This implies that:

$$\log\left(\frac{da}{dN}\right) = m\log(\Delta K) + \log C \tag{3.4}$$

$$\frac{da}{dN} = C(\Delta K)^m \tag{3.5}$$

Where a is the crack length, N is the number of load cycles, C and m are material constants, and ΔK is the range of the SIF. This law quantifies the residual life of a specimen given a particular crack size. Finding the beginning of the initiation of fast crack initiation:

$$K = \sigma Y\sqrt{\pi a} \tag{3.6}$$

Where σ is a uniform tensile stress perpendicular to the plane of the crack, and Y is dimensionless geometric parameter. One can then find the remaining lifetime using the following simple mathematical manipulations given as follows;

$$\frac{da}{dN} = C(\Delta K)^m = C\left(\Delta\sigma Y\sqrt{\pi a}\right)^m \tag{3.7}$$

$$\int_0^{N_f} dN = \int_{a_1}^{a_2} \frac{da}{C\left(\Delta\sigma Y\sqrt{\pi a}\right)^m} \tag{3.8}$$

4. Experimental investigations

In general, a series of experiments are performed in order to determine the strength, reliability, deflection behavior, and fatigue strength of the stainless steel structures for washing machine drums. The component is considered to be reliable if it passed through all the experimental tests and satisfies the required output objectives in terms of fatigue strength and reliability. However, the experimental program conducted for the investigation of fatigue strength and failure analysis can be divided into two categories. First part consists of the experiments performed at the development stage, to evaluate the performance of the drum under the fatigue conditions. The second part consists of the experiments performed at the production stage in order to determine the structural static limit of the drum. In this chapter the procedures used to perform these experiments and the results from the experimental investigations are presented.

4.1 Procedures used in experimental investigations

A detail description of the procedures used to perform the experimental investigations and the methods to measure the output is presented in the following section.

4.1.1 Drum lifetime test

This experiment is performed at the product development stage and the main purpose of this test is to evaluate the performance of the drum under the fatigue conditions. This is an accelerated life test and gives an indication of the drum behavior under fatigue conditions. Generally, this test follows a complete appliance life test to guarantee drum lifetime performances.

4.1.1.1 Experimental setup

In this test rubber plates are used to incorporate the loads which act on the drum during operating conditions. The distributed load rubber plates are placed between the lifters, starting from the drum middle till a position, where the distance between the rubber plates and the drum front/rear is between 10 and 20 mm. Figure 4.1 demonstrates the position of the distributed load rubber plates.

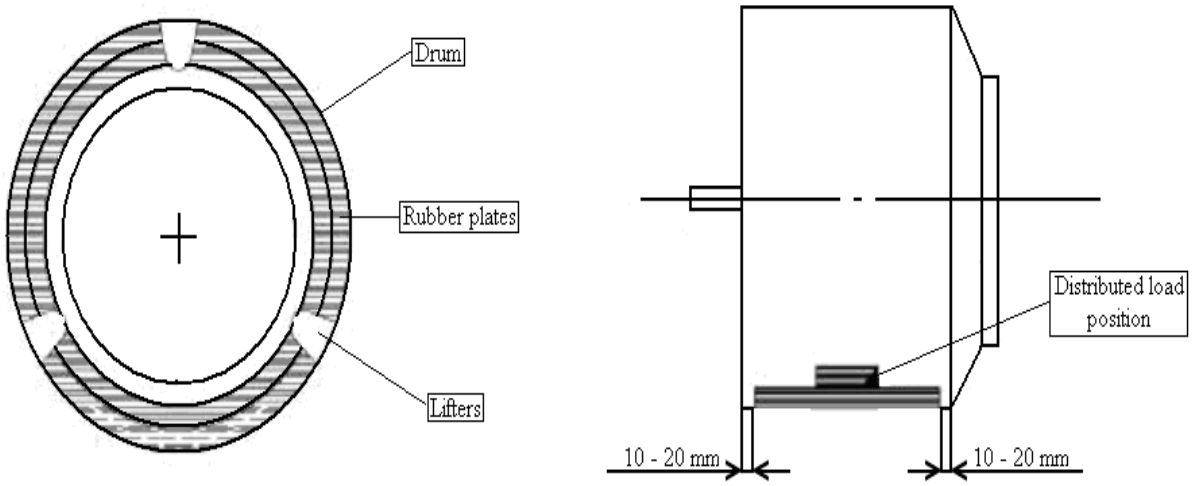

Figure 4.1: Position of the distributed load rubber plates.

In addition to the distributed load rubber plates, unbalanced rubber plates are also placed between the two lifters, beside the longitudinal seam, in direct contact with the drum front as shown in figure 4.2.

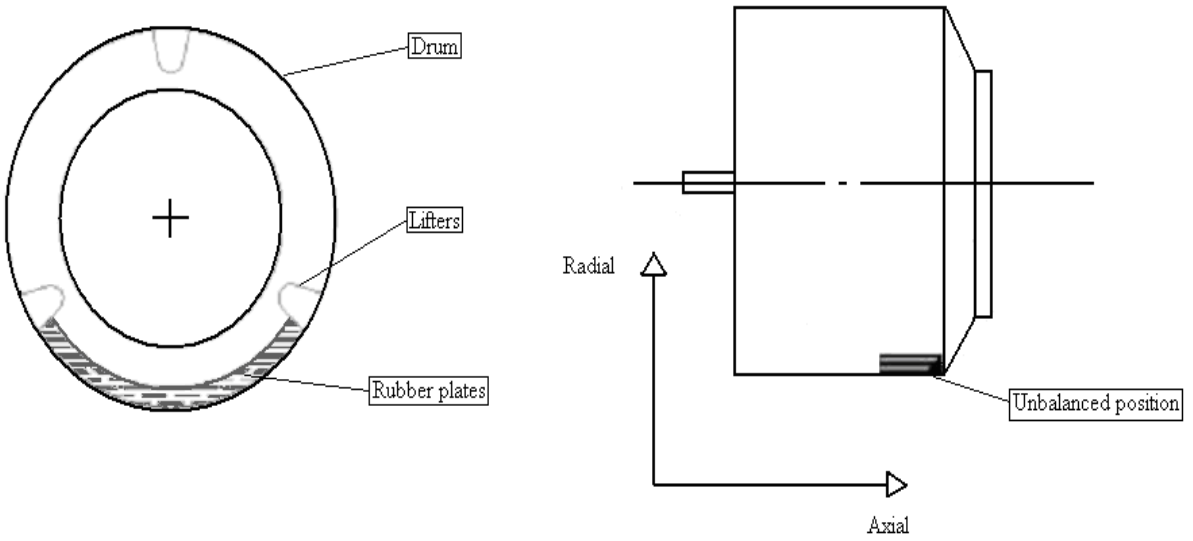

Figure 4.2: Position of unbalanced rubber plates.

4.1.1.2 Testing conditions

The conditions considered in order to perform the drum lifetime test are given as follow;

- The distributed load applied in this test consists of declared load and the rest moisture content (RMC). Usual values for RMC are between 50-80 percent of the dry load weight depending on the spinning speed of the appliance.

- The unbalanced load is taken as 10% of the declared load for appliances without inertia detection or 0,5 kg for appliances with inertia detection.
- A load cycle consists of three parts including ramp up till the maximum spinning speed, maintaining the speed, ramp down and rest as shown in the figure 4.3

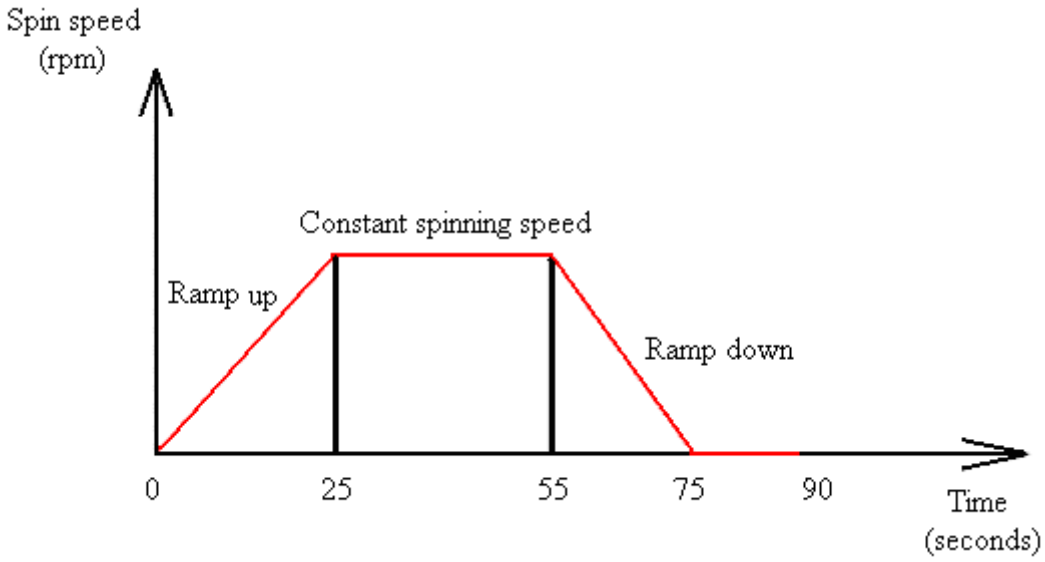

Figure 4.3: Three parts of a load cycle.

4.1.1.3 Inspection criteria

While performing this experiment, certain inspection criteria are used in order to collect the data from the experiment and later, this data is used to analyze the final results in terms of structural deformations and the overall structural damage. The inspection criteria used in this experiment are given as follows;

- Drum dimensions are continuously measured in order to make sure that the dimensions are inside the tolerance limits.
- After every 1000 cycles, a visual check is made to avoid cracks, in general and especially in the outer drum surface area and in the lifter area since failure mode is expected at these locations.

4.1.2 Forced failure test

This experiment is performed at the production stage and the main purpose of this test is to determine the structural static limit of the drum. The details of experimental setup and the testing conditions used in this test are given as follows:

4.1.2.1 Experimental setup

Like the drum lifetime test, rubber plates are used in this test to incorporate the loads act on the drum during operating conditions and the distributed load rubber plates are placed between lifters as shown in figure 4.1; however, no unbalance is used in this test because of the reasons given as follows;

- The lifters are made up of plastic material and they are not considered as a strong contributor of load.
- The rubber plates are packed between the lifters which make it easy to carry out the tests.

4.1.2.2 Testing conditions

The conditions used to perform the forced failure test consist of two main stages;

- In the first stage the drum spinning is brought at maximum nominal spinning speed but the rate doesn't affect the test result because the forced failure test is used to determine the spinning speed at which damage occurred and this speed is usually 400 ~ 600 rpm higher than nominal speed.
- In this stage the spin speed is gradually increased at the maximum rate of 50 rpm/min until the drum fails at a specific spinning speed which is much higher than the ones used for appliance delivered to the customers.

4.1.2.3 Inspection criteria

While performing this experiment, certain inspection criteria are used in order to collect the data from the experiment. The inspection criteria used in this experiment are given as follows;

- Like the drum lifetime test, the drum dimensions are continuously measured in this test in order to make sure that the dimensions are inside the tolerance limits.
- Once the drum failed, a general visual inspection of the failure area is made in order to determine reasons of failure and to determine the failure mode.

4.2 Results and discussion

While performing these tests the drum dimensions are continuously measured after certain time periods in order to make sure that the dimensions are inside the tolerance limits. The data collected from these experiments is in the form of measurements of dimensions and number of cycles for final failure.

The results from drum lifetime test are depending on the visual check and measurements of different parts of the drum after each 1000 cycles. The results from this test have demonstrated the deformations in the drum structure under the applied loading conditions. It has been observed that damage and most of the deformations are in the area which is near the lifter holes as shown in figure 4.4.

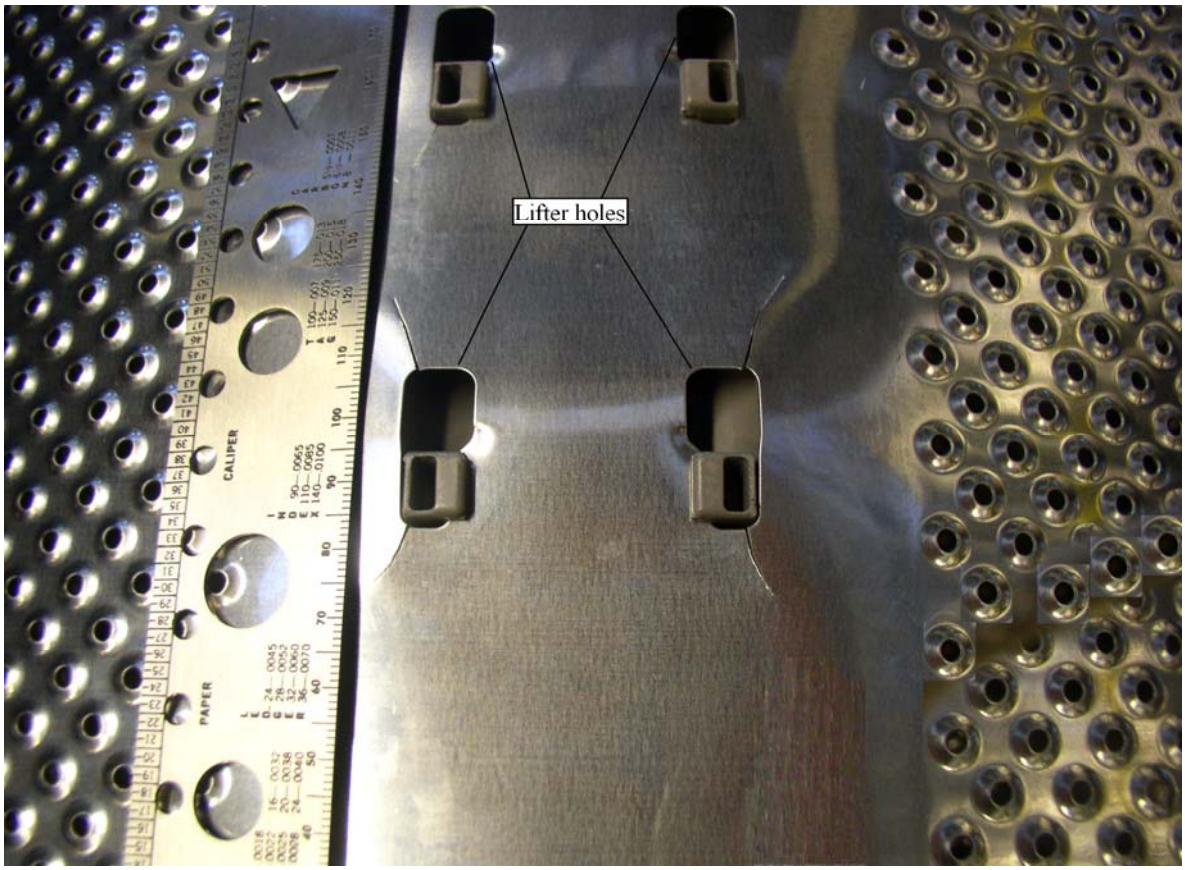

Figure 4.4: Structural deformations and cracks near the lifter holes.

The results from forced failure tests are based on the visual check of different part in order to evaluate the failure behaviour in the form of the crack propagation. As discussed previously, in this test the spin speed is gradually increased at the maximum rate of 50 rpm/min until the drum fails. It has also been observed from the results of this test that the final failure occurred

after 3 times of the total life time of the drum. Figure 4.4 demonstrates the damage occurred in the drum structure. The cracks only appear around the lifter holes and the propagation of these cracks follows approximately the same pattern around each lifter hole. It has also been observed that the damage shown in figure 4.4 occurred after 15000 cycles.

Hence, on the basis of the results obtained from the experimental investigations it can be concluded that the lifter holes are the most critical part of the whole drum because all cracks are found around the lifter holes. In the next chapter, different computational techniques will be used in order to verify these experimental findings.

5. Finite element model

5.1 Introduction

Most of the engineering analysis can be performed by using mathematical models which lead to differential equations. These models basically represent certain engineering phenomenon. The main purpose of using numerical techniques is to solve complicated problems, which can not be solved by analytical methods.

There are many numerical techniques available such as FEM and finite difference technique, but the most widely used technique is the FEM. In this technique, general differential equations are solved to get an approximate solution. In contrast to analytical methods, where solutions are found that hold over the entire region, in FEM the whole region is divided into a finite number of parts, finite elements, and the approximation can be carried out over each element. The behavior for each element can then be determined because the approximation made over each element is fairly simple.

Today, most of the engineering analyses are performed with the help of very powerful computers. But still the knowledge about the basic concepts and theories used in the FEM programs is very important for the proper understanding of the problem. The main questions that have to be answered by the researcher are: how to model a problem, what are the assumptions and limitations of certain FEM code and finally how to judge the results if they are realistic or not.

5.2 Model formulation

5.2.1 Geometric model

First step in all numerical analysis methods is to develop a finite element (FE) model which includes geometry, set of assumptions and loading conditions used to define the real physical problem. Modeling is an unambiguous representation of the parts of an object which is suitable for computer processing. The model for the FEA is created with all the actual dimensions using Pro/ENGINEER [35]. Pro/ENGINEER is a parametric, feature-based solid modeling system. The main features of the geometric model of the drum are demonstrated in Figure 5.1 which includes crosspiece connection holes, lifter holes and the wrapper

connection. The detailed engineering drawing of the drum including the dimension of internal holes is provided in Appendix 1.

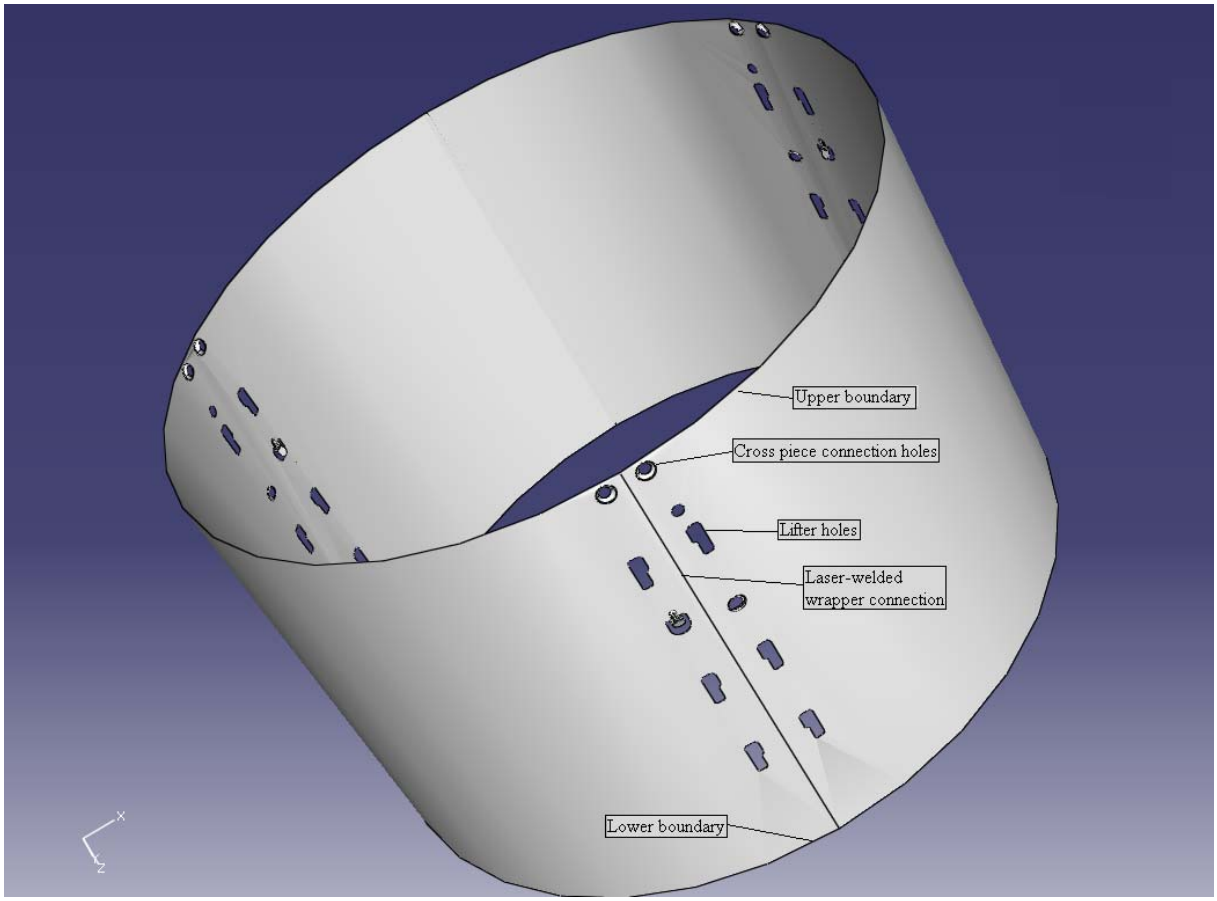

Figure 5.1: Geometric model of the drum created with Pro/ENGINEER.

5.2.2 Assumptions

In most of the cases it is not possible to develop a FE model that can exactly represent the real physical system particularly in the case of complex engineering systems. In order to develop a FE model which is close to the reality, the researchers have to consider all aspects of the problem which make the FE model complex and increase the computational time. In order to simplify the complex FE models the researcher relay on a certain set of assumptions. The assumptions used in this project are described as follows;

- Low cycle fatigue is expected for the rotating structure because of the loading conditions.
- One spinning cycle can basically be considered as one load cycle, however, with reduced forces over time, since water is getting extracted from the laundry during the cycle.

- Based on the past research conducted at the company it was concluded that all kind of loads acting on the structure during operating conditions can be modeled with an equivalent internal pressure $P_i = 0.145MPa$ on the whole drum (see section 5.2.5).
- Since spinning occurs under RT after rinsing with cold water, temperature effects can be neglected during the structural analysis.

5.2.3 Material Properties

The drum structure is modeled by a linear elastic isotropic stainless steel material with a young's modulus $E =$ 200 GPa, and a poisson's ratio $\nu =$ 0.3. Because of the thin wall thickness of 0.5mm, the model is idealized by shell elements [24].

5.2.4 Boundary conditions

During the operating conditions different types of loadings are acting on the drum boundary. Because of the vibrant nature of the drum it is very difficult to model such a drum with actual operating conditions. For the analysis purpose, certain set of boundary conditions are defined. The purpose of these conditions is to simplify the model without loosing a realistic approximation of the drum. The set of boundary conditions that are used in this project are demonstrated in Figure 5.2. The detail description of these boundary conditions is given as follows;

- It is considered that the upper and lower boundary of the drum is fixed so that displacements in all degrees of freedom (DOF) are fixed.
- The crosspiece connection holes are also considered to be fixed in all DOF because the drum is fixed with the external structure due to the screw connection at the crosspiece connection holes.

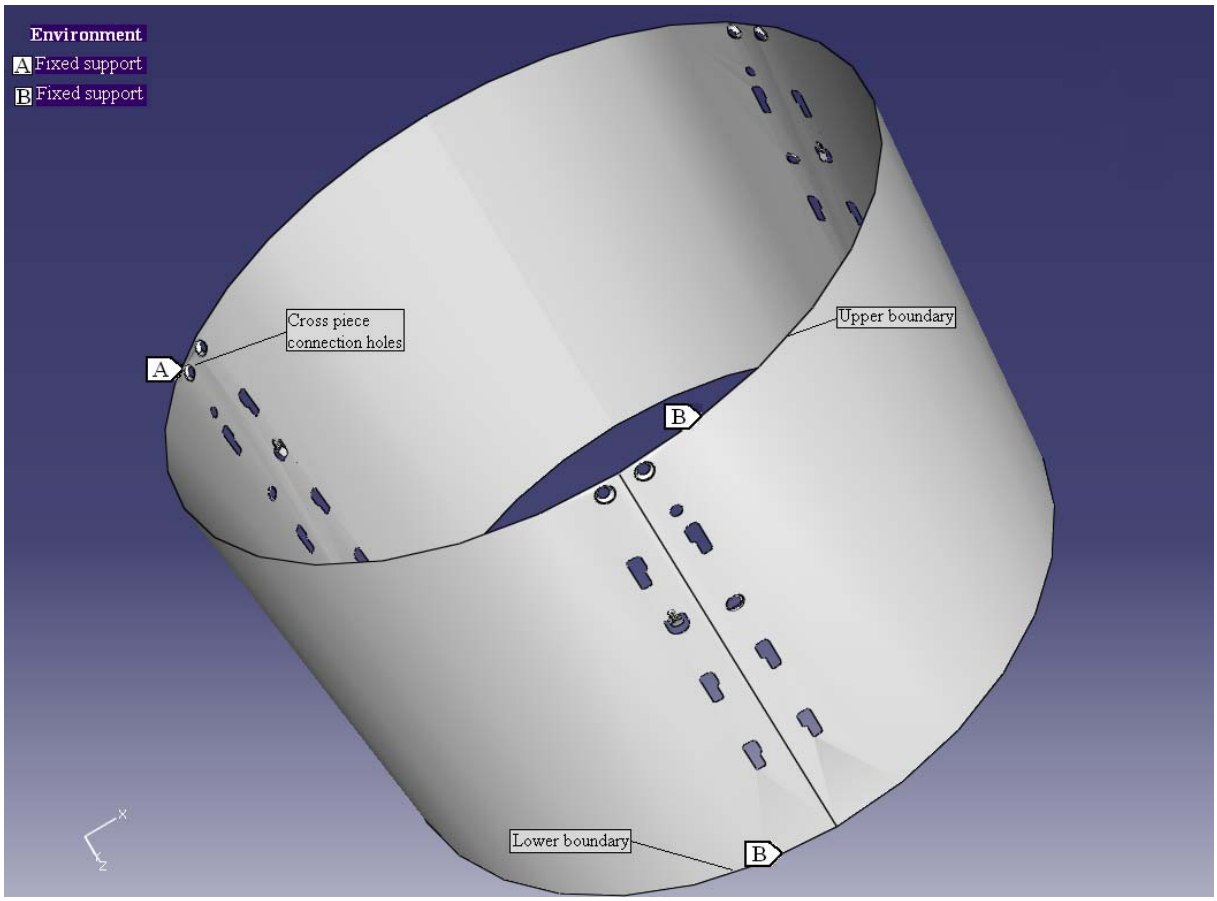

Figure 5.2: Boundary conditions used in the FE model.

5.2.5 Loading conditions

The overall loading conditions are very complex because of the above mentioned operating conditions such as spinning speed effects, centrifugal forces and forces due to the mass of laundry. In order to make a best approximation of the loading conditions, a complete research is conducted at the company to determine an equivalent load that can be used instead of the real complex loading conditions. After several investigations it is concluded that the overall loadings can be replaced with an equivalent internal pressure $P_i = 0.145MPa$ along with a set of boundary conditions explained in section 5.2.4. Figure 5.3 demonstrate the loading condition used in this FE model.

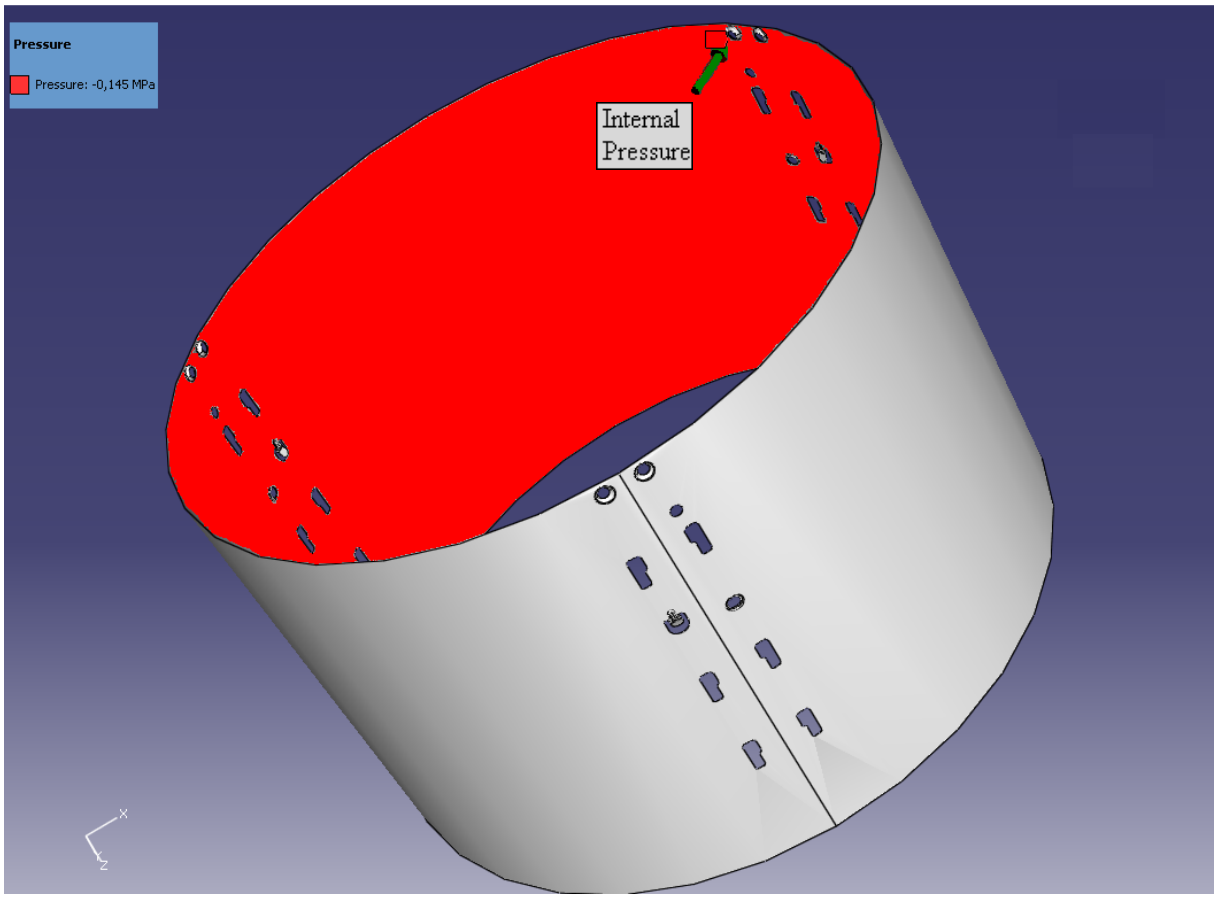

Figure 5.3: Loading conditions used in the FE model.

6. Finite element analysis

In this chapter a brief summary of the different analysis approaches that have been used and the corresponding simulation results are presented. The main purpose of numerical simulations is to understand the shape deformation and stress distribution behaviour of the drum, and to compare these results with the experimental findings. The FE model defined in chapter 5 is imported first into ANSYS [25] in order to perform the simulations and the results are obtained in the form of shape deformations and stress distribution.

Based on the results obtained from simulations performed in ANSYS certain modifications are made in the FE model in order to improve the results. The modified FE models are created in PATRAN and then the ABAQUS input file is generated with all information of the FE model, as an output from PATRAN. Later, the input files are submitted to the solver using ABAQUS. The solver performs the analysis and finally sends the information regarding final results back to ABAQUS/Viewer for the final evaluation of the results.

6.1 Initial FEA analysis

The main purpose of these simulations is to compare the results with experimental findings. ANSYS provides several different analysis types such as static analysis, transient dynamic analysis and buckling analysis but for this FE model static analysis procedure is used because of the applied loading conditions. Generally, in this analysis type a sequence of events are defined and the state of the FE model at the end of each step provides the initial state for the next step. A detailed description of the simulations performed with ANSYS is presented in the following section.

6.1.1 Finite element model

The FE model defined in chapter 5 is imported into ANSYS with the same boundary conditions, loading conditions and material properties. The FE model is meshed in ANSYS using SHELL93 elements [26]. The SHELL93 elements are particularly well suited to model curved shell structures. The element has six DOF at each node; three translations and three rotations DOF. The deformation shapes are quadratic in both in-plane directions. The demonstration of SHELL93 elements is shown in figure 6.1.

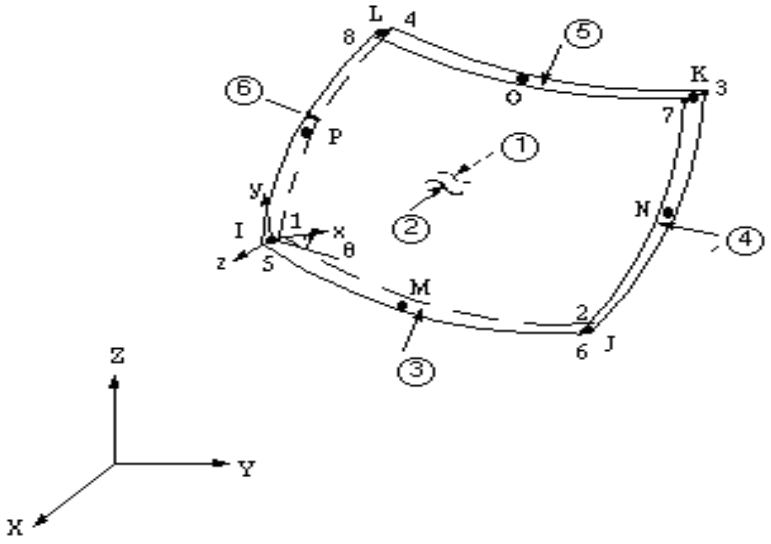

Figure 6.1: A SHELL93 element implemented in ANSYS.

The thickness of the shell elements is a defined parameter and therefore do not have any elements in that direction. The computational savings come about because the mid-surface of the structure is modeled; the thickness and other cross-sectional properties are incorporated into the element stiffness matrix and input as "real constants" in ANSYS. A fine mesh is used around the lifter holes as shown in figure 6.2

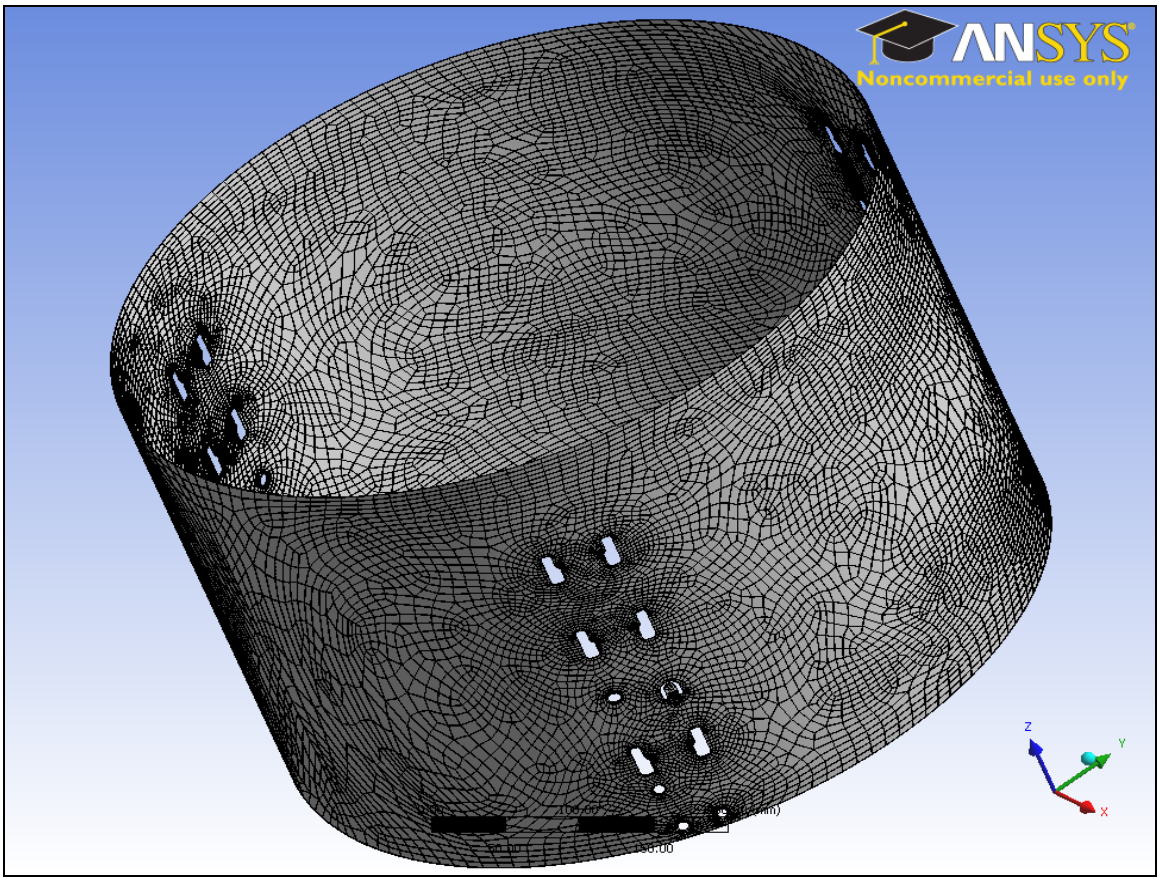

Figure 6.2: FE mesh of the drum model in ANSYS.

6.1.2 Simulation results

After performing the simulation in ANSYS the results are obtained in the form of deformations and stress distributions. The results obtained from ANSYS are described as follows;

6.1.2.1 Deformation results

The deformation behaviour obtained from FE analysis is found to be close to the deformation results obtained from the experimental investigations. It has been found, that the structural deformation behaviour is non-symmetric. The values obtained are in good acceptable range and the maximum value is found to be 0.311 mm as shown in figure 6.3.

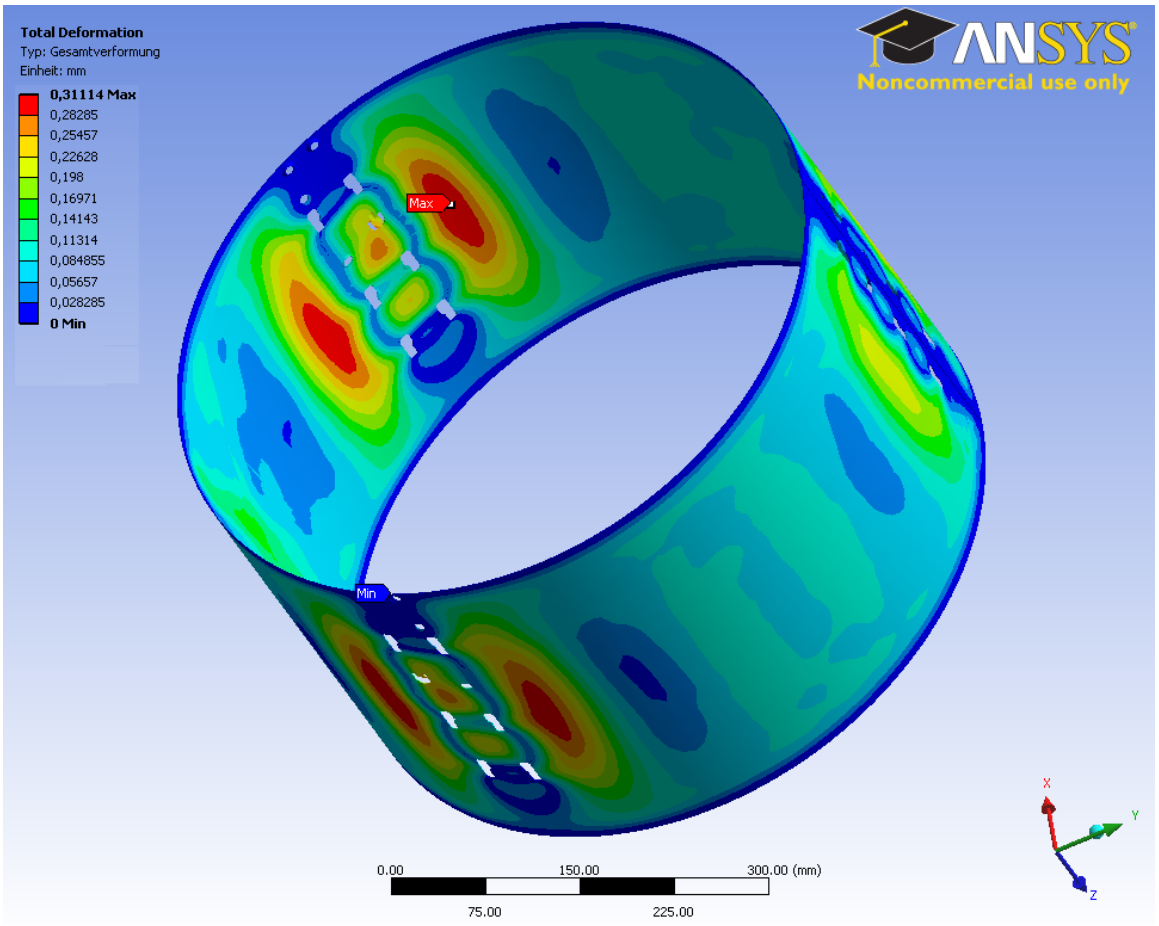

Figure 6.3: Total deformation plot.

6.1.2.2 Stress distribution results

The stress distribution results are obtained in the form of Von-Misses stresses and a maximum value is found to be 466 MPa. The Von-Misses stress distribution obtained from ANSYS is shown in figure 6.4. Like the deformation results, the stress distribution is also non-symmetric and the maximum stresses are found around the lifter holes. It has been observed that the stress distribution behaviour around each lifter hole is consistent as seen in the experimental findings that, the crack propagation behaviour around each lifter holes was consistent. Figure 6.5 demonstrates the location of the maximum Von Misses stress and the stress distribution behaviour around the lifter holes.

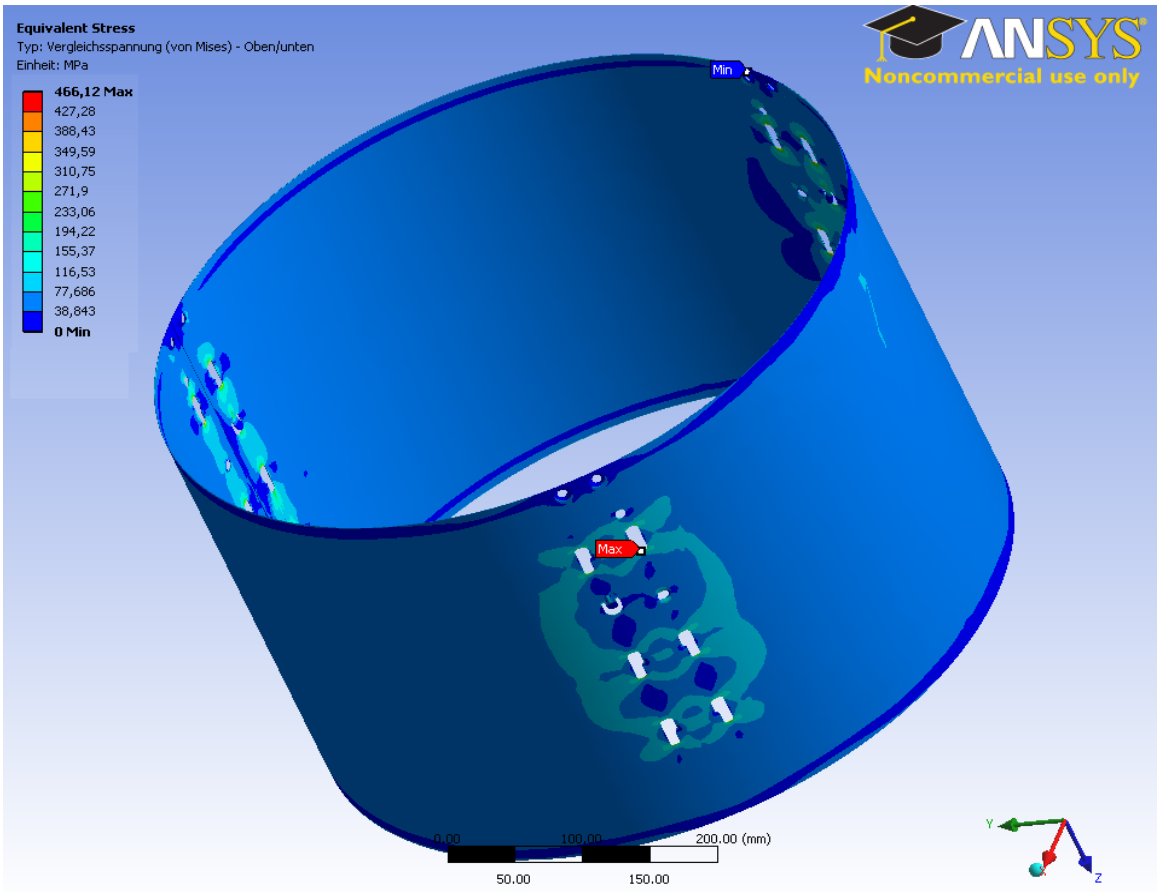

Figure 6.4: Von-Misses stress distribution.

Figure 6.5: Location of maximum Von Misses stress.

Another important fact about the stress distribution is that there is not much variation of stresses in the internal geometries of the holes. The internal geometries of the holes are demonstrated in figure 6.6. It has been observed that, there is not much variation in the stress distribution around each hole. These results show that there are no significant effects of these internal geometries on the simulation results.

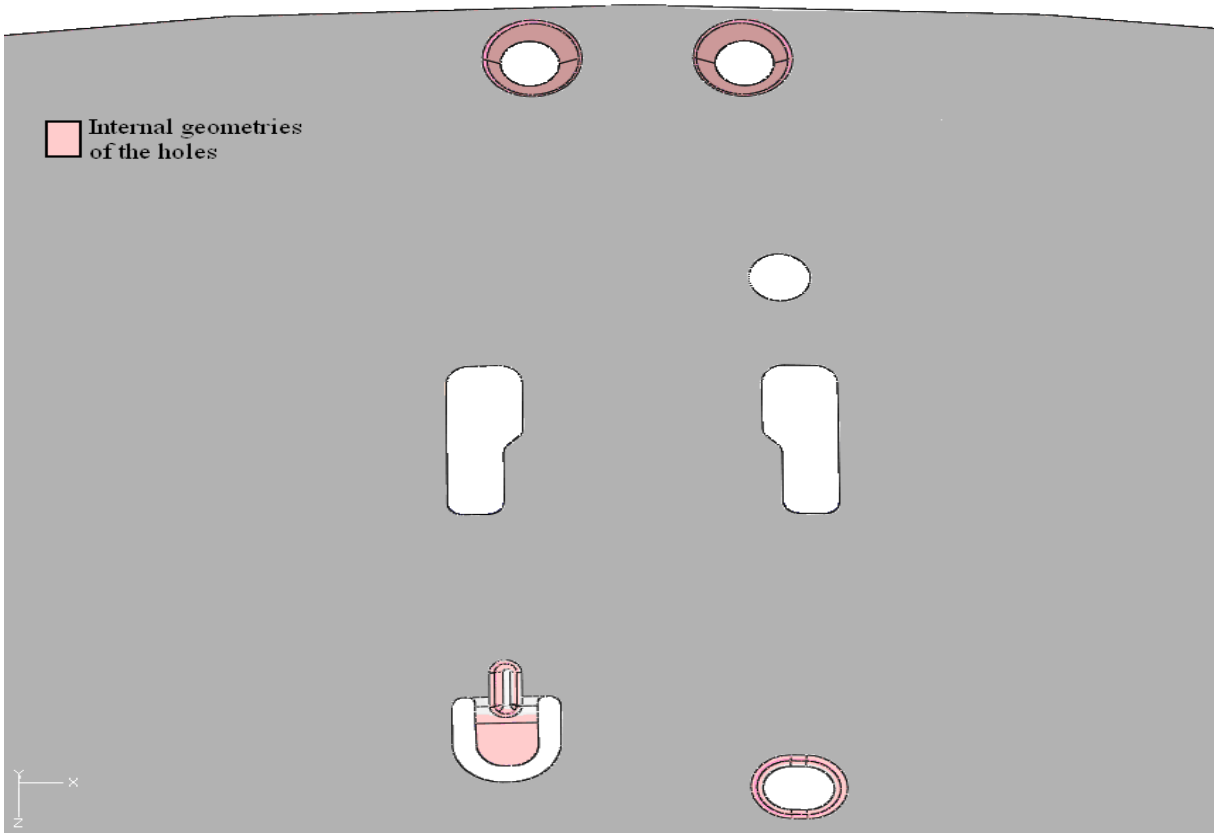

Figure 6.6: Internal geometries of the holes in the FE model.

6.1.3 Discussion

The results obtained from the numerical simulation performed with ANSYS show good agreement with the experimental findings. The important conclusions drawn from the simulation results are as follows;

- The structural deformation results obtained from the FE analysis are close to the experimental findings and the location of the maximum deformations obtained from FE analysis is somehow coincide with the experimental findings, which is around the lifter holes.
- The Von-Misses stress distribution results obtained from the FE analysis shows that the maximum stresses are around the lifter holes.

- Both the deformation and stress distribution results are non-symmetric.
- The results show that the internal geometries of the holes have no significant influence on the results and one can ignore these geometries in order to simplify the model.

These simulation results are verified in the next section by using ABAQUS, and based on the simulation results from ANSYS, some geometric modifications are made to simplify the model.

6.2 Modifications in the FE model

The modifications made in the FE model are based on the simulation results obtained from ANSYS simulations. The modified FE model is created in PATRAN and the simulations are performed in ABAQUS. The main purpose of using ABAQUS is to verify the results obtained from simulations performed in ANSYS by using a simplified FE model.

6.2.1 Geometric modifications

It has been observed from the simulation results obtained from ANSYS, that the deformations and stress distributions around the internal geometries of holes as shown in figure 6.6 does not have significant effects on the overall results of the simulation, therefore, these unnecessary parts can be removed.

The FE model defined in chapter 5 is imported into PATRAN with the same boundary conditions, loading conditions and material properties, however, without internal geometries as shown in figure 6.7.

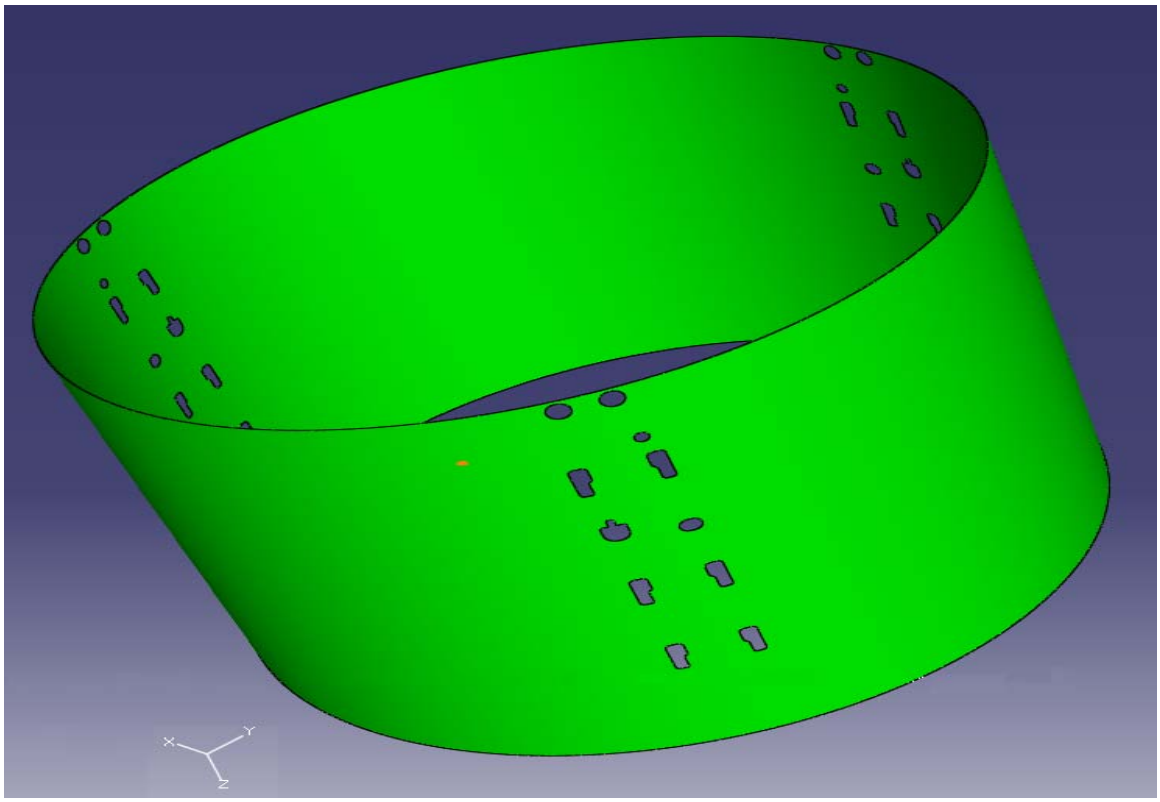

Figure 6.7: Modified geometric model.

6.2.2 Generating the FE mesh

PATRAN has an extensive library of FE types and topologies. The FE names are denoted by a shape name and its number of associated nodes, such as *Bar2*, *Quad4*, *Hex20*. PATRAN provides a choice of using either the *IsoMesh* method or the *Paver* method depending on the type of surface to be meshed. *Paver* is best suited for trimmed surfaces, including complex surfaces with more than four sides, such as surfaces with holes. In general, for a quadrilateral element mesh the *Paver* requires the total number of elements around the perimeter of each surface to be an even number. It will automatically adjust the number of elements on a free edge to ensure this condition is met.

6.2.2.1 The element type

The shell element library is divided into three categories consisting of general-purpose, thin, and thick shell elements. Thin shell elements provide solutions to shell problems that are adequately described by classical (Kirchhoff) shell theory, thick shell elements yield solutions for structures that are best modeled by shear flexible (Mindlin) shell theory, and general-purpose shell elements can provide solutions to both thin and thick shell problems [27].

The Discrete Kirchhoff Constraint (DKC), which refers to the satisfaction of the Kirchhoff constraint at discrete points on the shell surface, is imposed in all thin shell elements. The solutions obtained with these elements converge to those corresponding to classical shell theory. For the thin shell element type (S8R5) the DKC is imposed numerically where the transverse shear stiffness acts as a penalty that enforces the constraint. Non negligible transverse shear flexibility is required for S8R5 element to function properly; hence, the element is suitable for the analysis of composite and sandwich structures. Irregular meshes of these elements converge very poorly because of severe transverse shear locking; therefore, special consideration is given while meshing the model with these elements.

6.2.2.2 Mesh optimization

The model is meshed using S8R5 elements, which is an 8 noded shell element with reduced integration. In order to get better results a fine mesh is used around the lifter holes. Different FE models are developed with different mesh densities in order to optimize the mesh and finally it has been observed that the FE model with 25418 elements gives good results. Based on this mesh optimization test the meshed FE model is shown in figure 6.8.

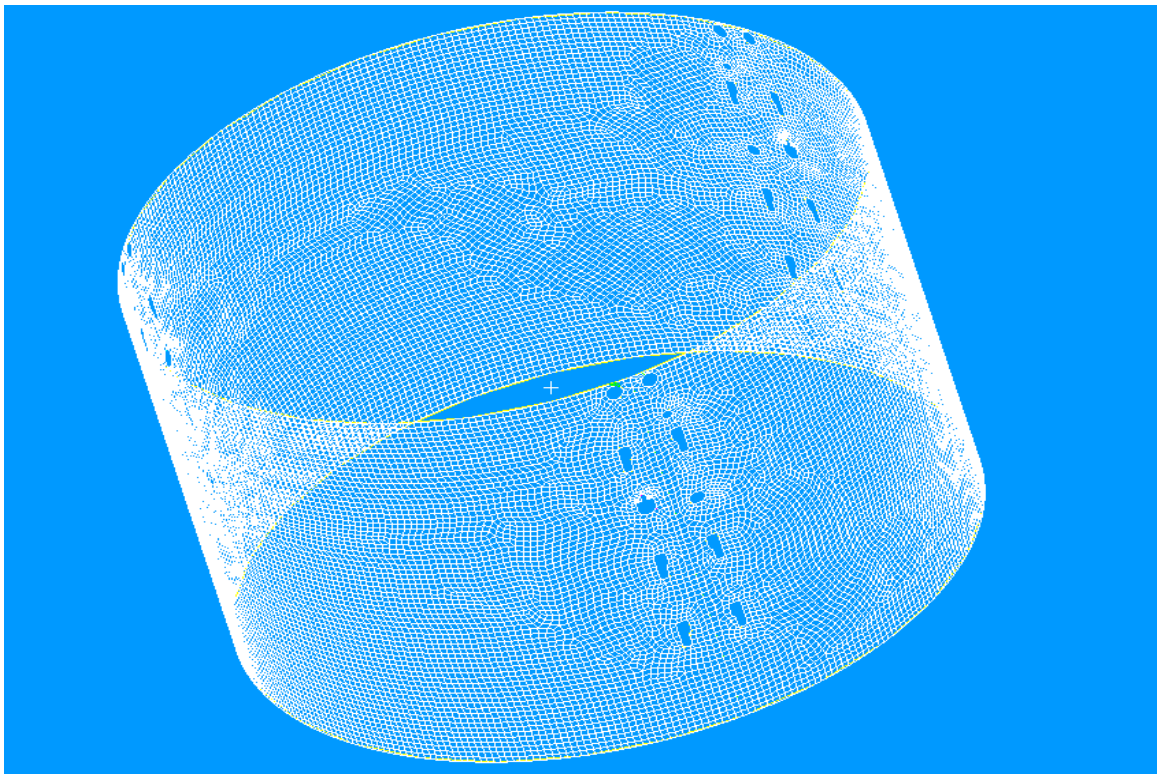

Figure 6.8: FE mesh of the drum model in PATRAN.

6.2.3 Simulation results

ABAQUS provides several different analysis types which are divided into two main categories: linear perturbation and general. Linear perturbation analysis provides the linear response of the model about the state reached at the end of last general nonlinear analysis. Whereas, general analysis is mostly used for both linear and nonlinear analysis and it is performed to analyzed the static behaviour such as deformation due to static loads.

The input file, generated in PATRAN, is imported into ABAQUS in order to carry out the simulations. After performing the simulations in ABAQUS the results are obtained in the form of structural deformation behaviour and stress distributions. The results obtained from ABAQUS are explained as follows;

6.2.3.1 Deformation results

The deformations in the model are analyzed in all three directions in order to understand the behaviour of the FE model under the applied conditions. The simulation results shows that the deformation behaviour of the modified FE model is the same as found from experimental investigations which is shown in figure 4.4. The maximum deformation values in x and y direction are 0.3971 mm and 0.3877 mm, respectively, as shown in figure 6.9 (a) and (b). These deformation results are close to the deformation results found from ANSYS simulations where the maximum deformation value was found to be 0.311 mm as illustrated in figure 6.3. The small difference in deformation values obtained from ANSYS and ABAQUS is probably due to the difference in the FE meshes used. The location of the maximum deformation obtained in both softwares is quite close to the experimental findings as shown in figure 4.4. However, the model deforms in non-symmetric manner in x and y directions whereas, the deformations are symmetric in z-direction. The deformation values in the z-direction are very small (almost negligible) as compared to the other directions as shown in figure 6.9 (c).

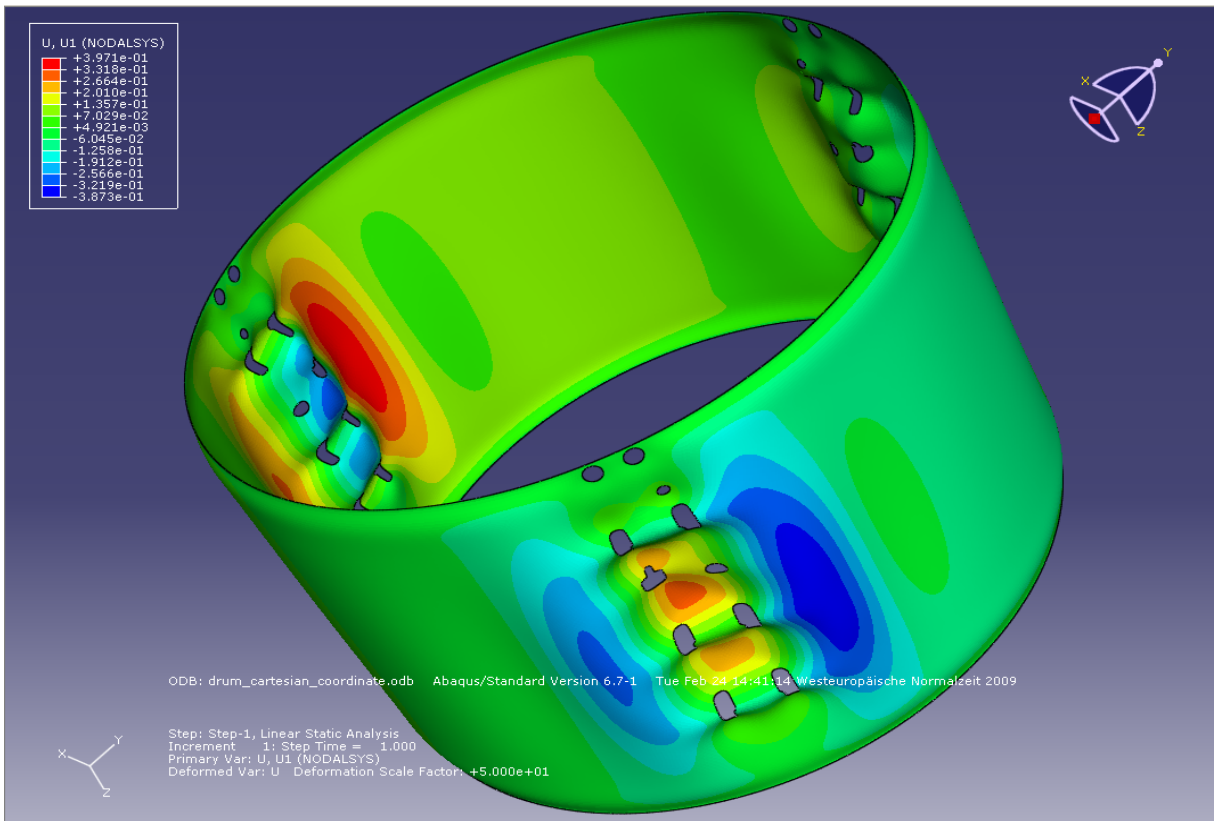

Figure 6.9 (a): *x* -deformations in the drum structure.

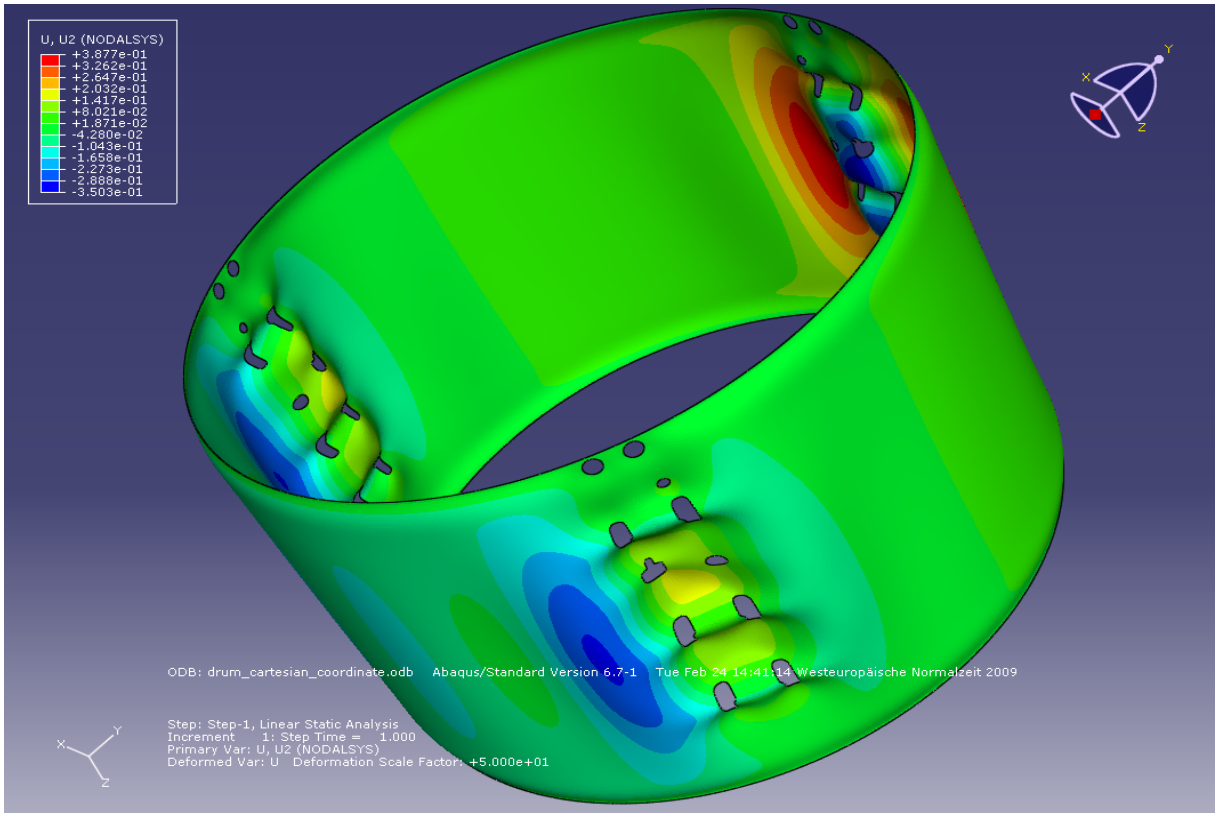

Figure 6.9 (b): *y* -deformations in the drum structure.

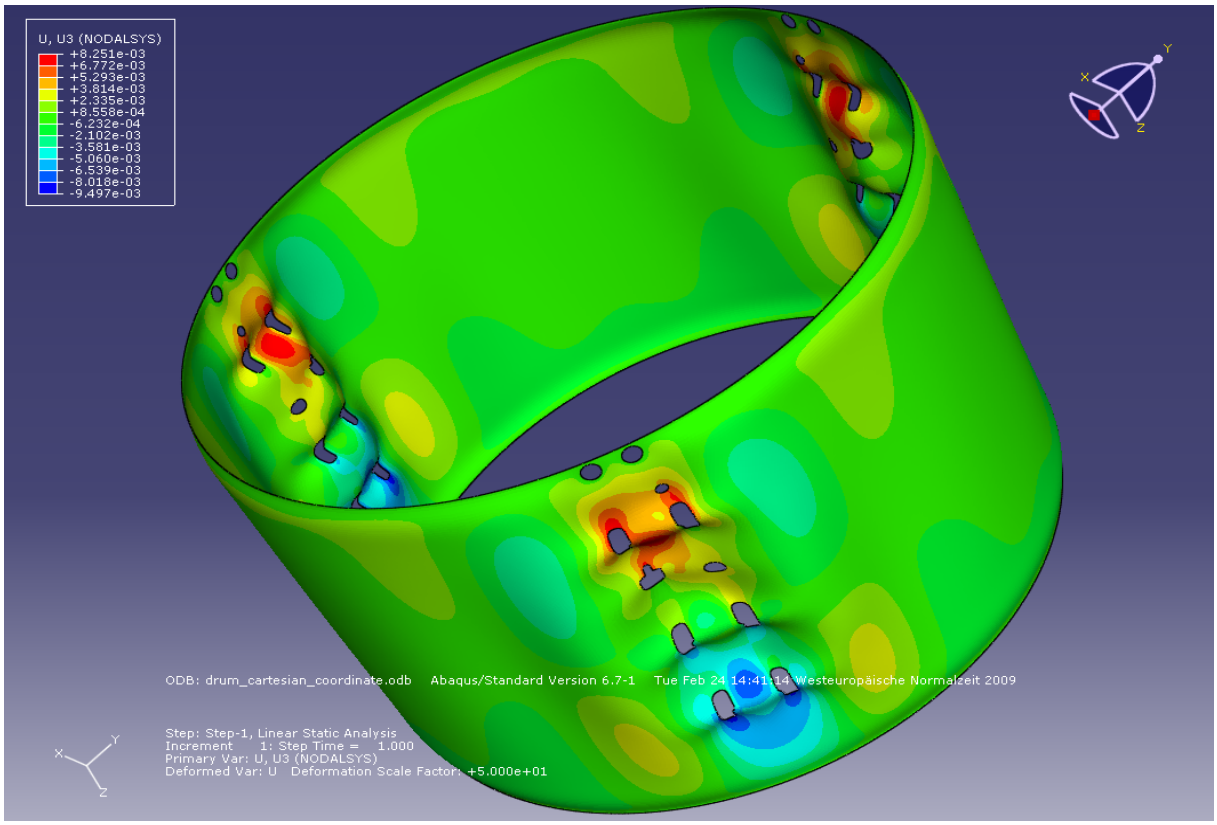

Figure 6.9 (c): z -deformations in the drum structure.

6.2.3.2 Stress distribution results

While analyzing the stress distribution results obtained from the simulations performed in ABAQUS, it has been observed that the stress distribution behaviour is symmetric in all three directions. As expected, the stresses in the z-direction (σ_z) are negligible because there is no loading is the axial direction. However, the maximum stress in the x direction (σ_x) is found to be 335.2 MPa and the maximum stress in the y direction (σ_y) is 169.6 MPa which is almost 50.6% less than the maximum value of σ_x. Figure 6.10 (a), (b) illustrate the stress distribution in x and y direction. Thus, the stress distribution results show that σ_x is the most dominant stress as compare to the other stresses and the maximum σ_x is found near the lifter holes. This effect can be seen in experimental findings since the cracks appear around the lifter holes and they initiated at the maximum stress locations.

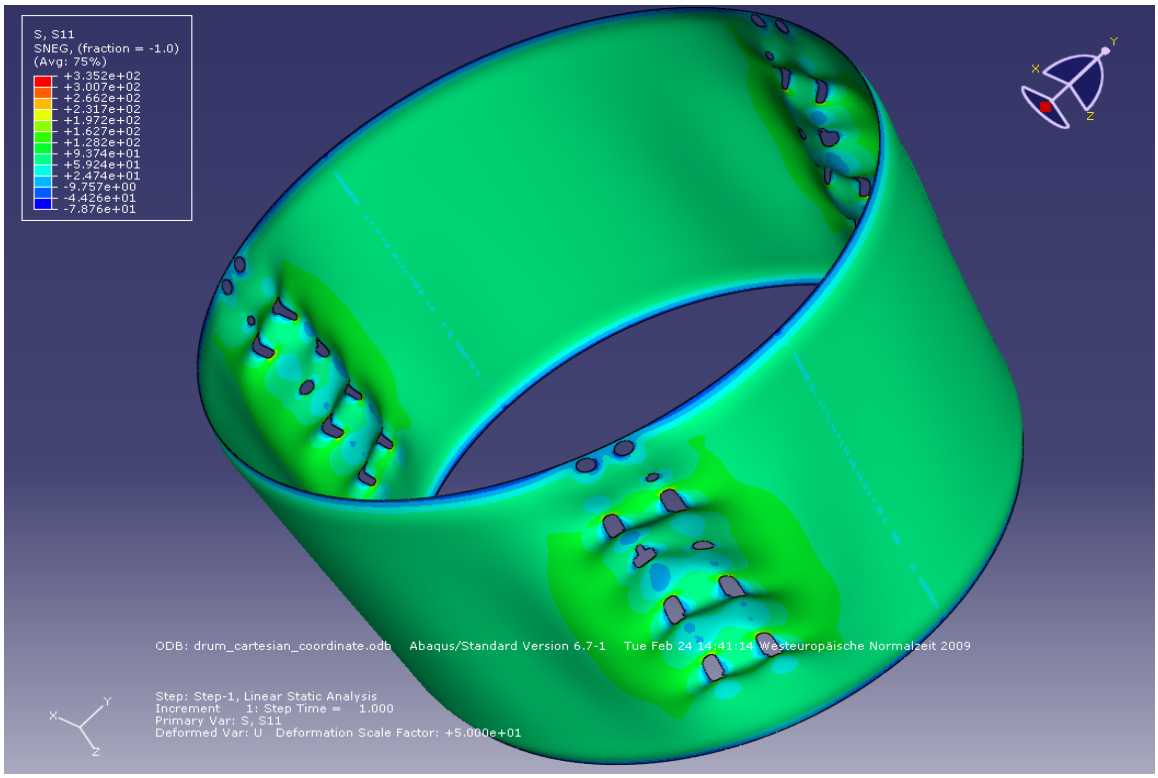

Figure 6.10 (a): σ_x distribution in the drum structure.

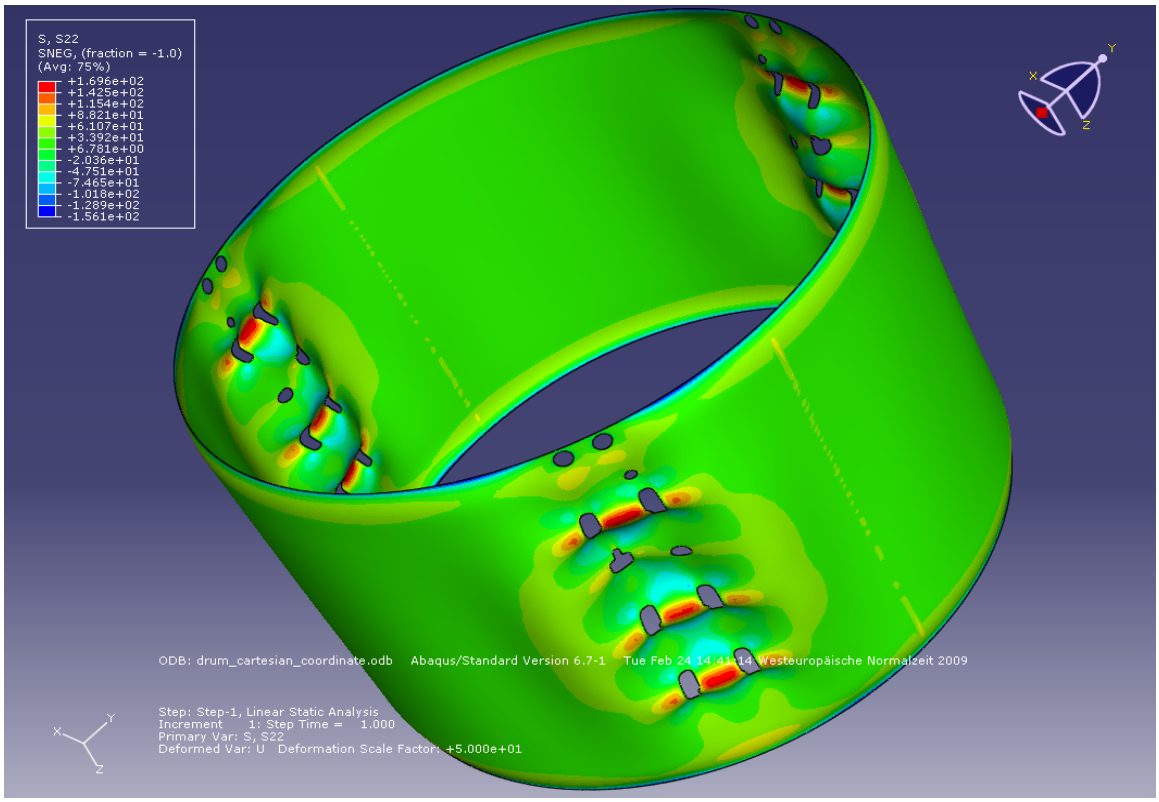

Figure 6.10 (b): σ_y distribution in the drum structure.

As discussed in chapter 4, the experimental investigation shows that crack appear around the lifter holes and propagate in the longitudinal direction, in the same way the σ_x distribution results shows that the maximum stresses are around the lifter holes as shown in figure 6.11.

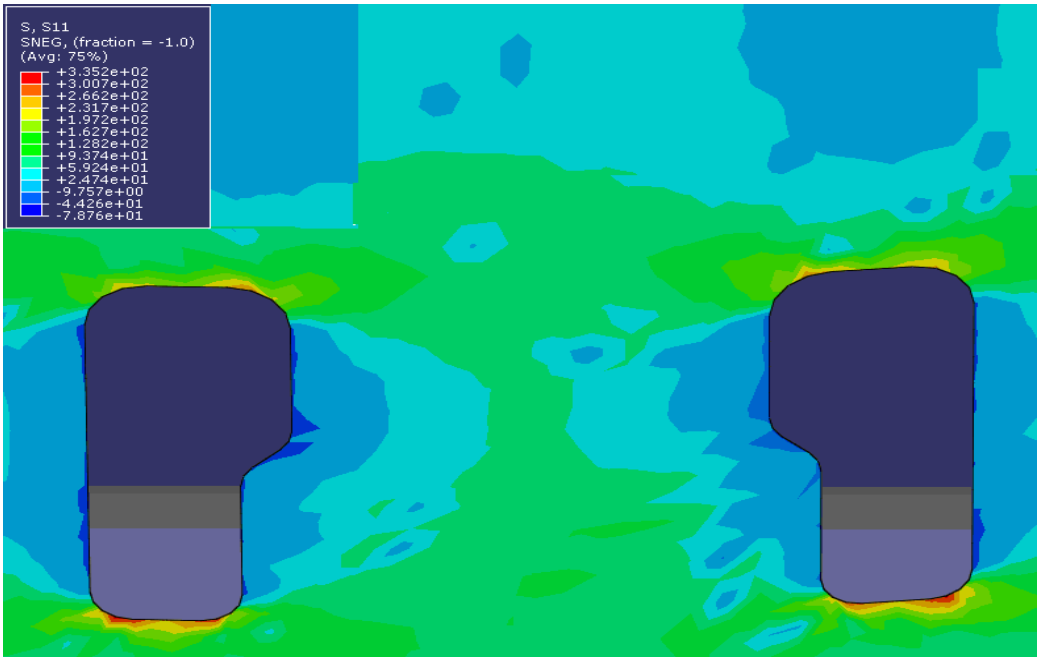

Figure 6.11: σ_x distribution around the lifter holes.

Hence, based on these facts it can be deduced that the results obtained from the simulations performed in ABAQUS verifies the ANSYS results in terms of shape deformation and these results are close to the experimental findings. The deformation results in all three directions are non-symmetric because of the usage of a Cartesian coordinate system. In the next section a cylindrical coordinate system is introduced and its effects on the simulation results are discussed in detail.

6.3 Application of a cylindrical coordinate system

The deformation results discussed in the previous section are found to be non-symmetric. In this section a FE model is defined in cylindrical coordinate system with same loading conditions. The general modeling procedures discussed in section 6.2 are used in developing this FE model.

6.3.1 Finite element model.

The FE model used in this section is defined in a cylindrical coordinate system (r,t,z) with its origin at the centre of the drum. As discussed in section 6.2, the geometric model is created

in PATRAN and the FE mesh is generated by using S8R5 (8 noded shell elements wit reduced integration). The material properties, boundary conditions and the loading conditions defined in chapter 5 are also used in this FE model.

6.3.2 Simulation results

The results obtained from the simulations performed in ABAQUS are described as follows;

6.3.2.1 Deformation results

The deformations in the model are analyzed in all three directions in order to understand the model behaviour under the applied conditions. The results show that the deformation results are symmetric in all three directions. Figure 6.12 (a), (b), (c) shows the deformation behaviour of the drum in radial, circumferential and axial direction, respectively.

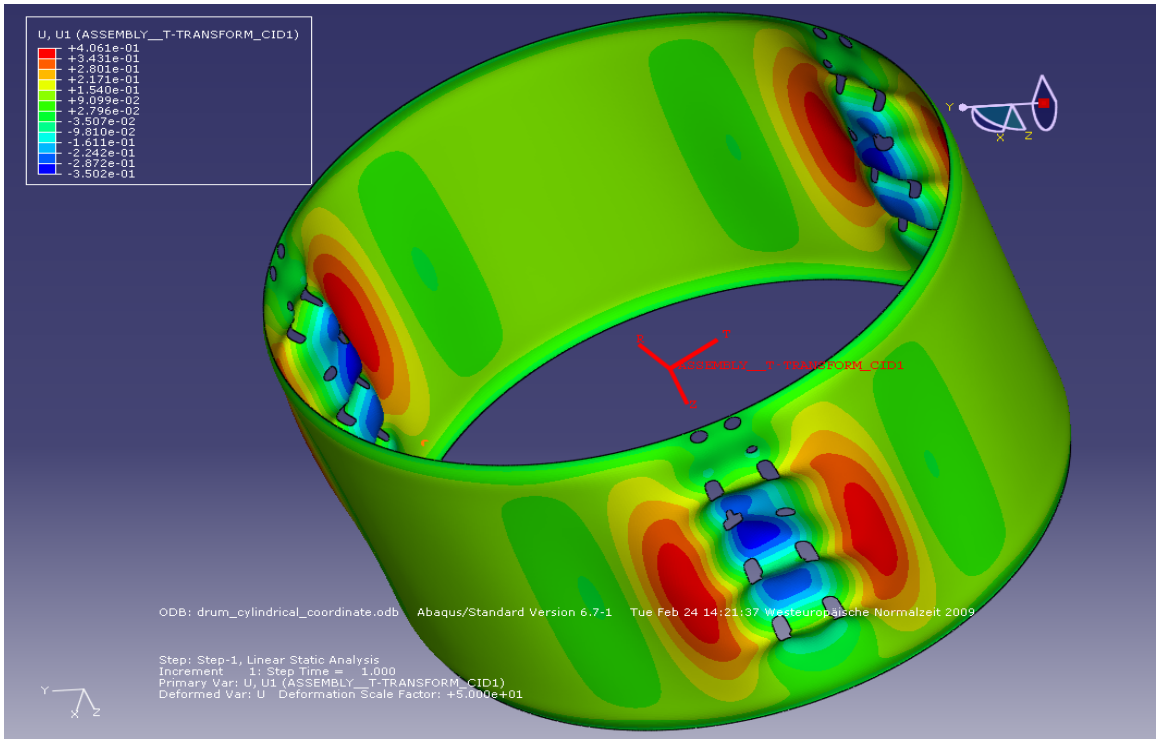

Figure 6.12 (a): Radial deformations in the drum structure.

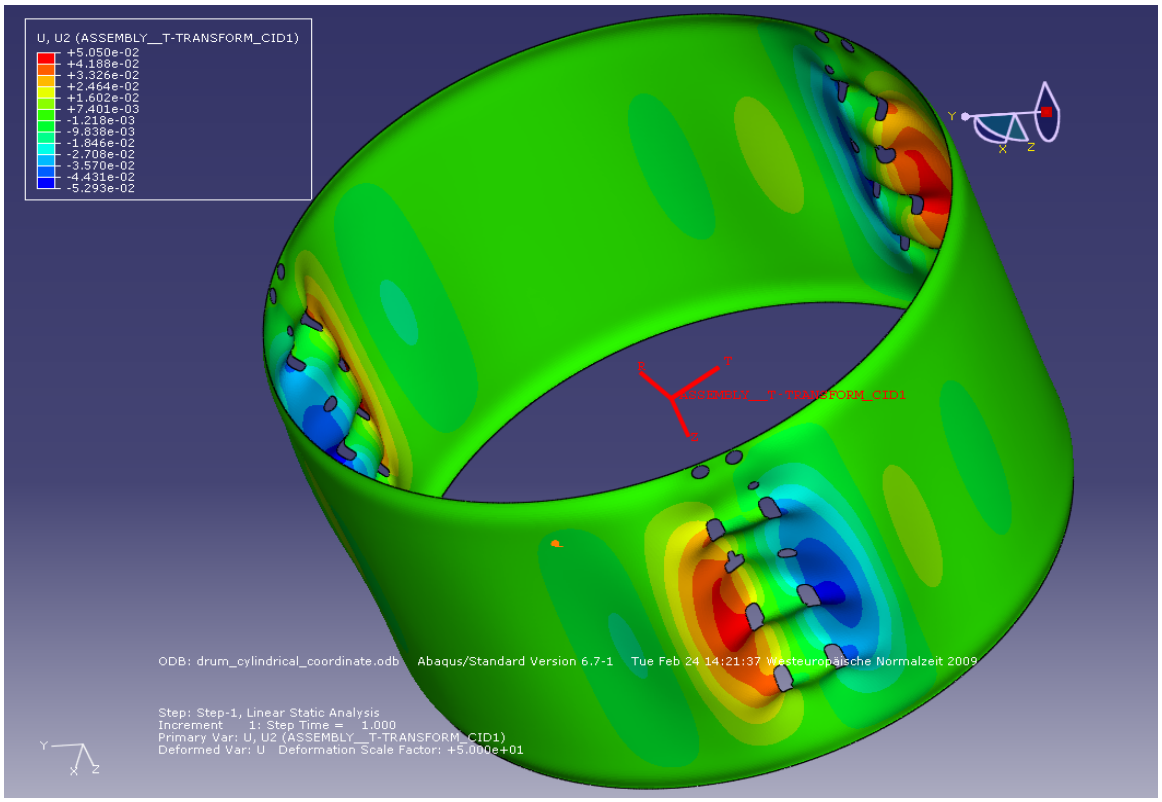

Figure 6.12 (b): Circumferential deformations in the drum structure.

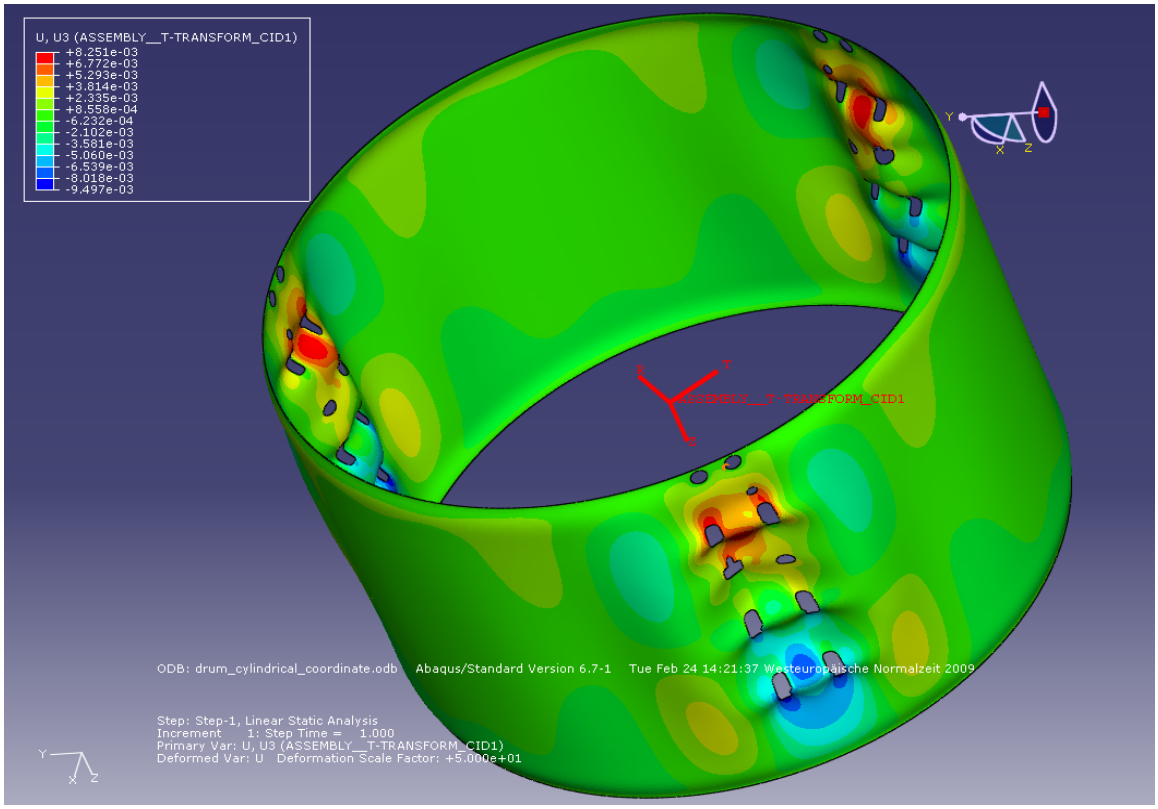

Figure 6.12 (c): Axial deformations in the drum structure.

The radial deformations are found to have a maximum value of 0.406 mm and the radial deformation near the holes are negative, which is due to the numerical instabilities because of a shell thickness of 0.5 mm. This deformation behaviour verifies the results found from experimental investigations as shown in figure 4.4. However, the effect of shell thickness on the radial deformation results is investigated by defining a FE model with a 10 times thicker shell. The radial deformation results show that there are no negative deformation values in this case as shown in figure 6.13; however, it is practically not possible to increase the thickness of the drum since it will definitely increase the weight of the drum and hence increase the cost of the whole product.

The deformations in axial direction are found to have the same behaviour as in the Cartesian coordinate system and the axial deformation values are very small (almost negligible) as compared to the deformation values in the other directions.

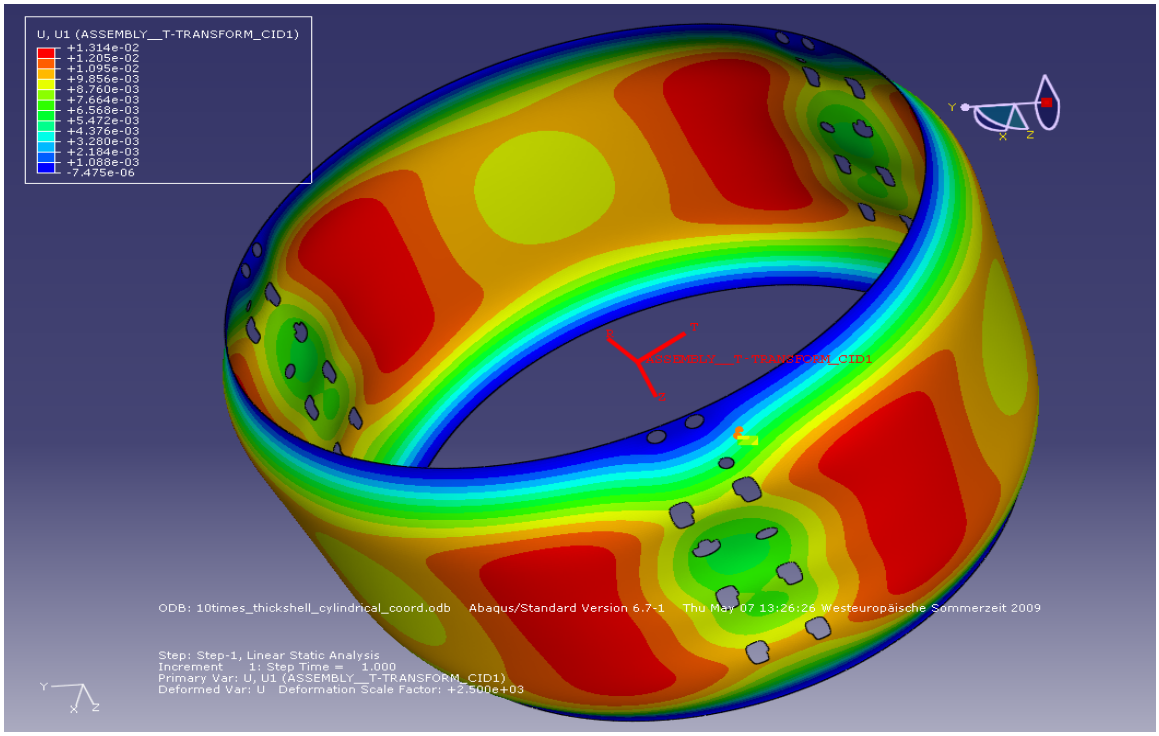

Figure 6.13: Radial deformation deformations in the drum: wall thickness = 5 mm.

6.3.2.2 Stress distribution results

The simulation results show that the stress distribution in the circumferential direction is the most dominant factor as compared to the stresses in the radial and axial directions because the loading is mainly acting in the circumferential direction due to the internal pressure. Figure 6.14 demonstrates the stress distribution in the circumferential direction.

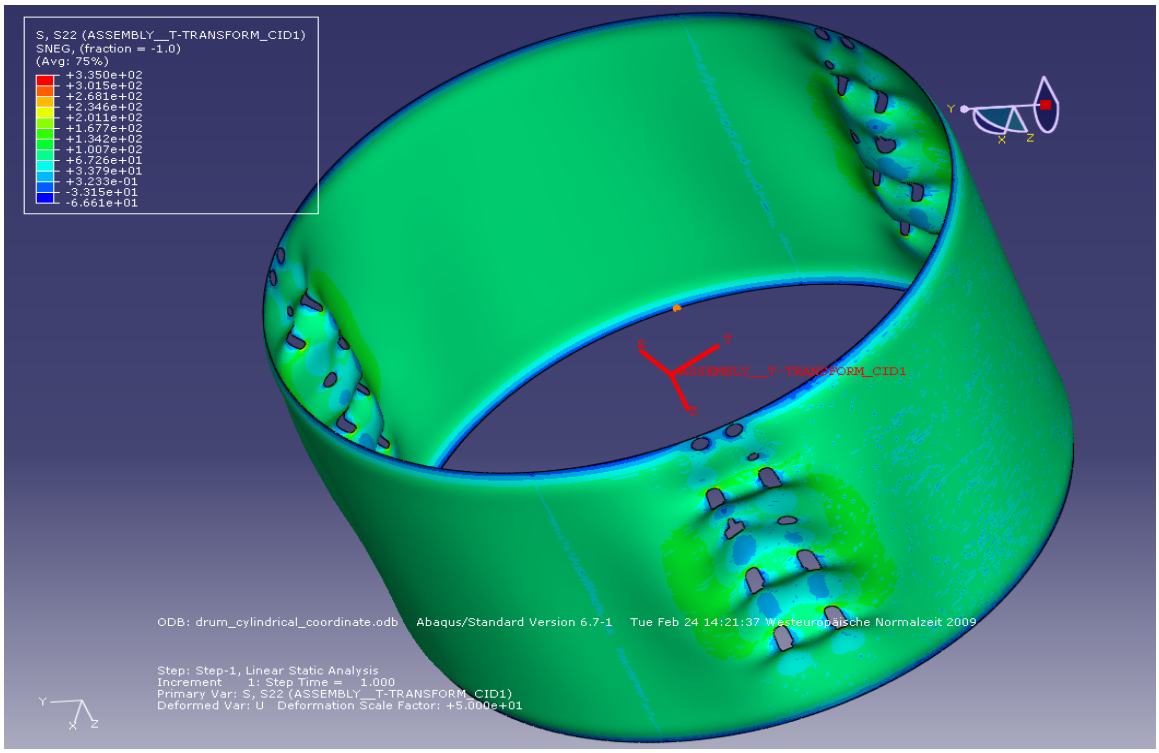

Figure 6.14: Circumferential stress distribution in the drum structure.

The simulation results show that the maximum circumferential stress value is 335 MPa and the maximum stress is found around the lifter holes, which verifies the simulation results presented in the previous sections and the results from experimental investigations also shows that the cracks appear around the lifter holes. The maximum circumferential stress around the lifter holes is demonstrated in figure 6.15. However, the stress distributions in the axial direction are almost negligible because there is no loading in this direction.

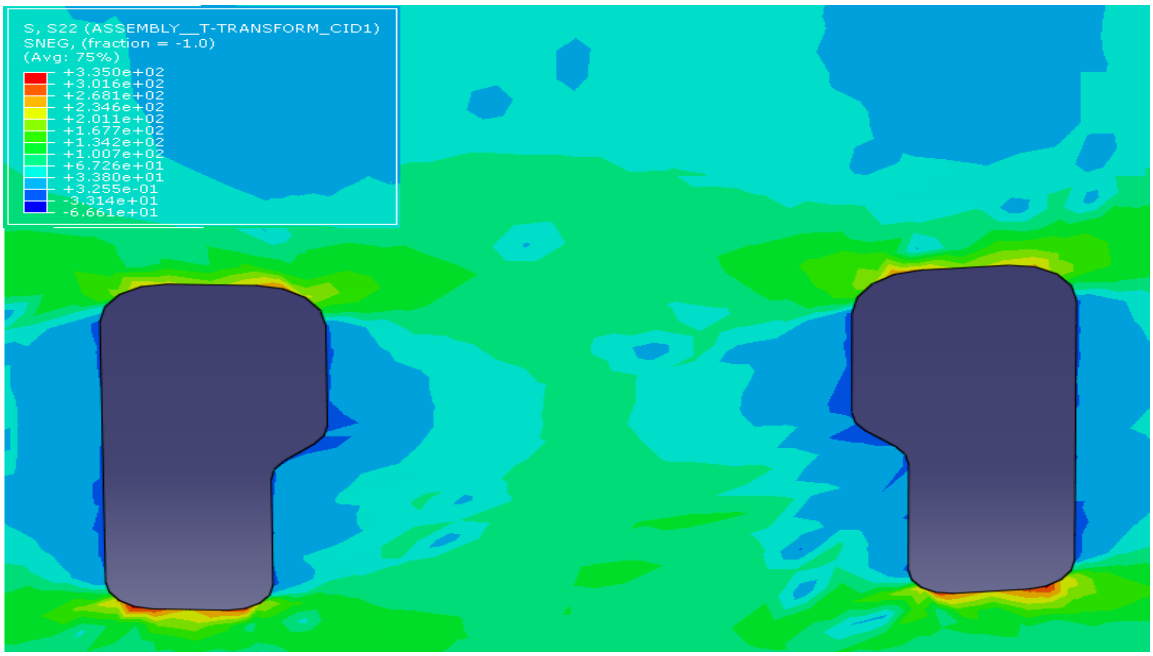

Figure 6.15: Circumferential stress distribution around the lifter holes.

Hence, based on these facts it can be deduced that the results obtained from the simulations performed in ABAQUS using a cylindrical coordinate system shows good agreement with the previous simulation results and these results are close to the experimental findings. It has been observed that the deformation and stress distribution results are symmetric in all directions; therefore, a symmetric feature can be used in order to simplify the FE model. The formulation of a simplified FE model using the symmetric features and the corresponding simulation results are discussed in the next section.

6.4 Model simplifications

The simplified FE model is based on the simulation results obtained in the last section which showed that the deformation and stress distributions in all directions are symmetric. Hence, by using the symmetric feature only one third of the whole drum is considered as a new simplified FE model.

6.4.1 Finite element model

In this FE model a one third of the whole drum structure is considered and the FE model is defined in a cylindrical coordinate system (r,t,z). This new cutout section is created in PATRAN as shown in figure 6.16.

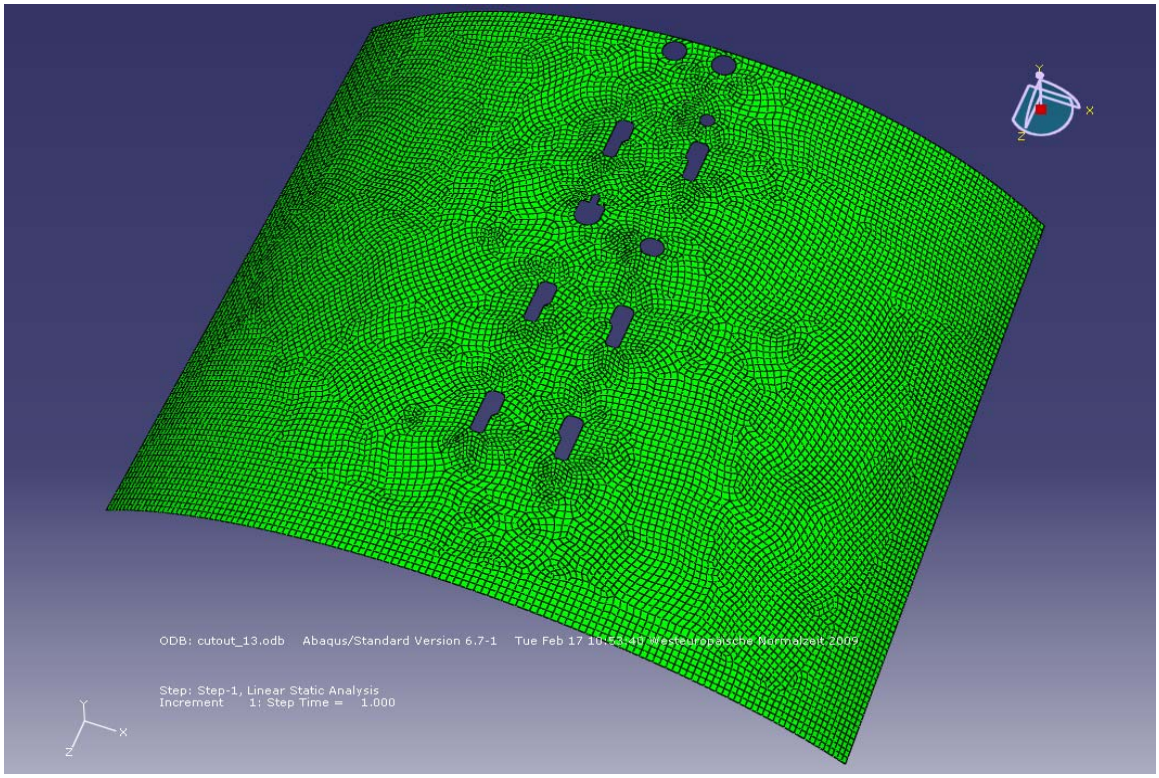

Figure 6.16: Simplified FE model (one-third of the whole drum model).

In this FE model a more refined mesh is generated on the FE model in order to get better results. Again S8R5 elements (8 noded thin shell elements with reduced integration) are used to generate the FE mesh as shown in figure 6.16. The material properties and the loading conditions defined in chapter 5 are again used in this FE model. However, some new boundary conditions are imposed because of the symmetric features used in this FE model.

6.4.1.1 Modified boundary conditions

The boundary conditions discussed in section 5.2.4 are used in this FE model along with one extra boundary condition which is due to the symmetry used in this FE model. Figure 6.17 demonstrates the boundary conditions used in this FE model. The boundary conditions used in the simplified FE model are described as follow;

- The outer periphery (upper and lower boundary) of the model is fixed in all DOF.
- The crosspiece connection holes are fixed in all DOF.
- The left and right side of the model is fixed in circumferential direction because of the symmetric feature.

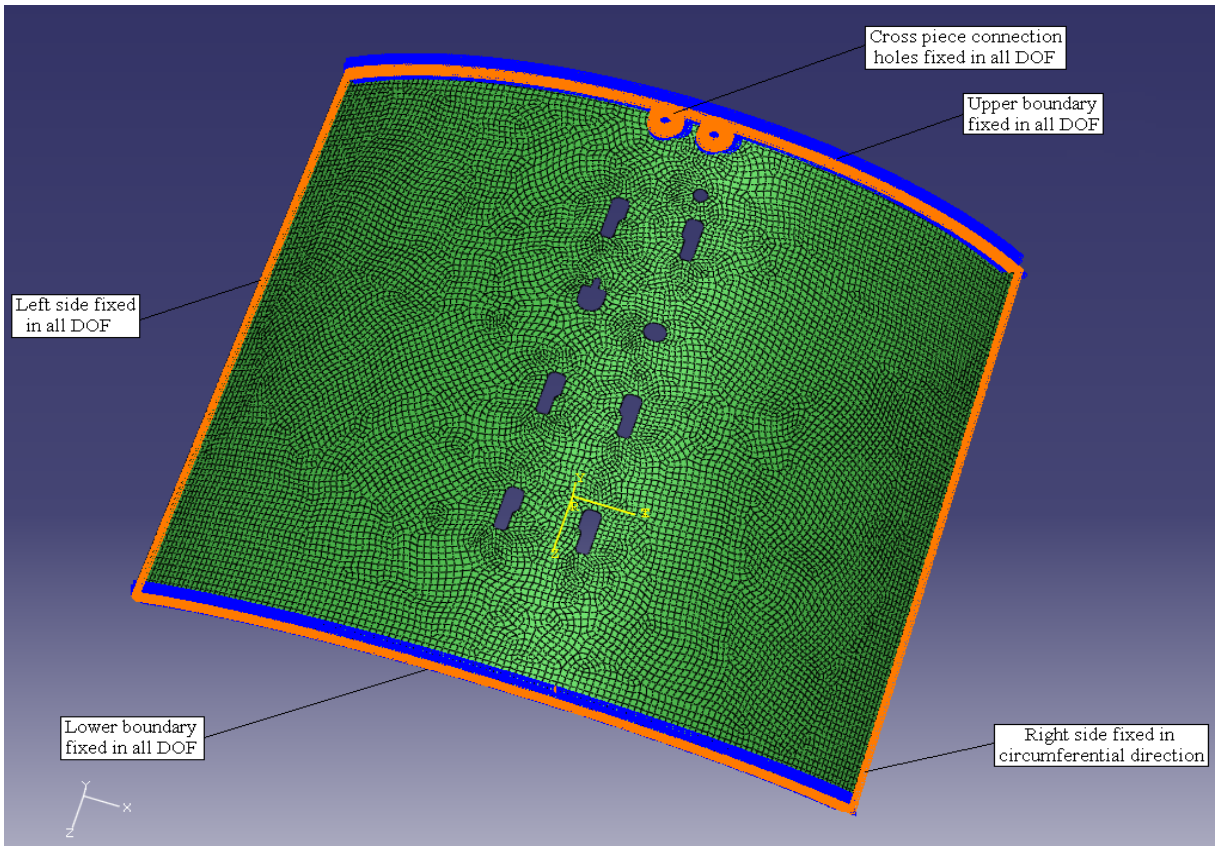

Figure 6.17: Boundary conditions used in the simplified FE model.

6.4.2 Simulation results

Again the input file, generated in PATRAN, is imported into the ABAQUS in order to perform the simulations. The results obtained from the simulations in ABAQUS are described as follows;

6.4.2.1 Deformation results

It has been observed that the deformations results obtained from simulations performed with the simplified FE model follows the same deformation behaviour as in the case of simulation performed with the full drum model. This resemblance in the results obtained from the simulations performed by using the full FE model and the simplified FE model, justifies the extra boundary conditions imposed due the application of the symmetric features. Figure 6.18 (a), (b), (c) shows the deformation results in radial, circumferential and axial direction, respectively. As observed in the results of the full FE model simulations, the radial deformations near the holes are negative, which is due to the numerical instabilities since we have a shell thickness of 0.5 mm. The deformations in the axial direction are very small (almost negligible) as compared to the deformations in the other directions as observed in the case of the full drum FE model simulation results.

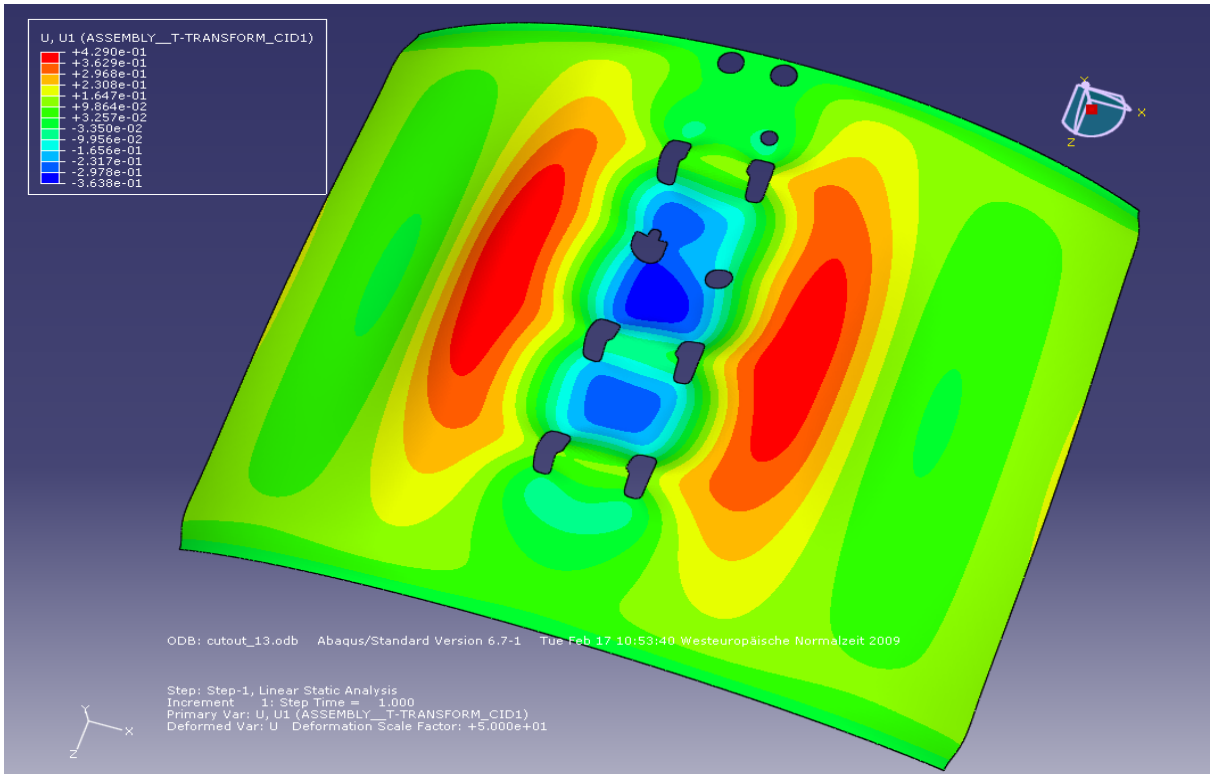

Figure 6.18 (a): Radial deformations in the drum structure (simplified FE model).

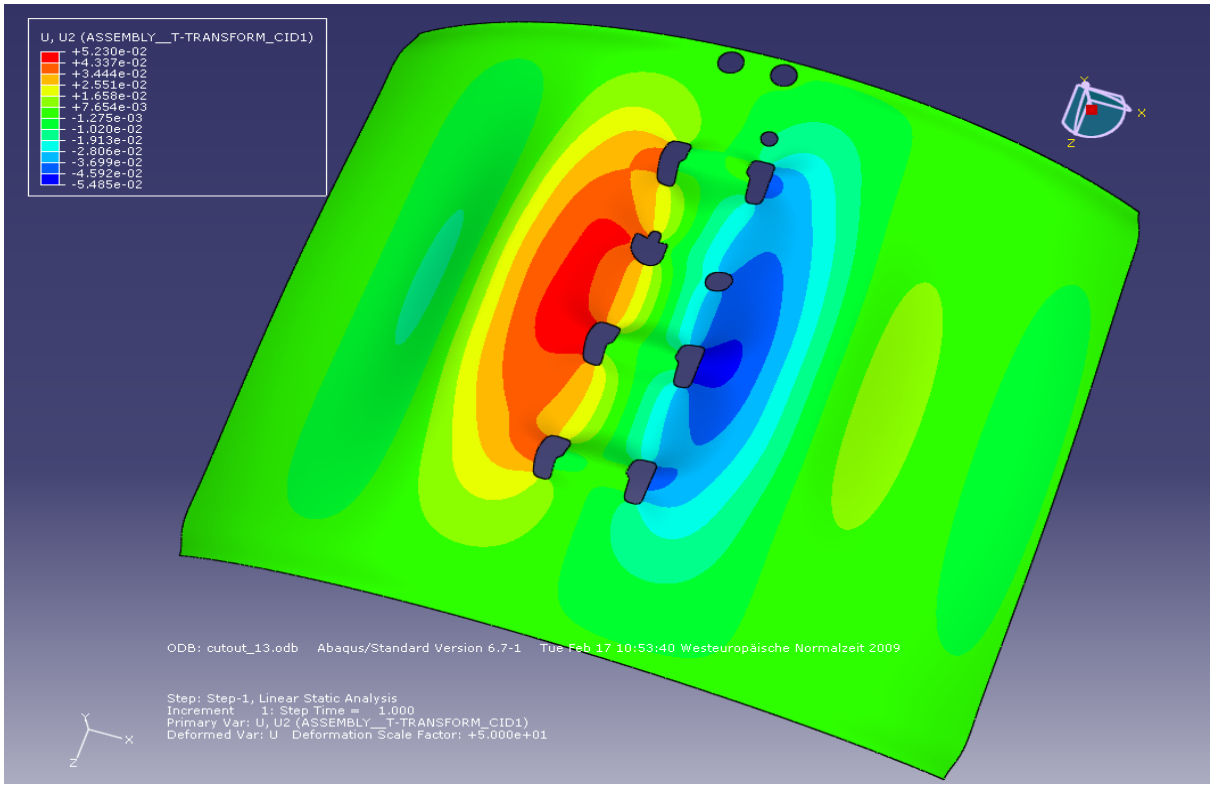

Figure 6.18 (b): Circumferential deformations in the drum structure (simplified FE model).

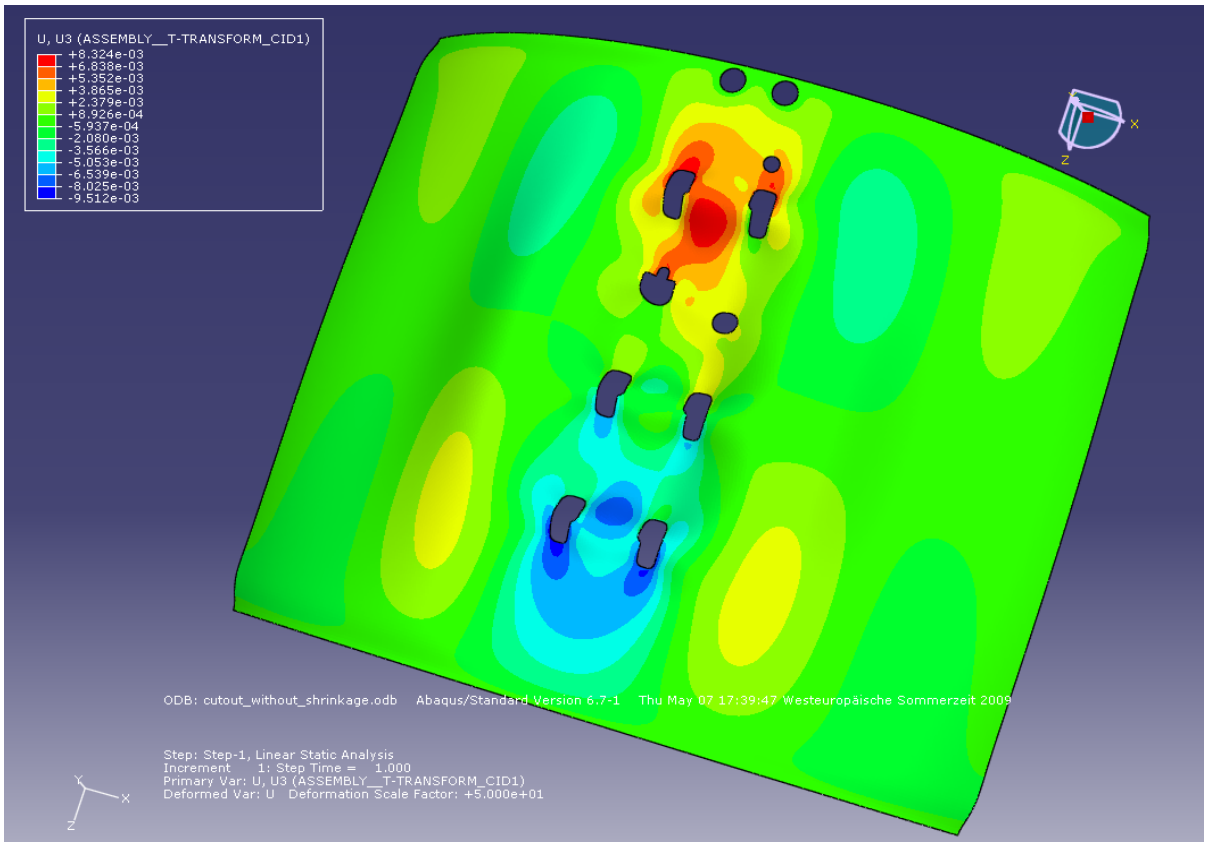

Figure 6.18 (c): Axial deformations in the drum structure (simplified FE model).

6.4.2.2 Stress distribution results

The analysis of circumferential stress distribution is performed in detail in order to understand the behaviour of the FE model under the applied loading conditions. The circumferential stress distribution obtained from simulations of the simplified FE model is shown in figure 6.19. It has been found that the value for maximum circumferential stress is 330.6 MPa and the location of maximum circumferential stresses is found again around the lifter holes as shown in figure 6.20.

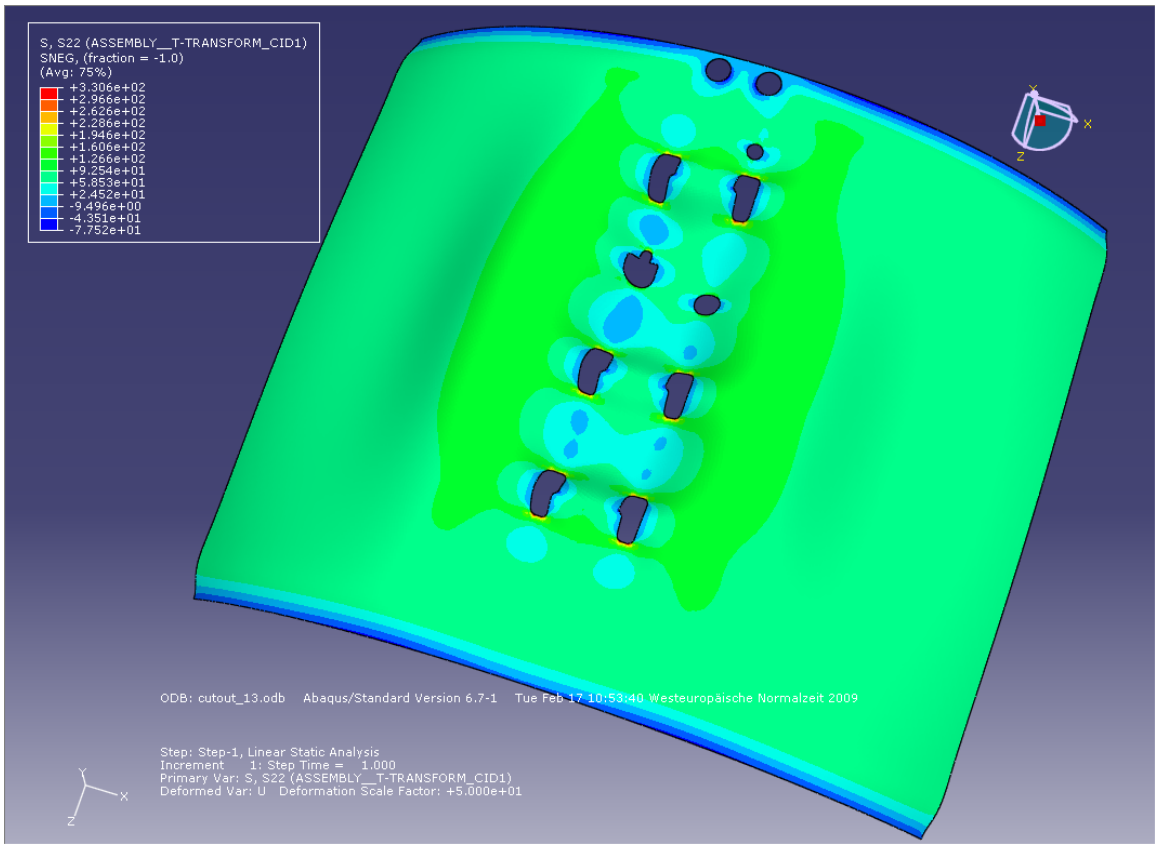

Figure 6.19: Circumferential stress distribution in the drum structure (simplified FE model).

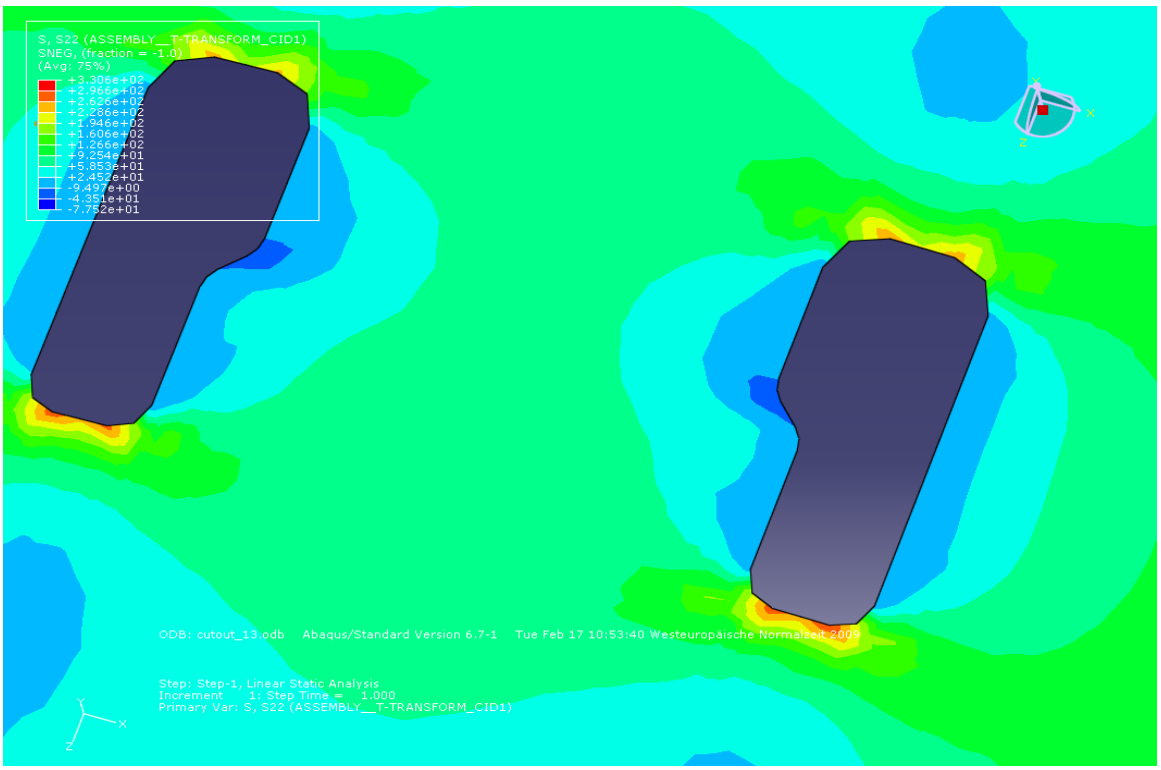

Figure 6.20: Circumferential stress distribution around the lifter holes (simplified FE model).

The deformation and the stress distribution results obtained from the simulations performed in ANSYS and ABAQUS again showed that the lifter holes are the most critical regions in the whole model and this fact is also found in the experimental findings which showed that the cracks more likely appear around the lifter holes. In the next chapter a new simplified FE model is used for the investigation of the crack propagation and the fatigue strength, based on the results obtained through the simulations performed using various FE models and the experimental findings.

7. Crack propagation and fatigue strength analysis

This chapter deals with the modelling techniques that are used to study the crack propagation and fatigue strength analysis using Franc2D [28]. In this project the FE model for Franc2D is created in CASCA which is a kind of mesh generating software, however, it is also possible to use meshes generated from other programs with similar features. The initial mesh is a basic requirement in order to perform the simulations in Franc2D.

7.1 Introduction

Computational techniques for evaluating fracture parameters, such as the SIF or crack propagation rate, requires either a refined mesh around the crack tip or the use of "special elements" which must possess the ability to incorporate the stress singularity near the crack tip. Although from the theoretical point of view the SIF and fatigue life can be obtained with the straight forward approaches which are explained in chapter 3.

7.1.1 Important facts about Franc2D

Franc2D (FRacture ANalysis Code) is available on Cornell Fracture Group web page [28]. Franc2D is a highly interactive program for the simulation of crack growth and this software is considered to be a significant step in the development of discrete fracture analysis because of its modular software design and topological data structure.

Franc2D uses standard eight or six noded elements with quadratic shape functions. These elements perform well for the elastic analysis and it also have the capability to incorporate the stress singularity in the solution by moving the side nodes to the quarter-point locations (Henshell and shaw, 1975).

Although, Franc2D have a lot of features which provide very useful information concerning fracture mechanics and fatigue life calculations, but some of the main issues concerning Franc2D are discussed as follows.

7.1.1.1 Crack propagation theories

The fracture calculations incorporated in Franc2D use two 2D LEFM concepts. The mode I SIF (K_I) governs the fracture process in the LEFM context [29]. Franc2D can also model quasi-static crack propagation and crack propagation due to fatigue loading. The crack

propagates in the direction predicted using any of the three propagation theories implemented in Franc2D. These are Sigma Theta Maximum theory [Erodogan and Sih, 1963], the G Theta Maximum theory [Hussain et al., 1974] and the S Minimum theory [Sih, 1974].

The Sigma Theta Maximum theory stated that the crack will move in the direction of maximum circumferential stress around the crack tip when a critical value of the stress is reached [30]. The G Theta Maximum theory states that the crack will move in the direction of maximum energy release rate when a critical value of the energy release rate is reached [31]. The minimum strain energy density theory, S Minimum, states that the crack will move in the direction where the strain energy density is minimum, and will move when a critical value is reached [32].

7.1.1.2 Analysis procedures used in Fracn2D

Franc2D uses two approaches in order to perform the simulation. The first is a direct linear equation solver for symmetric systems. The other one is a dynamic relaxation solver. Although, the linear equation solver is used in almost all cases except when nonlinear interface elements are being used.

7.2 FE model formulation

The simulation results from ABAQUS provide the foundation for the development of a FE model for crack propagation and fatigue strength analysis. The results from FEA showed that the circumferential stresses are most dominant as compared to the stresses in the other directions and the maximum stresses are found near the lifter holes as discussed in chapter 6. The results from experimental findings have also demonstrated that the crack initiation is located around the lifter holes as shown in figure 4.4. Hence, by comparing the simulation results with the experimental findings it is quite clear that the locations of maximum circumferential stresses effect the crack initiation. The results showed that the circumferential stress distribution around all lifter holes is consistent as shown in figure 6.15, a single crack model is considered in this project in order to perform an in-depth investigation of the crack propagation behaviour and the fatigue strength analysis.

CASCA is used in order to generate a mesh. CASCA is a mesh generating program which is used to two main functions for example, defining the geometry of the model and then generating a mesh using the given element types.

7.2.1 Geometric outline of the FE model

In order to develop a FE model for the crack propagation and fatigue strength analysis, a geometric outline of the FE model is created in CASCA. It has a lot of features which can be used to specify the outline of the FE model. Since the model is based on the circumferential stress distribution, so the outline of the FE model is defined at a certain distance where the variation in stress distribution is minimum. Figure7.1 demonstrates the geometric outline of the model created in CASCA. However, the detail drawings of the actual drum and the lifter holes with the exact dimension are provided in the Appendix 1.

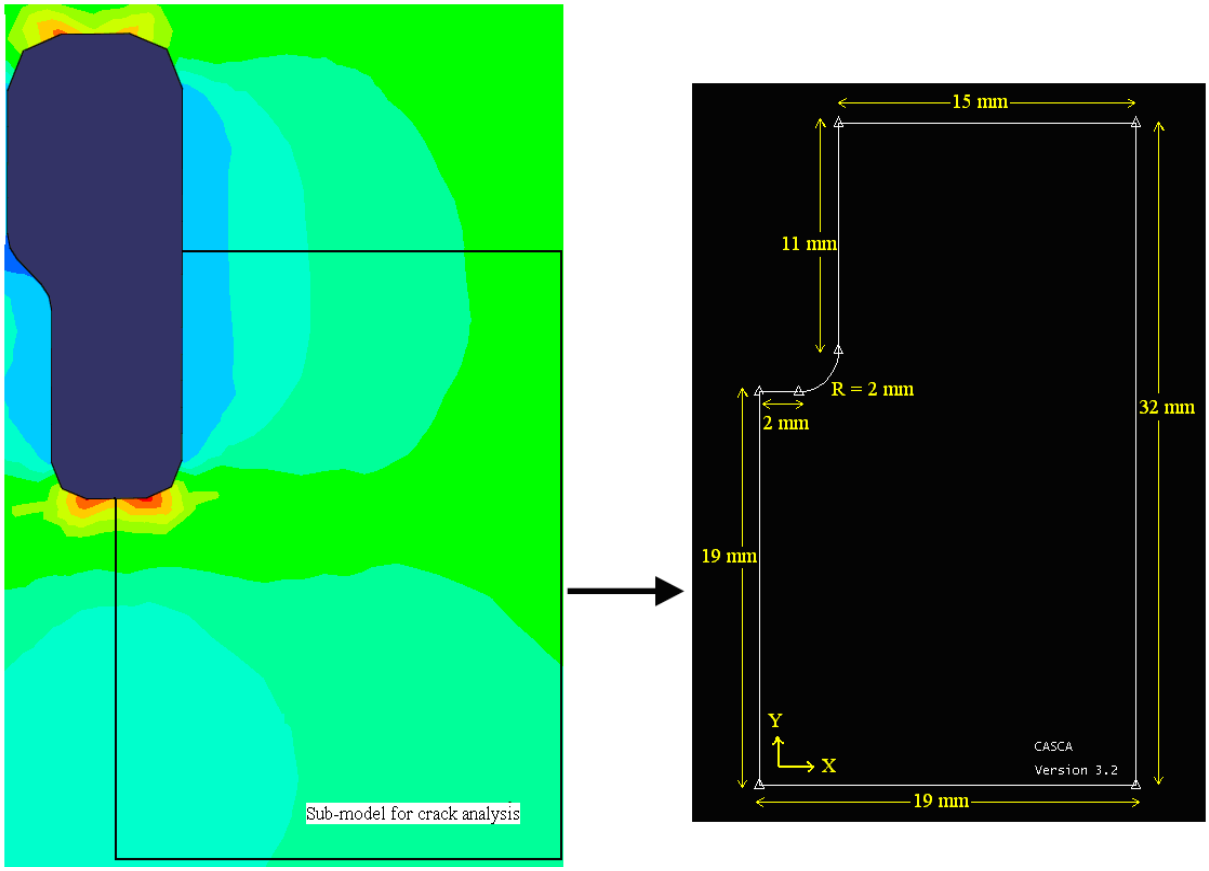

Figure7.1: Geometric model (around one lifter hole) for the fatigue strength analysis.

7.2.2 Generating the FE mesh

In order to perform the crack propagation and fatigue strength analysis it is always preferred to have a very fine mesh typically at critical locations, which is the region around the lifter holes because of the notch effect which results in stress concentration. For this purpose the model is divided into different sub-regions with specific mesh densities. In CASCA the process of generating a FE mesh involves three different steps and the detail description of these steps is given as follows:

1. Adding subregions: This allows breaking the model up into a number of simpler regions that are more convenient for meshing. It also allows defining the patch geometry. In this project the model is divided into five different regions as shown in figure 7.2

2. Adding subdivisions: After defining the subregions the next step is to specify the nodal densities along the boundaries for all the regions in the model and this is done by using subdivision options. The arrows along all the edges indicate their orientation, and are used to grade the nodal spacing along the edges. In this project a very dense mesh is specified around the notch in order to take stress concentration effects into consideration. Figure 7.2 illustrates the nodal densities along the edges of all regions of the model.

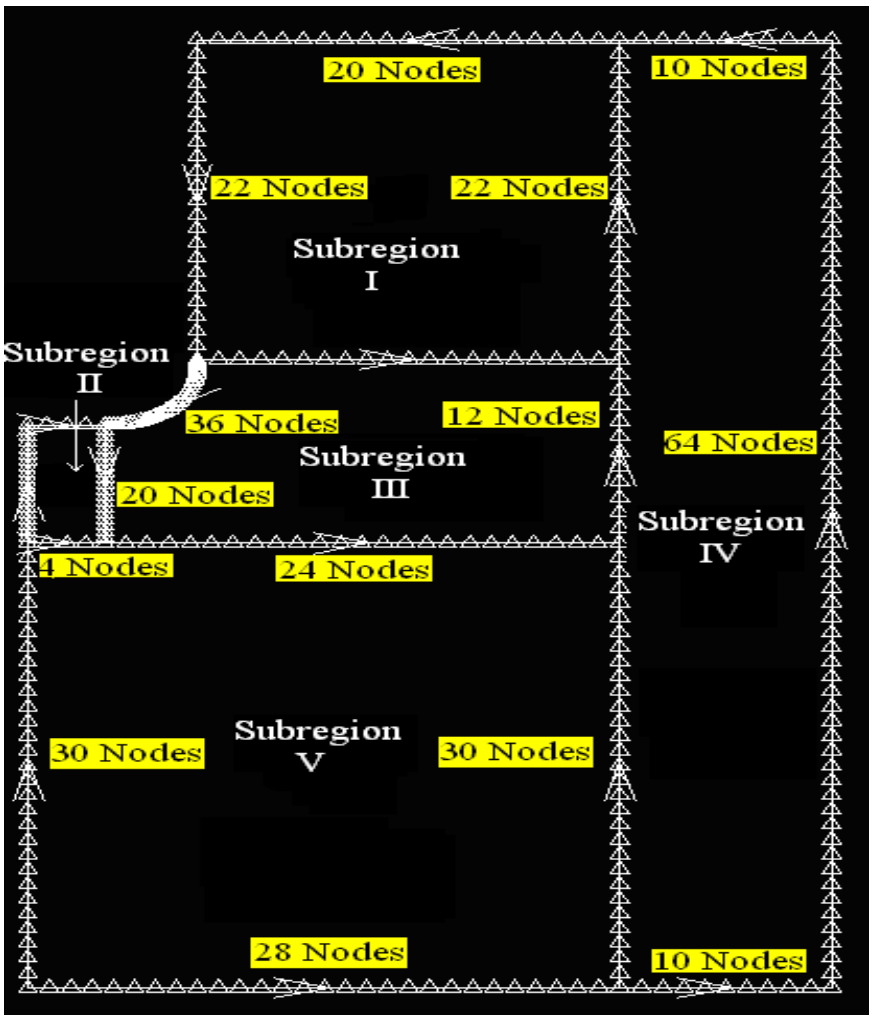

Figure 7.2: Subregions and subdivisions created in CASCA.

3. Mesh generation: After defining the subregions and specifying the subdivions, the final step is to generate the mesh for the five subregions. All five subregions of the model are meshed with the four sided meshing algorithm (Bilinear 4side). This algorithm requires a rectangular

region with equal number of nodes on opposite sides. For the meshing, Q8 quadrilateral elements are used which are basically 8 noded elements.

These elements perform well in the elastic analysis and also have the capability to incorporate the stress singularity in the solution by moving the side nodes to the quarter-point locations (Henshell and shaw, 1975). Figure 7.3 illustrates the mesh generated for Franc2D.

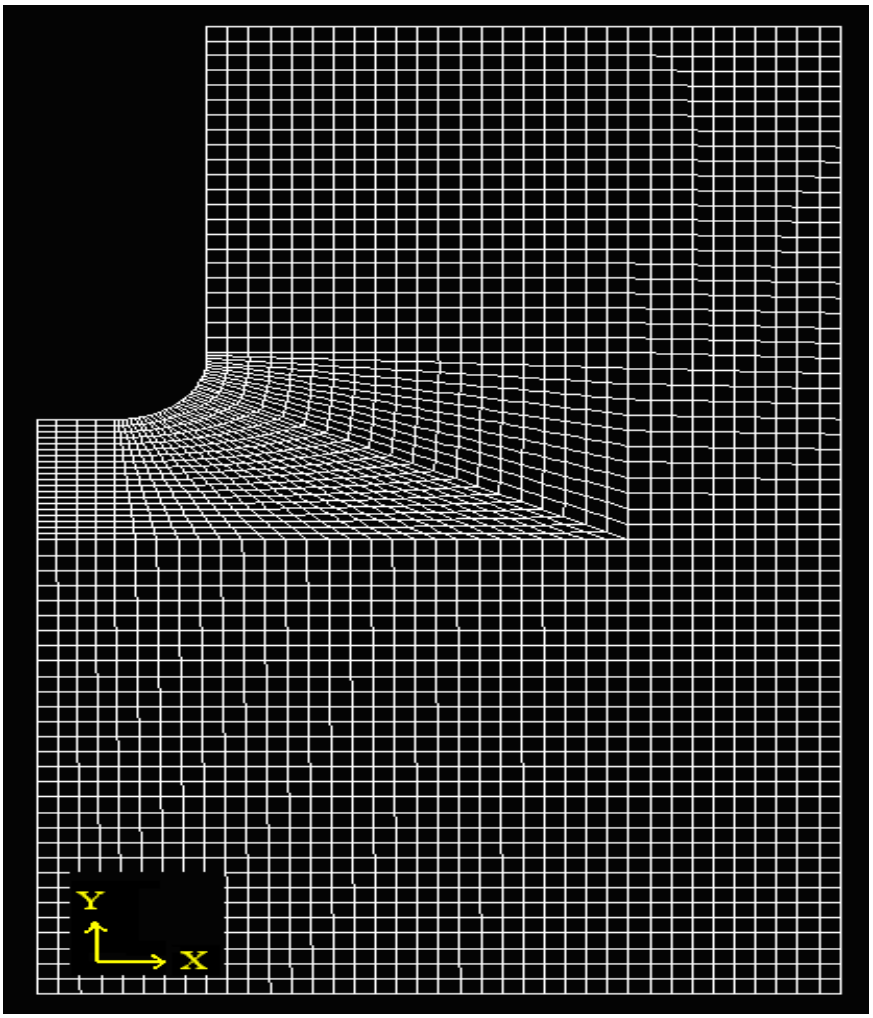

Figure7.3: Mesh generation using Q8 quadrilateral elements.

7.3 Loading conditions

As discussed above, the FE model for the crack propagation and fatigue strength analysis is developed on the basis of circumferential stress distribution results obtained from ABAQUS. Displacements in both x and y direction are applied as boundary conditions. The values of these displacements are taken from the deformation results obtained from the ABAQUS simulation. The mesh density of the FE model used in Franc2D is different than the one used

in previous simulation performed in ABAQUS. Hence, the displacement values can not be directly transformed into the Franc2D model. Figure 7.4 illustrates the difference in meshing used in ABAQUS and Franc2D.

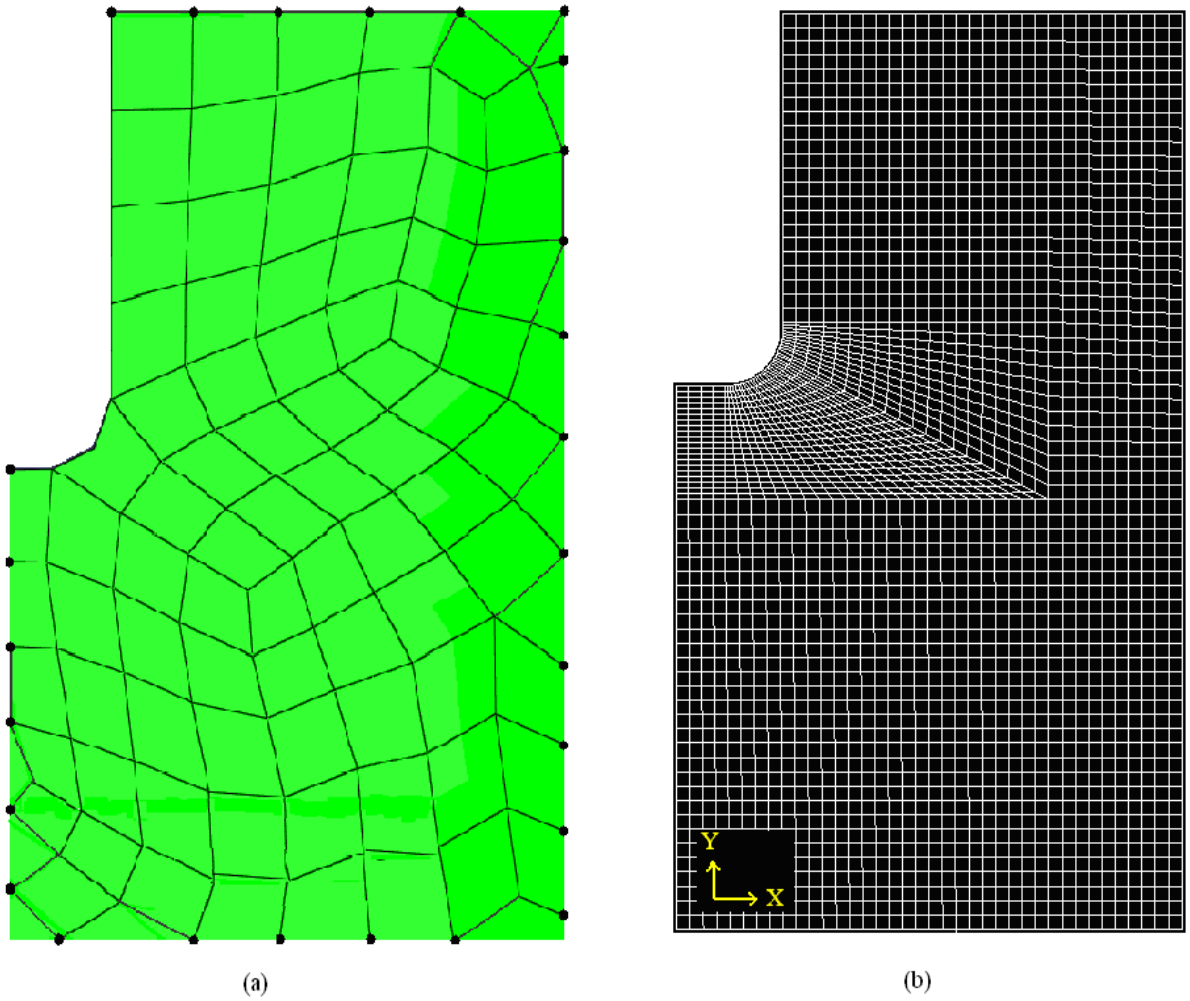

Figure 7.4: Comparison of the mesh used in (a) ABAQUS and (b) Franc2D.

In order to approximate the displacement values at each node of the Franc2D model an interpolation technique is used. The details description of this technique is given as follows;

7.3.1 Multiple linearization technique

This technique is used to approximate the displacements on each node of the Franc2D model. In this technique linear interpolation is performed on many small steps in order to approximate the displacements on each node of the model. Generally, it is a method of curve fitting using linear polynomials.

First step in this technique is to plot the displacement values obtained from ABAQUS simulation results against the position (location) in x and y direction. After getting the curve the next step is to cut the whole curve into a number of linear curves. Finally, for each linear step, a linear interpolant is defined which is actually a slope of that linear line. Then, using this slope a linear equation is defined which represents that part of curve. Following the same procedure for each part of the curve, finally, a function is defined which represents the whole curve. Then, displacement values (x, y) for each node are found by using this curve fitting technique. A description of this methodology is shown in figure 7.5.

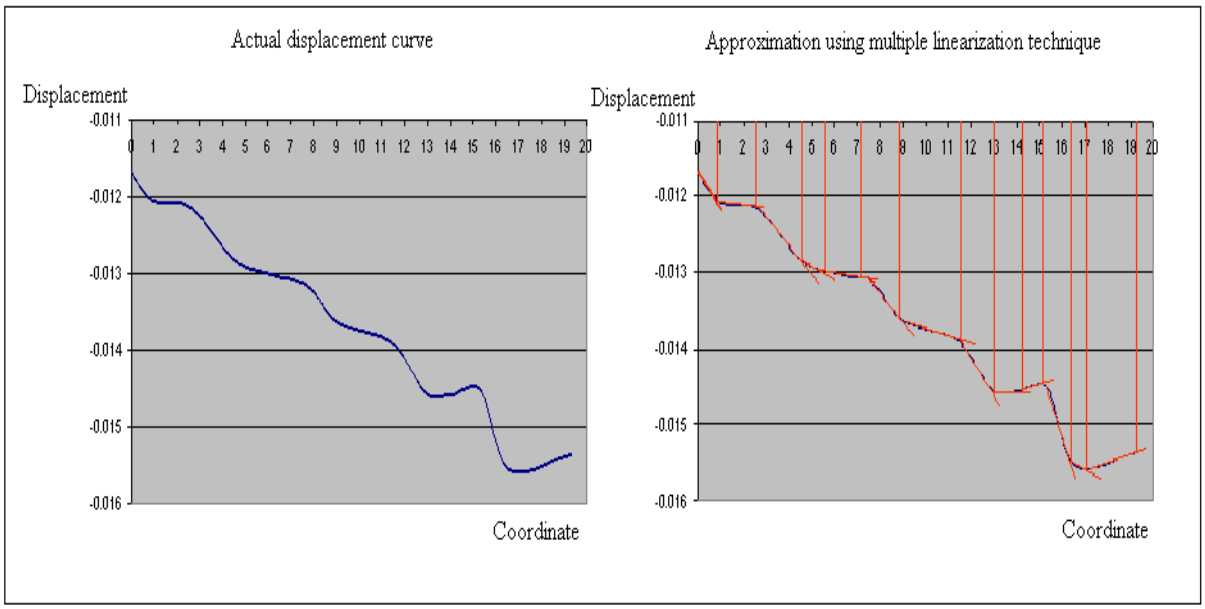

Figure 7.5: Multiple linearization technique to transform ABAQUS deformations to Franc2D.

Using the multiple linearization techniques, both x and y displacements are found for each node. Figure 7.6 illustrates the loading condition used in this FE model. Later on the FE model is verified by performing the simulation in Franc2D and then comparing the stress distribution results with the actual ABAQUS simulation results. The values of x and y displacements on each node are given in Appendix 2.

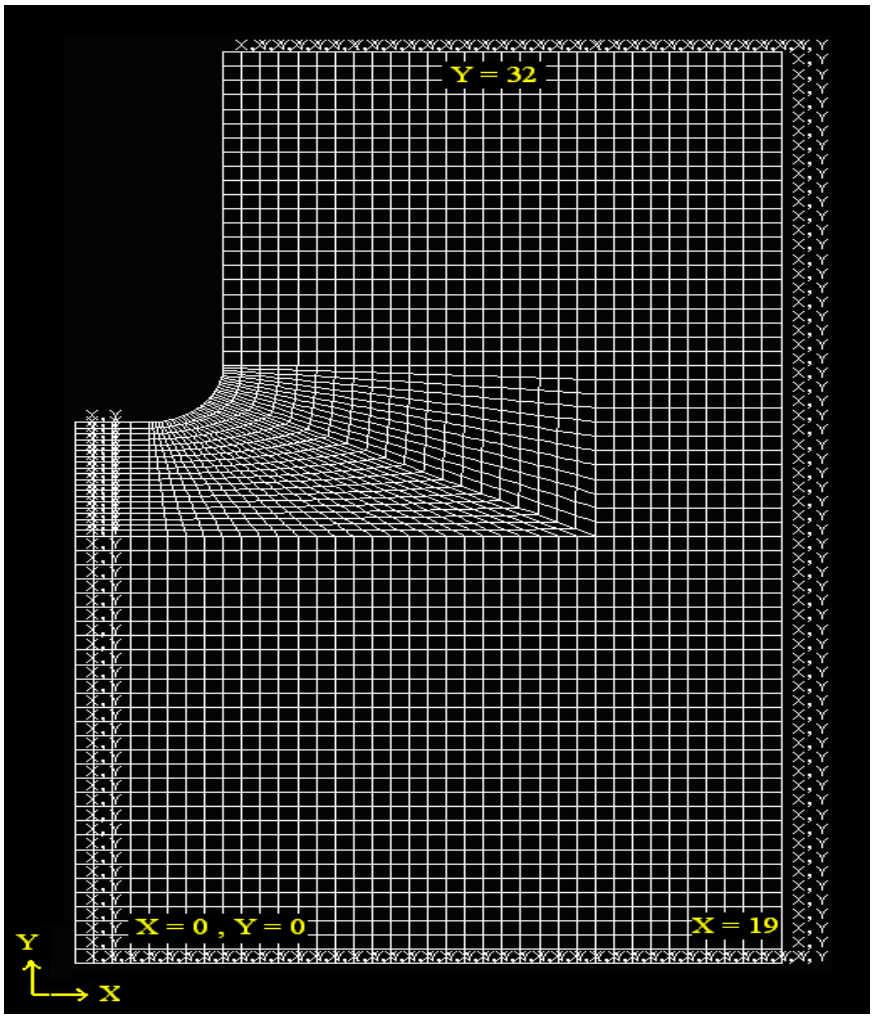

Figure 7.6: Loading conditions used in the Franc2D model

7.4 Simulations results

After developing a FE model for the crack propagation and fatigue strength analysis, the simulations are performed in Franc2D. The loading conditions used in this FE model are obtained from the deformation results of the ABAQUS simulation of the simplified FE model and an interpolation technique is used to transform the results. The results from Franc2D simulations are compared with the results from ABAQUS simulation in order to verify the conditions used to develop this FE model. The results obtained from Franc2D simulations are describe as follows;

7.4.1 Deformation results

After performing the simulation in Franc2D the results are compared with the simulation results obtained in ABAQUS and it has been observed that the deformation results in x and y directions obtained from Franc2D simulations shows good agreement with the deformation

results obtained from ABAQUS simulations. Figure 7.7 and 7.8 shows the comparison of deformation results in x and y direction, respectively. The deformation range is in good agreement and the deformation bevahiour near the lifter hole corner is almost consistent in both analyses.

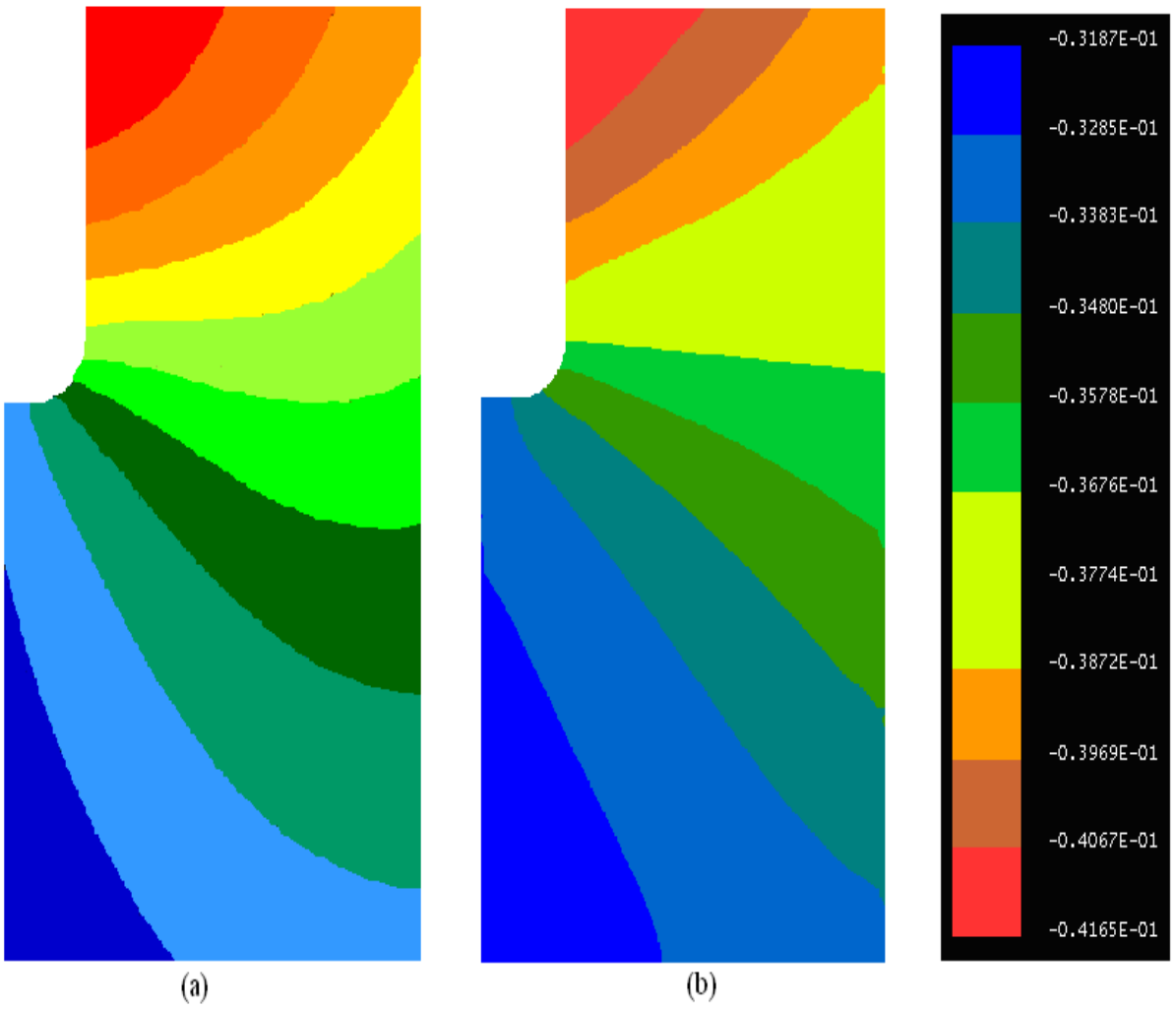

Figure 7.7: x-deformation results from simulations in (a) ABAQUS and (b) Franc2D.

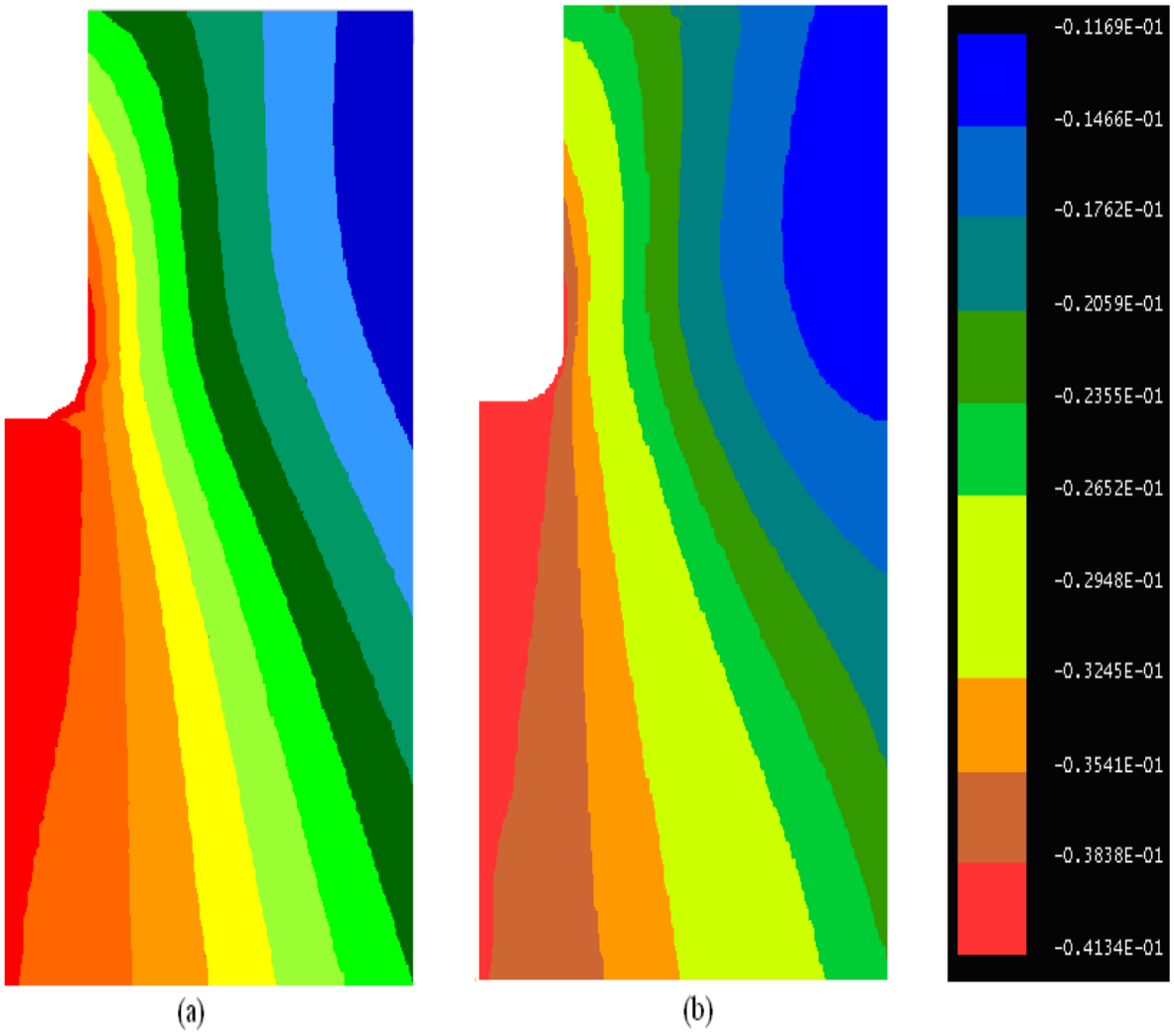

Figure 7.8: y -deformation results from simulations in (a) ABAQUS and (b) Franc2D.

7.4.2 Stress distribution results

The stress distribution results obtained from simulations performed in Franc2D show good agreement with the stress distribution results obtained from simulations in ABAQUS. Since the results from numerical simulations and the experimental findings have shown that the cracks appear around the lifter hole, so the main concern is to compare the stress distribution around this area. The comparison of the circumferential stress distribution obtained from simulations performed in Franc2D and ABAQUS is demonstrated in figure 7.9. The maximum stress value of 343.4 MPa is found at the same location where cracks have been found from experimental findings shown in figure 4.4.

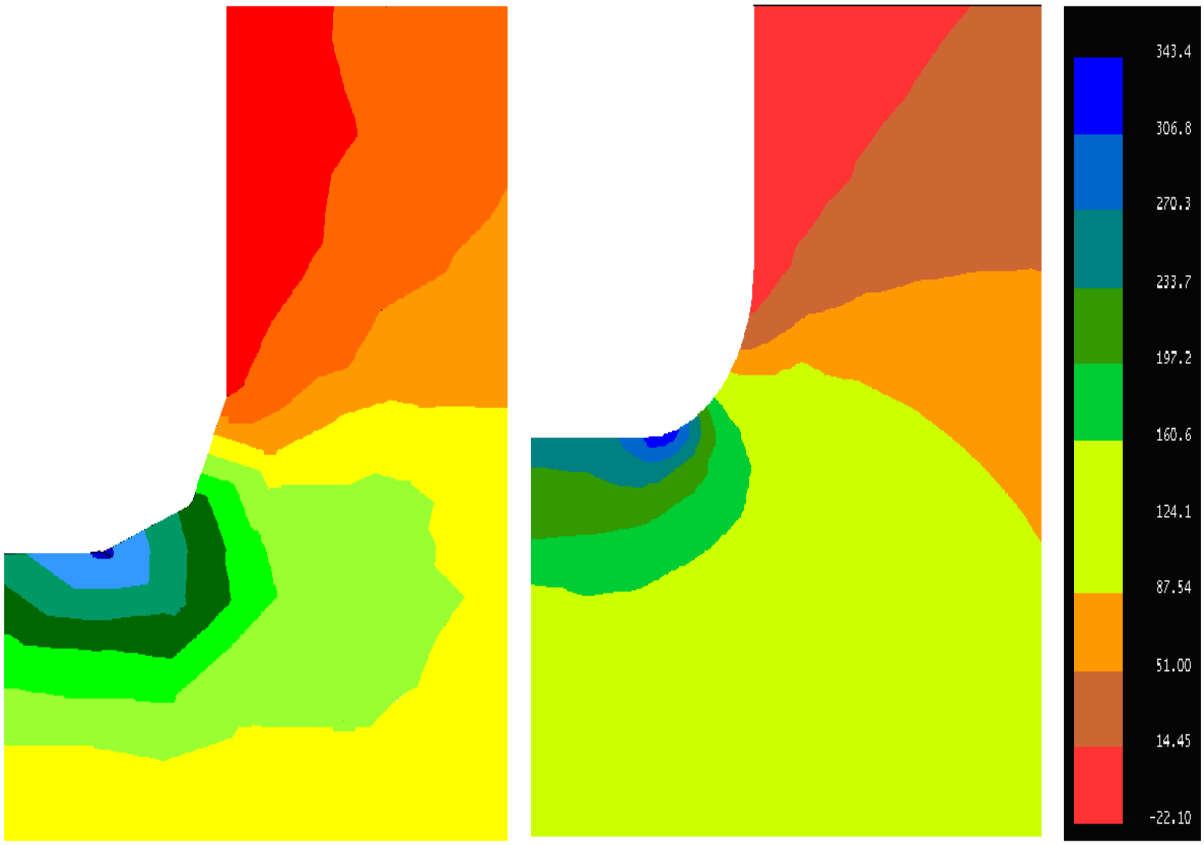

Figure 7.9: Stress distribution around the lifter hole obtained from simulations in (a) ABAQUS and (b) Franc2D.

7.4.3 Determining the crack propagation direction

The simulations are performed in Franc2D in order to obtain an expected crack propagation direction. For this, a crack is initiated at a point of maximum stress and an automatic remeshing strategy is used as shown in figure 7.10. The automatic remeshing strategy used in Franc2D consists of the following steps:

i. Delete the elements in the vicinity of crack tip.
ii. Move the crack tip
iii. Insert a trial mesh to connect the new crack to the existing mesh

In general, the crack propagates in the direction of maximum hoop stresses. It has been observed that the expected crack propagation direction obtained from the results of simulations performed in Franc2D shows good agreement with the actual crack propagation direction. Figure 7.10 demonstrates the resemblance between the actual crack propagation

direction obtained from experimental investigations and the expected crack propagation direction obtained from Franc2D simulations.

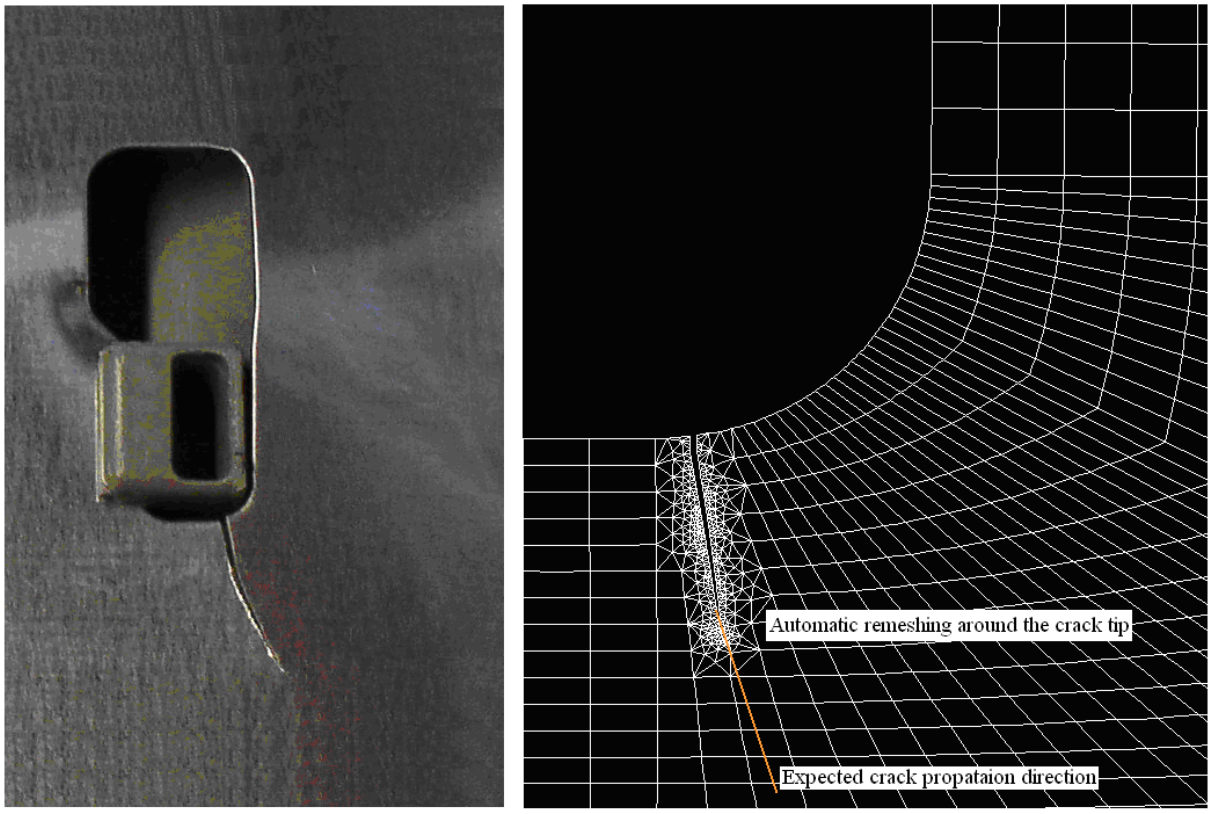

Figure 7.10: Crack propagation direction obtained from (a) experimental investigations and (b) simulations in Franc2D.

7.4.4 Calculating the stress intensity factor (K_I)

The simulation results showed that the circumferential stresses are mainly responsible for the crack propagation because of the applied loading conditions. It has been found from the results that K_I governs the crack propagation behaviour because the values found for K_{II} are almost negligible compared to the K_I values and the maximum value for K_{II} has been found to be 2.6 $MPa\sqrt{mm}$. However, the maximum value for K_I is found to be 320 $MPa\sqrt{mm}$ and the maximum value is reached with a crack length of 0.86 mm. A set of K_I values is obtained for different crack lengths and finally the K_I values are plotted as a function of crack length in order to understand the crack propagation behaviour. Figure 7.11 demonstrates the variation of K_I with respect to the crack length.

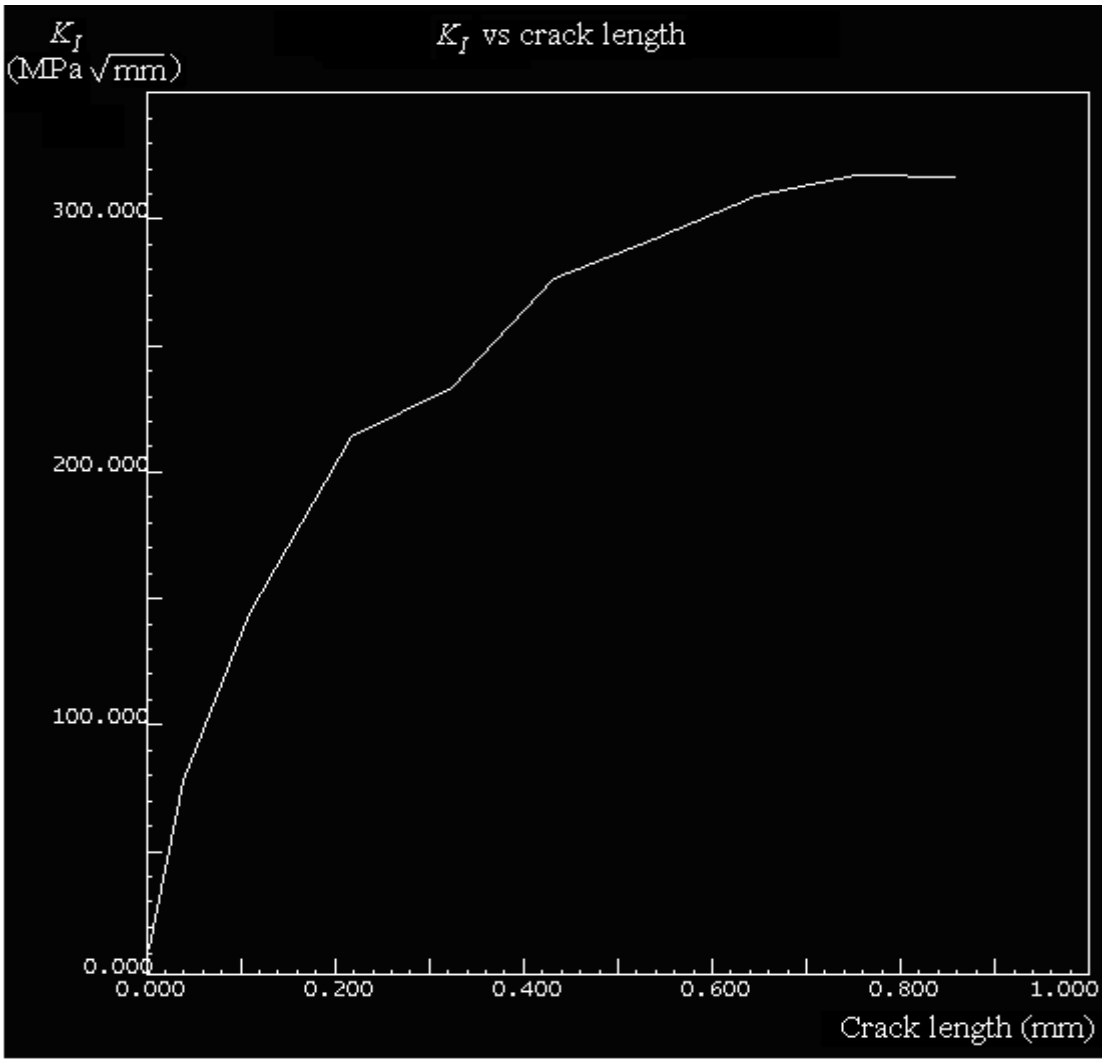

Figure 7.11: K_I as function of crack length.

7.4.5 Fatigue life analysis

A simple fatigue life analysis is performed in Franc2D which is based on Paris law. As mentioned in section 3.3, the Paris law states that the crack growth rate is an exponential function of the ΔK :

$$\frac{da}{dN} = C(\Delta K)^m \tag{7.1}$$

where C and m are the material specific input parameters. In Franc2D only mode I values of the stress intensity ranges are used. Generally, for metals, values for m ranges from 2.5 ~ 3.5 [33] and the C values ranges from 1^{-9} ~ 1^{-11} [34]. However, no specific values of these parameters were available for this FE model. Following values of these parameters are assumed for the basic understanding of the fatigue strength behaviour of the FE model.

$$m = 3$$
$$C = 1^{-10} \tag{7.2}$$

The results obtained from the fatigue life analysis show that it takes 14600 cycles for a crack to reach a crack length of 0.9 mm. However, the fatigue life is greatly dependens on the material parameters and a small variation in these material parameters effect the fatigue life results significantly. The fatigue life plot as a function of crack length is demonstrated in figure 7.12.

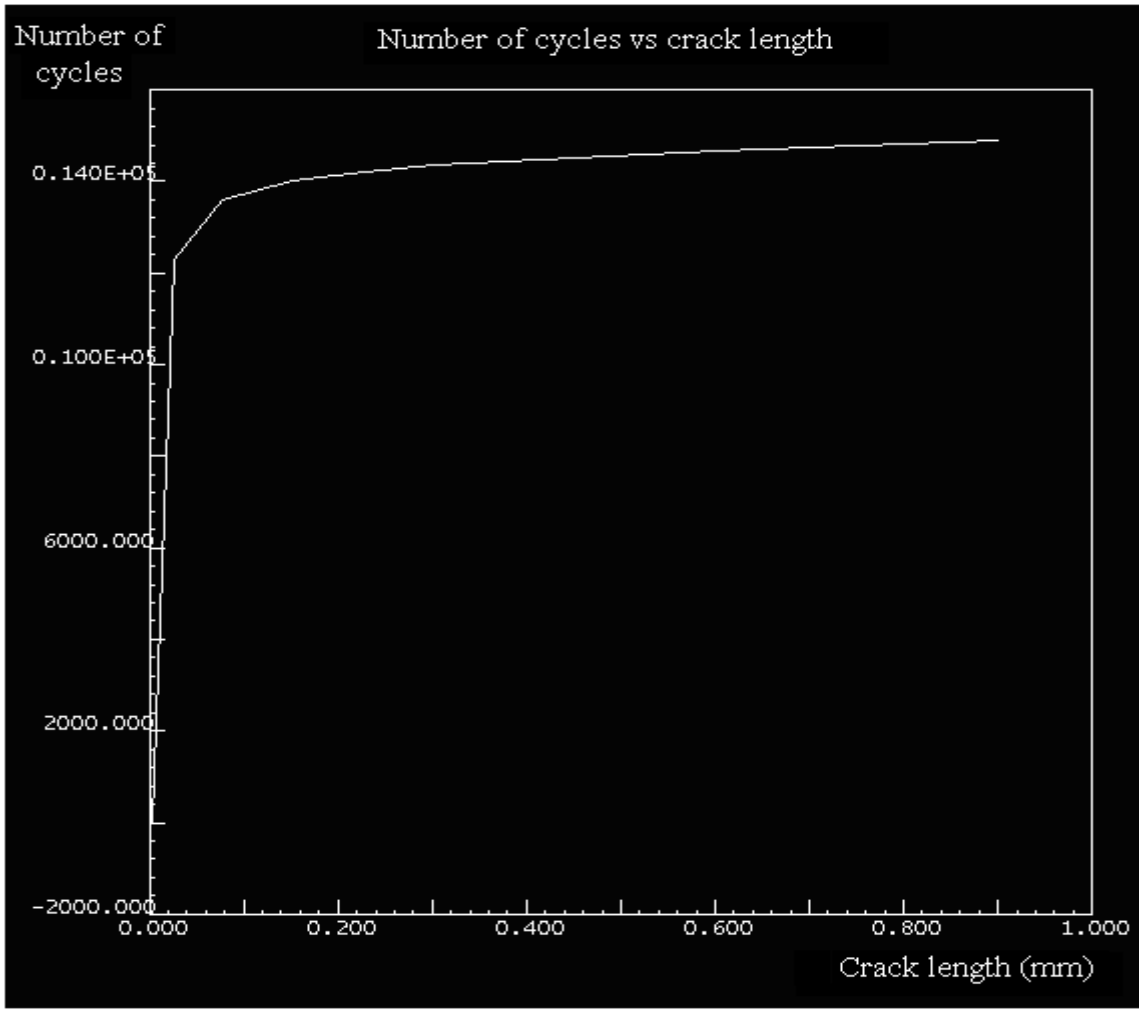

Figure 7.12: Fatigue life as function of crack length.

7.5 Effects of loading conditions on fatigue life

In general, the analytical models demonstrate that the loading has direct impact on the stresses value and higher the level of stresses, faster the crack will grow. A detailed description of the models considered in order to understand the effect of loading on the fatigue life is given in the following section.

7.5.1 FE model with increased loading

In order to study the influence of loading conditions on the crack propagation and the fatigue life of the component used in this Master thesis, two different FE models are created with the same geometry, material properties, meshing and boundary conditions but different loading conditions. In one FE model actual loads are applied in the form of displacements taken from the simulation results obtained from ABAQUS, while in other FE model an extra load of 50% is applied, hence the load in the second FE model is 1.5 times the actual load. Then, the simulations are performed in Franc2D and the results obtained in each case are discussed in the following section.

7.5.2 Simulation results

The simulation results are obtained in the form of maximum stresses and crack propagation rate. It has been found that the crack tip location is same in both cases which show that the location of maximum stress remains the same. However, the value of maximum stress increases from 334.7 MPa to 495.2 MPa when 50% extra loading is applied. In order to understand the effect of loading on the FCG, simulations are performed with both FE models until the crack length reaches a value of 1 mm in both cases. For the comparison of the fatigue life results, same values of material parameters are assumed in these simulations as discussed in section 7.4.5. It has been observed that it takes 14800 cycles for a crack to reach a length of 1 mm in the case of actual loading. However, in case of 50% extra loading, crack reaches a length of 1 mm with only 5050 cycles. Table 7.1 summarizes the results obtained from the FE simulations performed.

Loading condition	Crack tip location		Maximum stress (Mpa)	Number of cycles to reach a crack length of 1 mm
	x (mm)	y (mm)		
Actual loads	2.26	19.01	334.7	14800
50% extra loads	2.26	19.01	495.2	5050

Table 7.1: Fatigue life results for FE models under different loading conditions

The simulation results shows that fatigue life is significantly affected by the applied loading, however, a detailed analysis of the results is performed for better understanding of the crack propagation behaviour. The fatigue life is plotted as a function of crack length for both FE models. Figure 7.13 demonstrate the effect of loading on the FCP.

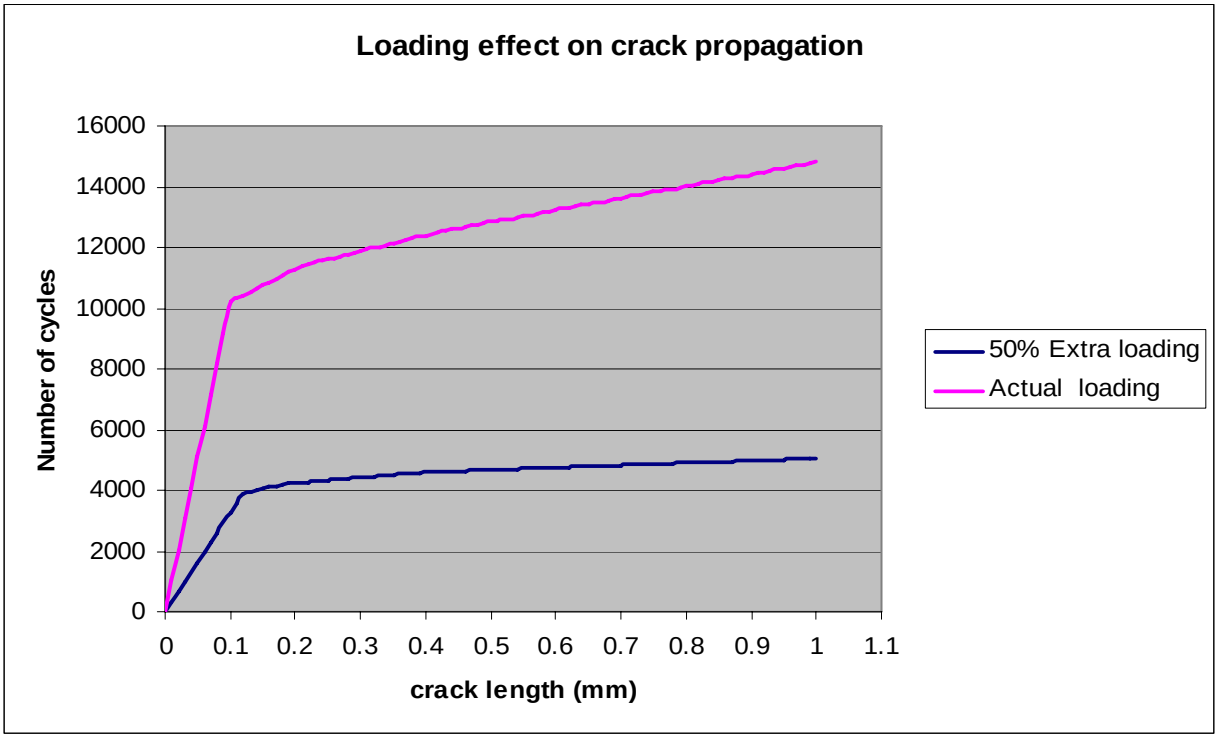

Figure 7.13: Comparison of fatigue life as function of crack length for the FE models under different loading conditions.

The simulation results show that a 50% increase in the applied load results in 48% increase of the maximum stress value and the fatigue life decrease by nearly three times. Hence, 50% increase in the applied load results in 65% increase in the rate of crack growth (see table 7.1).

7.6 Effect of notch size on the fatigue life

A notch is basically a geometric discontinuity which results in stress concentrations. The FE results have shown that cracks are usually expected near the areas of stress concentrations. In this section the influence of notch size on the crack propagation and fatigue life is studied in detail and the results obtained from simulations performed in Franc2D are also presented in this section.

7.6.1 FE models with different notch sizes

In order to study the influence of notch size on the crack propagation and the fatigue life of the component, three FE models are created with lifter holes of radius of 1 mm, 2 mm and 3 mm. The other features including material properties, meshing and loading conditions are same in all three FE models as discussed in section 7.2 and 7.3. Figure 7.14 demonstrate the

three FE models used for the study of notch size effects on the fatigue life. The simulations are performed in Franc2D for these three FE models and the results obtained in each case are explained in the following section.

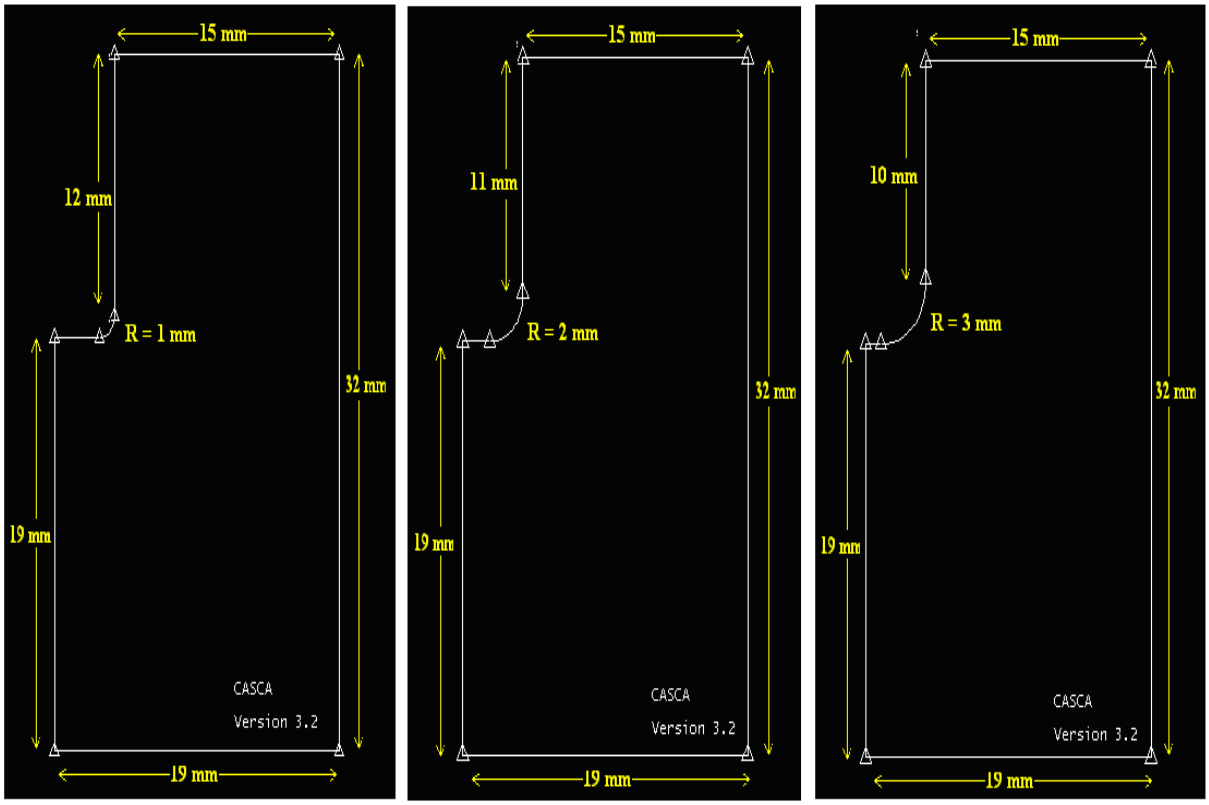

Figure 7.14: FE models having notch radius of (a) R = 1 mm (b) R = 2 mm (c) R = 3 mm.

7.6.2 Simulation results

The simulation results are obtained in the form of maximum stresses and crack propagation rate. As expected, it has been found that the value of maximum stress decreases with an increase in the notch radius. The maximum stress of 388 MPa is found in the FE model with notch radius of 1 mm. In order to understand the effect of notch size on the FCG, simulations are performed until the crack length reaches a value of 1 mm in all three cases. For the comparison of the fatigue life results, same values of material parameters are assumed in these simulations as discussed in section 7.4.5. It has been observed that the number of cycles required for a crack to reach a length of 1 mm increases with an increase in the notch radius. The maximum of 17200 cycles are required for a crack to reach a length of 1 mm in the case of 3 mm notch radius. Table 7.2 summarizes the results obtained from the FE simulations

performed. Finally, the fatigue life is plotted as a function of crack length for all three cases. Figure 7.15 demonstrates the effect of notch radius on the FCP.

Notch radius (mm)	Crack tip location		Maximum stresses (MPa)	Cycles to reach a crack length of 1 mm
	x (mm)	y (mm)		
1	3.29	19.03	388.0	13000
2	2.26	19.01	334.7	14800
3	1.48	19.0	321.4	17200

Table 7.2: Fatigue life results for the FE models having different notch radius.

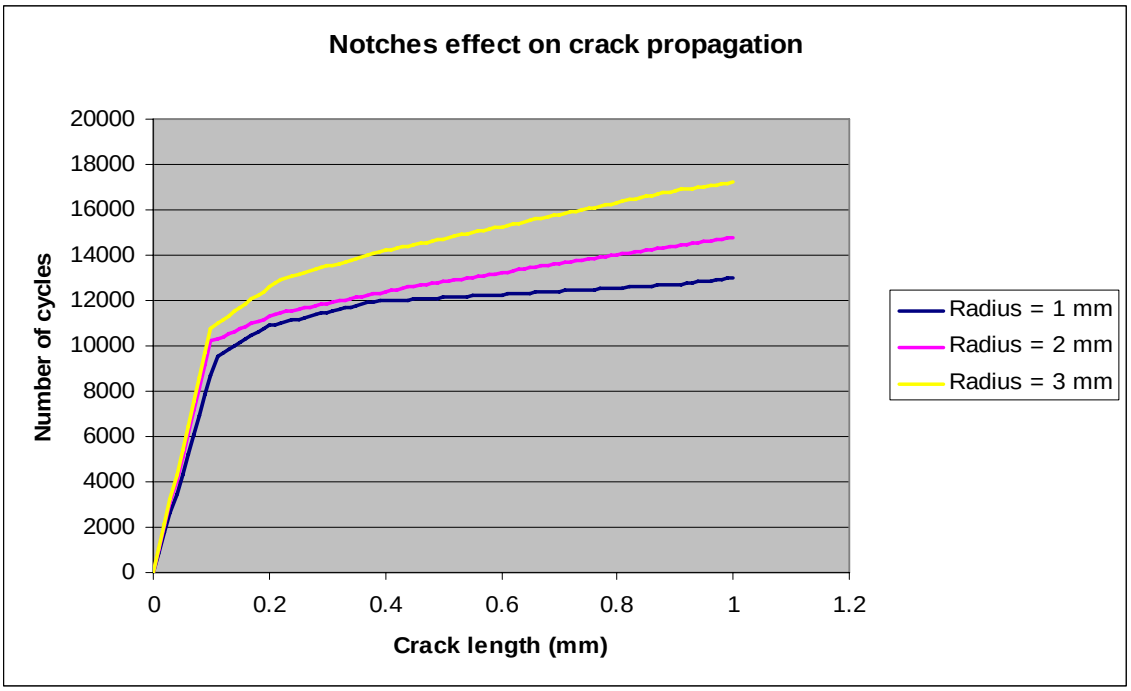

Figure 7.15: Comparison of fatigue life as function of crack length for different notch radii.

The simulation results showed that the value of maximum stress and the crack growth rate both decreases with an increase in the notch radius. Hence, the crack growth rate increases with the sharper notch as expected.

8. Conclusions and recommendations

The purpose of this thesis was to study the fatigue strength and crack propagation behaviour of the stainless steel structures based on both the experimental investigations and FEA. The FEA is done with ANSYS and ABAQUS. An important aspect of this research was to compare the results from the experimental investigations and FEA to see if it is possible to obtain similar results. The success in this manner depends both on the evaluation methods of the experiments and accuracy of FE models used in FEA. The crack propagation and fatigue strength analysis is done with Franc2D. A detailed study concerning different FE models with different geometries based on symmetry assumptions under static loading conditions were performed. The modeling approaches and the issues related to different FE meshes were also studied in detail.

The results from experimental investigations showed that the lifter holes are the most critical part of the drum structure because all the cracks were found around the lifter holes and the propagation of these cracks follows approximately consistent pattern around each lifter hole. It has been found from the forced failure that the structural damage obtained from experiments occurred after 15000 load cycles.

The simulation results obtained from the FE analysis performed with ANSYS showed good agreement with the experimental findings and the maximum deformations are also found near the lifter holes and the value of maximum deformation is found to be 0.311 mm. An important conclusion from these results is that the internal geometries of the holes have no significant influence on the simulation results and one can ignore these geometries in order to simplify the FE model. In the light of this conclusion it is recommended to use simplified model without internal geometries of the holes because these internal geometries sometimes also create problems during meshing due to the shape of these internal geometries.

The simulation results from FE analysis performed with ABAQUS verified the results of FE analysis performed with ANSYS in terms of structural deformations and stress distribution behaviour of the FE model. However, the maximum deformation value was found to be 0.38 mm and this small difference in the maximum deformation values obtained from ANSYS and ABAQUS is probably due to the difference in the FE meshes used. The deformation behaviour obtained from simulations performed in both ANSYS and ABAQUS was found to be non-symmetric and the stresses in the axial direction were negligible because of the

applied loading condition. Further simplification of the FE model using symmetry features is not possible due to this non-symmetric behaviour. Hence, it is recommended to use cylindrical coordinate system in order to have symmetry in the results and then the model can be simplified due to the symmetry and thus, an in-depth investigation can be made to understand the crack propagation behaviour.

The crack propagation and fatigue strength analysis was performed in Franc2D. The deformation and stress distribution results from simulations performed in Franc2D showed good agreement with the results obtained from simulations performed in ANSYS and ABAQUS and the crack initiation location and crack propagation direction obtained from Franc2D simulations was close to experimental finding. It has also been found from the results obtained from simulations performed in Franc2D that K_I governs the crack propagation behaviour because the K_{II} values obtained were almost negligible compared to the K_I values. The fatigue life prediction results showed that the fatigue life prediction is strongly dependent on the material parameters (C and m) used in Paris law. It is highly recommended to use the exact values for these material parameters in order to get the exact crack propagation behaviour and to get a better understanding of the fatigue strength of the component. However, the procedure used in this project with assumed values of these parameters provide a good basic understanding of the crack propagation behaviour because of the fact that the crack propagation behaviour coincide with the experimental findings.

In the end, simulations were performed in Franc2D to study the influence of the applied loads and the notch size on the fatigue life of the component. The results from the study of loading effects on the fatigue life showed that in the case of the actual loading, 14800 cycles are required for a crack to reach a length of 1 mm but in the case of 50% extra loading, the crack growth rate increased by 65% and the crack length of 1 mm was reached with 5050 cycles. The simulations performed in Franc2D to study the effects of notch size on the fatigue life of the structure showed that the value of maximum stress and the crack growth rate both decreases with an increase in the notch radius as expected.

8.1 Scope for future work

There is a lot of room for future research in this relatively new field. The simulation results provide an estimated fatigue life of the component but have in mind that these results were based on the assumed values of material parameters (C and m) used in Paris law. Therefore,

the calculated crack propagation rate and the fatigue life can be used for the basic understanding of the crack propagation behaviour and fatigue strength of the component but these results can not determine the exact fatigue life of the component. One of the suggested future improvements to determine the exact fatigue life can be to perform experimental investigations to get the exact values of these parameters and then the same model can be used to get better results for the fatigue life prediction. Similarly, the simulation results concerning the influence of the applied loads and the notch size on the fatigue life of the component can also be improved by using the exact values for the material parameters. Metallographic studies can be performed in order to get an in-depth understanding of the crack propagation behaviour and to determine the factors which influence the fracture process (other than geometric factors).

9. References

[1] Y. Murakami and K.J. Miller., What is fatigue damage? A view point from the observation of low cycle fatigue, *International journal of fatigue*, 27 (2007) pp. 991-1005.

[2] Hoeppner, D.W., and Krupp, W.E., Prediction of component life by application of fatigue crack growth knowledge, *Engg. Fracture Mech.* Vol., 6 (1974), pp.47-70.

[3] Smith,R.A., Fatigue crack growth 30 years of progress, pergamon press, 1986.

[4] L. P. Pook N. E. Frost and K. Matsh. Metal Fatigue. Oxford University Press, 1974.

[5] ASTM: E1150/87 standard definitions of terms relating to fatigue. *American Society for testing and Materials*, (1987), pp. 1–10.

[6] K.J. Miller., A historical perspective of the important parameter of metal fatigue; and problems for the next century. In: X.R. Wu and Z.G. Wang, Editors, Proceedings of the seventh international fatigue congress. Fatigue'99, Beijing 99, Higher Education Press EMAS (1999), pp. 15–39.

[7] Y. Murakami, S. Harada, T. Endo, H. Tani-ishi and Y. Fukushima., Correlations among growth law of small cracks, low-cycle fatigue law and applicability of Miner's rule, *Eng Fract Mech*, 18 (1983) (5), pp. 909–924.

[8] Stephens, Ralph I., Metal Fatigue in Engineering (Second edition ed.). John Wiley & Sons, Inc. 2001, pp. 69.

[9] Callister, W. D., Material Science and Engineering an Introduction, John Wiley & Sons, Inc. 2000.

[10] Material Technologies, Inc. Completes EFS Inspection of Bridge in New Jersey Press release regarding metal fatigue damage to the Manahawkin Bay Bridge in New Jersey.

[11] Broek, D., 1986, Elementary Engineering Fracture Mechanics, Martinus Nijhoff Publishers, Dordrecht.

[12] O. Vardar., Effect of single OL in FCP. *Engineering Fracture Mechanics*, V-30, n-3 (1988), pp. 329-335.

[13] J. J. Coner Julie A. Bannantine and J. Hand Rock., Fundamentals of metal fatigue analysis. Printice Hall, 1990.

[14] Sanford, R. J., 2003, Principles of Fracture Mechanics, Prentice Hall, Upper Saddle River, NJ.

[15] Sih, G. C., Some Basic Problems in Fracture Mechanics and New Concepts, *Eng. Fracture Mech.*, Vol. 5 (1973), pp. 365-377.

[16] Atkinson, B.K., Fracture Mechanics of Rock, pp. 534, Academic Press, London UK, 1987. Chapter 1, 2, 4.

[17] Anderson T.L., Fracture Mechanics Fundamentals and Applications, Second Edition, Taylor and Francis Ltd, Boca Raton, Florida, 1995, pp. 31-90, 566-598, 627-631.

[18] Dahlberg T. and Ekberg A., Failure Fracture Fatigue an Introduction, First Edition, Studentlitteratur, Sverige, 2002, pp. 63-205.

[19] Anderson, T.L., Fracture Mechanics: Fundamentals and Applications (CRC Press, Boston 1995).

[20] Cook R.D., Malkus D.S., Plesha M.E. and Witt R.J., Concepts and Application of Finite Element Analysis, Fourth Edition, John Wiley and Sons Ltd, New York, 2001, pp. 202-219, 283-286.

[21] Sato,T., and Shimada,H., Evaluation of fatigue crack initiation life from a notch, *Int. journal fatigue*, Vol. 10, No. 4 Oct. 1988, PP. 243-247.

[22] P. Paris and F. Erdogan ., A critical analysis of crack propagation laws, *Journal of Basic Engineering*, Transactions of the American Society of Mechanical Engineers, December 1963, pp.528-534.

[23] P. C. Paris, M. P. Gomez and W. E. Anderson., A rational analytic theory of fatigue. The Trend in Engineering (1961). 13, pp. 9-14.

[24] Ashwell, D. G., and R. H. Gallagher, Editors, Finite Elements for Thin Shells and Curved Members, John Wiley and Sons, London, 1976.

[25] Madenci, E., and Guven, I., 2006, The Finite Element Application in Engineering using ANSYS®, Springer.

[26] http://uic.edu/depts/accc/software/ansys/html/elem_55/chapter4/ES4-93.htm.

[27] Hibbit, Karlsson, and Sorensen. ABAQUS/Standard User's Manual 6.3 ed. Hibbit, Karlsson, and Sorensen Inc, Pawtucket, 2002.

[28] Cornell Fracture Group, Cornell University, Ithaca, New York. http://www.cfg.cornell.edu/.

[29] Banks-Sills L., Application of the Finite Element Method to Linear Elastic Fracture Mechanics, *ASME Applied Mechanics Reviews*, Vol. 44, No. 1 (1991), pp. 447-460.

[30] Erdogan & Sih., On the crack extension in plates under plane loading and transverse shear, *ASME J Basic Engr*, 85 (1963), pp. 519-527.

[31] Hussain, Pu, & Underwood., "Strain energy release rate for a crack under combined mode I and II," *Fracture Analysis*, ASTM STP 560 (1974), pp. 2-28.

[32] Sih, "Strain-energy-density factor applied to mixed-mode crack problems," *Int J Fracture Mech*., 10 (1974), pp. 305-321.

[33] Fuad M. Khoshnaw, Nazhad A. Hussain., Geometry factor determination of round specimens using fracture mechanic approaches in Al 2024-T3, *Int J of Aircraft Engineering and Aerospace Technology*, 79 (2007), pp. 469 – 474.

[34] N. Pugno,M. Ciavarella, P. Cornetti, A. Carpinteri., Ageneralized Paris' law for fatigue crack growth, *Journal of the Mechanics and Physics of Solids*, 54 (2006) pp. 1333–1349.

[35] http://www.ptc.com/products/proengineer/

[36] http://www.ansys.com/products/workbench/default.asp

[37] www.rrzn.uni-hannover.de/fileadmin/aws_dok/msc/patran.pdf

[38] http://caedoc.hlrs.de/v6.7/index.html

Appendix 1

Detailed drawings of the drum structure

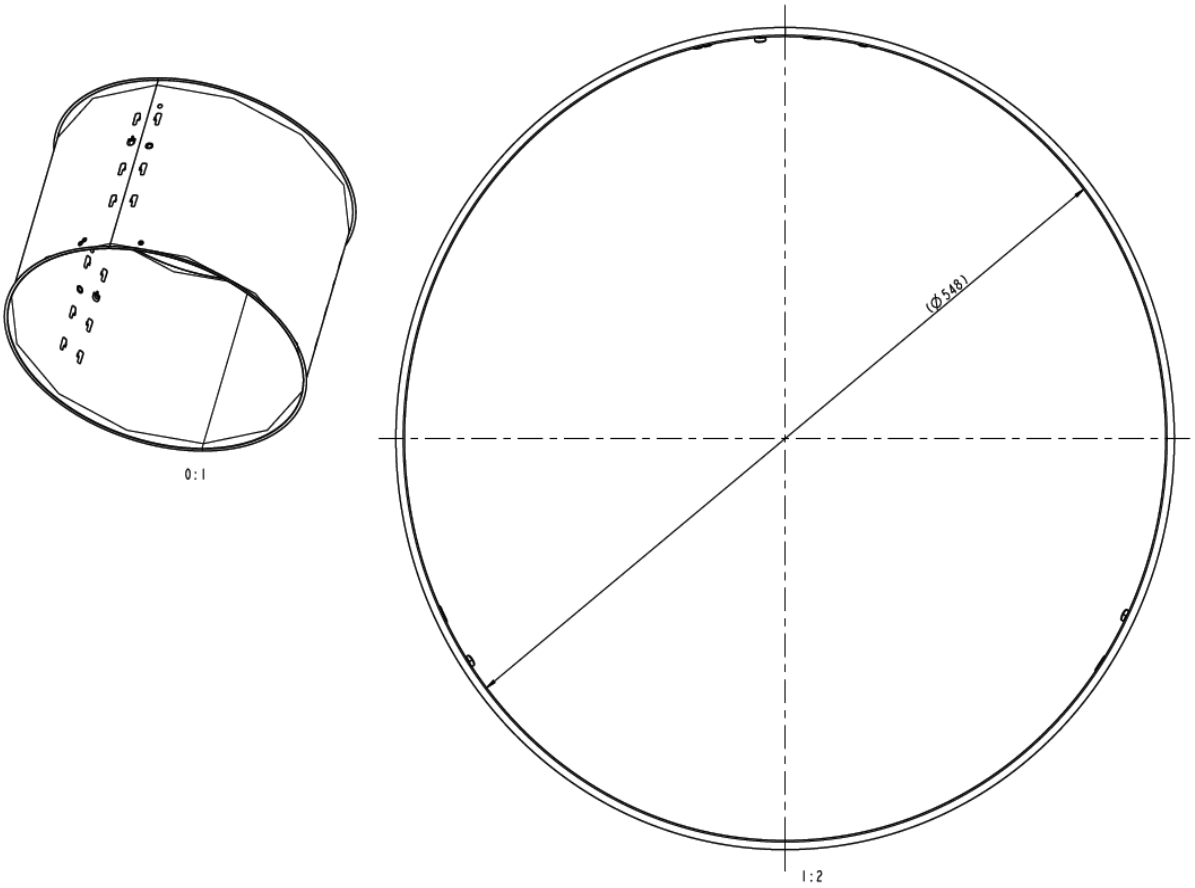

Figure A1.2: Detail drawing of the drum model.

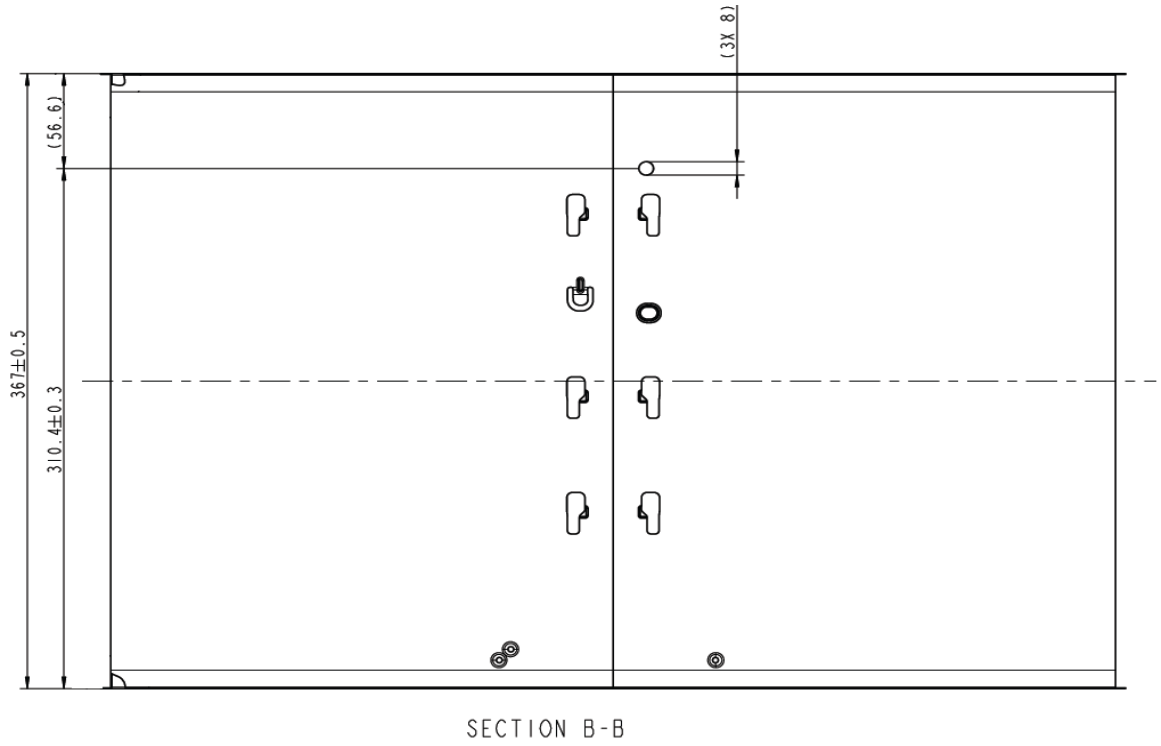

Figure A1.2: Detail drawing of the internal holes in the drum model.

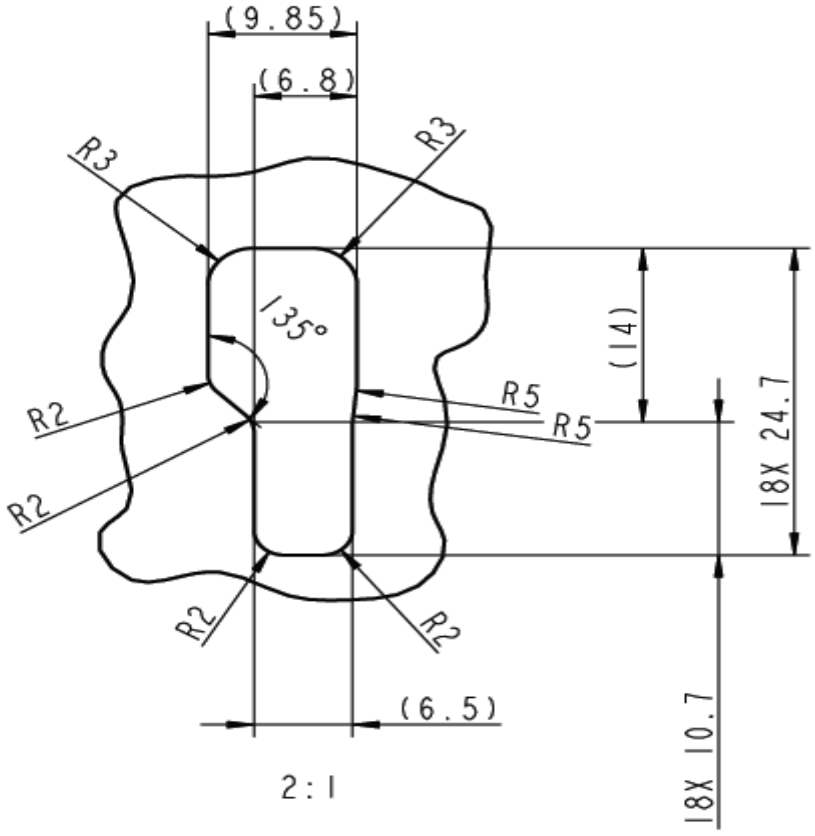

Figure A1.3: Detail drawing of the lifter hole.

Appendix 2

Displacement loading applied in the Franc2D model.

As discussed in section 7.3, the displacement loads are determined by using an approximation technique for each node as shown in figure 7.6. The detail description of the displacement loads applied on each node of the model used for the crack propagation and fatigue strength analysis is given in the following tables:

Displacement values on the left side of the model (x = 0)					
Y coord. (mm)	X-Displacement (mm)	Y-Displacement (mm)	Y coord. (mm)	X-Displacement (mm)	Y-Displacement (mm)
0	-0.01169	-0.04073	13.0	-0.01459	-0.04142
0.5	-0.01190	-0.04072	13.5	-0.01455	-0.04146
1.0	-0.01207	-0.04071	14.0	-0.01455	-0.04150
1.5	-0.01210	-0.04074	14.5	-0.01454	-0.04154
2.0	-0.01212	-0.04076	15.0	-0.01454	-0.04158
2.5	-0.01215	-0.04080	15.2	-0.01454	-0.04160
3.0	-0.01228	-0.04080	15.4	-0.01458	-0.04162
3.5	-0.01245	-0.04081	15.6	-0.01474	-0.04163
4.0	-0.01262	-0.04081	15.8	-0.01491	-0.04165
4.5	-0.01279	-0.04081	16.0	-0.01507	-0.04166
5.0	-0.01290	-0.04083	16.2	-0.01523	-0.04161
5.5	-0.01294	-0.04087	16.4	-0.01540	-0.04157
6.0	-0.01299	-0.04090	16.6	-0.01556	-0.04152
6.5	-0.01303	-0.04094	16.8	-0.01556	-0.04148
7.0	-0.01308	-0.04097	17.0	-0.01556	-0.04143
7.5	-0.01313	-0.04100	17.2	-0.01554	-0.04138
8.0	-0.01327	-0.04103	17.4	-0.01552	-0.04134
8.5	-0.01344	-0.04105	17.6	-0.01551	-0.04129
9.0	-0.01362	-0.04108	17.8	-0.01549	-0.04125
9.5	-0.01369	-0.04112	18.0	-0.01547	-0.04120
10.0	-0.01375	-0.04116	18.2	-0.01546	-0.04115
10.5	-0.01381	-0.04121	18.4	-0.01544	-0.04111
11.0	-0.01387	-0.04125	18.6	-0.01542	-0.04106
11.5	-0.01394	-0.04130	18.8	-0.01541	-0.04102
12.0	-0.01416	-0.04134	19	-0.01539	-0.04097
12.5	-0.01438	-0.04138			

Table A2.1: Displacements on the left edge (x = 0)

Displacement values on the right side of the model (x =19 mm)					
Y coord. (mm)	X-Displacement (mm)	Y-Displacement (mm)	Y coord. (mm)	X-Displacement (mm)	Y-Displacement (mm)
0	-0.01666	-0.03589	16.5	-0.02490	-0.03326
0.5	-0.01691	-0.03581	17.0	-0.02515	-0.03316
1.0	-0.01716	-0.03573	17.5	-0.02540	-0.03307
1.5	-0.01741	-0.03565	18.0	-0.02565	-0.03297
2.0	-0.01766	-0.03557	18.5	-0.02590	-0.03287
2.5	-0.01791	-0.03549	19.0	-0.02615	-0.03278
3.0	-0.01816	-0.03541	19.5	-0.02640	-0.03270
3.5	-0.01841	-0.03534	20.0	-0.02665	-0.03262
4.0	-0.01866	-0.03526	20.5	-0.02690	-0.03254
4.5	-0.01891	-0.03518	21.0	-0.02716	-0.03246
5.0	-0.01916	-0.03510	21.5	-0.02741	-0.03239
5.5	-0.01941	-0.03502	22.0	-0.02767	-0.03231
6.0	-0.01966	-0.03494	22.5	-0.02793	-0.03223
6.5	-0.01991	-0.03487	23.0	-0.02818	-0.03215
7.0	-0.02016	-0.03479	23.5	-0.02848	-0.03213
7.5	-0.02041	-0.03472	24.0	-0.02880	-0.03212
8.0	-0.02066	-0.03464	24.5	-0.02911	-0.03210
8.5	-0.02091	-0.03457	25.0	-0.02942	-0.03209
9.0	-0.02116	-0.03450	25.5	-0.02973	-0.03207
9.5	-0.02141	-0.03442	26.0	-0.03004	-0.03206
10.0	-0.02166	-0.03435	26.5	-0.03035	-0.03204
10.5	-0.02191	-0.03427	27.0	-0.03068	-0.03203
11.0	-0.02216	-0.03420	27.5	-0.03095	-0.03201
11.5	-0.02241	-0.03413	28.0	-0.03123	-0.03199
12.0	-0.02266	-0.03405	28.5	-0.03151	-0.03198
12.5	-0.02291	-0.03398	29.0	-0.03178	-0.03196
13.0	-0.02315	-0.03391	29.5	-0.03206	-0.03195
13.5	-0.02340	-0.03383	30.0	-0.03233	-0.03193
14.0	-0.02365	-0.03376	30.5	-0.03261	-0.03192
14.5	-0.02390	-0.03365	31.0	-0.03289	-0.03190
15.0	-0.02415	-0.03355	31.5	-0.03316	-0.03189
15.5	-0.02440	-0.03346	32.0	-0.03344	-0.03187
16.0	-0.02465	-0.03336			

Table A2.2: Displacements on right edge (x = 19 mm)

Displacement values on the bottom edge of the model (y = 0)					
X coord. (mm)	X-Displacement (mm)	Y-Displacement (mm)	Node No. (mm)	X-Displacement (mm)	Y-Displacement (mm)
0	-0.01169	-0.04073	10.0	-0.01503	-0.03853
0.5	-0.01187	-0.04067	10.5	-0.01514	-0.03839
1.0	-0.01206	-0.04060	11.0	-0.01525	-0.03825
1.5	-0.01225	-0.04053	11.5	-0.01536	-0.03811
2.0	-0.01243	-0.04046	12.0	-0.01547	-0.03797
2.5	-0.01262	-0.04039	12.5	-0.01558	-0.03783
3.0	-0.01280	-0.04032	13.0	-0.01569	-0.03769
3.5	-0.01299	-0.04021	13.5	-0.01581	-0.03755
4.0	-0.01318	-0.04011	14.0	-0.01588	-0.03740
4.5	-0.01334	-0.04001	14.5	-0.01596	-0.03725
5.0	-0.01351	-0.03991	15.0	-0.01604	-0.03710
5.5	-0.01367	-0.03979	15.5	-0.01612	-0.03695
6.0	-0.01384	-0.03965	16.0	-0.01619	-0.03680
6.5	-0.01401	-0.03951	16.5	-0.01627	-0.03665
7.0	-0.01417	-0.03937	17.0	-0.01635	-0.03649
7.5	-0.01434	-0.03923	17.5	-0.01643	-0.03634
8.0	-0.01450	-0.03909	18.0	-0.01650	-0.03619
8.5	-0.01467	-0.03895	18.5	-0.01658	-0.03604
9.0	-0.01483	-0.03881	19.0	-0.01666	-0.03589
9.5	-0.01492	-0.03867			

Table A2.3: Displacements on lower edge (y = 0)

Displacement values on the top edge of the model (y = 32 mm)					
X coord. (mm)	X-Displacement (mm)	Y-Displacement (mm)	Node No. (mm)	X-Displacement (mm)	Y-Displacement (mm)
4.0	-0.04134	-0.03610	12.0	-0.03766	-0.03384
4.5	-0.04114	-0.03596	12.5	-0.03734	-0.03370
5.0	-0.04094	-0.03581	13.0	-0.03703	-0.03356
5.5	-0.04073	-0.03567	13.5	-0.03671	-0.03342
6.0	-0.04053	-0.03553	14.0	-0.03640	-0.03328
6.5	-0.04033	-0.03539	14.5	-0.03608	-0.03314
7.0	-0.04012	-0.03525	15.0	-0.03577	-0.03300
7.5	-0.03992	-0.03511	15.5	-0.03545	-0.03286
8.0	-0.03974	-0.03497	16.0	-0.03514	-0.03272
8.5	-0.03949	-0.03483	16.5	-0.03483	-0.03257
9.0	-0.03924	-0.03469	17.0	-0.03451	-0.03243
9.5	-0.03899	-0.03455	17.5	-0.03423	-0.03229
10.0	-0.03874	-0.03441	18.0	-0.03396	-0.03215
10.5	-0.03849	-0.03426	18.5	-0.03370	-0.03201
11.0	-0.03824	-0.03412	19.0	-0.03344	-0.03187
11.5	-0.03799	-0.03398	19.0	-0.03766	-0.03384

Table A2.4: Displacements on top edge (y = 32 mm)